A Surface Acoustic Wave based Biosensor for the detection of Hepatitis B Surface Antigen

A
Thesis Submitted
in Partial Fulfillment of the Requirements
for the Degree of
DOCTORATE OF PHILOSOPHY
By

NAMAMI GOSWAMI

Centre for Nanotechnology
Indian Institute of Technology Guwahati
December, 2019


भारतीय प्रौद्योगिकी संस्थान गुवाहाटी
Indian Institute of Technology Guwahati

DECLARATION

This is to certify that the thesis entitled "**A Surface Acoustic Wave based Biosensor for the detection of Hepatitis B Surface Antigen**", submitted by me to the *Indian Institute of Technology Guwahati*, for the award of the degree of Doctorate of Philosophy, is a bonafide work carried out by me under the supervision of Prof. Roy Paily Palathinkal and Dr. Biplab Bose. The content of this thesis, in full or in parts, have not been submitted to any other University or Institute for the award of any degree or diploma. I also wish to state that to the best of my knowledge and understanding nothing in this report amounts to plagiarism.

Signed: ____

Namami Goswami
Centre for Nanotechnology,
Indian Institute of Technology Guwahati,
Guwahati-781039, Assam, India.

Date: ____

Dedicated

To

My Family

CERTIFICATE

This is to certify that the thesis entitled "**A Surface Acoustic Wave based Biosensor for the detection of Hepatitis B Surface Antigen**", submitted by Namami Goswami (136153002), a research scholar in the *Centre for Nanotechnology*, *Indian Institute of Technology Guwahati*, for the award of the degree of Doctorate of Philosophy, is a record of an original research work carried out by her under our supervision and guidance. The thesis has fulfilled all requirements as per the regulations of the institute and in our opinion has reached the standard needed for submission. The results embodied in this thesis have not been submitted to any other University or Institute for the award of any degree or diploma.

Supervisor: Prof. Roy Paily Palathinkal
Centre for Nanotechnology &
Department of Electronics and Electrical Engineering
Indian Institute of Technology Guwahati,
Guwahati-781039, Assam, India.

Date:

Co-Supervisor: Dr. Biplab Bose
Centre for Nanotechnology &
Department of Biosciences and Bioengineering
Indian Institute of Technology Guwahati,
Guwahati-781039, Assam, India.

Date:

ACKNOWLEDGEMENTS

I have been very fortunate to pursue my doctorate degree at the Centre for Nanotechnology, IIT Guwahati, where I had the opportunity to interact with many extraordinary people. I whole-heartedly thank my supervisor, Prof. Roy Paily Palathinkal, who helped me in every possible way in providing the guidance as well as facilities that gave a shape to my research. I fall short of words for my co-supervisor Dr. Biplab Bose, for guiding me wherever and whenever I was stuck in the intricacies of biological research. I would also like to thank my supervisors for making time to read and correct my dissertation. I would like to acknowledge the contributions of the members of my doctoral committee, Prof. Arun Chattopadhyay, Prof. Siddartha Sankar Ghosh and Prof. Harshal B. Nemade, who kept me going with their encouraging remarks and valuable suggestions from time to time. Interacting with them was a pleasant learning experience for me.

Special mention must be made of my labmates who have contributed significantly to my growth as a person: seniors Basudeb Behera, Brajesh Rawat, Jitendra Kumar, Shyam Trivedi, Vivek Sir and Santosh Golapuddi, for guiding me and making me feel at home in the lab; juniors Siddhant, Paromita, Himakshi, Monica and Sophia for pestering me with all sorts of technical and non-technical queries and helping me enhance my knowledge in various topics. I would like to acknowledge the support of my labmates from the Centre of Excellence, BSBE: Mahesh Agarwal, Poulami, Vimalathithan, Satendra, Kamlesh and Priya Praness, for being so supportive. I thank my juniors from EEE Department: Pralay, Satya and Vimal for all the technical help. Ujjwol, Vimalathithan and Paromita deserve special mention, as they went out of their ways to aid me in the proof-reading process. A special thanks to the officers from the Centre for Nanotechnology: Paran Sir, Pranjoli Ma'am, Kaustubh Sir, Indrajit Sir and Naba Sir, who always found time to check if the students had any difficulties and facilitated the solutions to those issues. I would also like to thank the CENTD Project staff: Gayatri Natu, Emlin Abraham, Thomas and Reena for their assistance in utilising the instrument facilities. I am really indebted to the facilitators of the INUP program at IISc Bangalore, especially the technologists involved in the fabrication of the devices.

I am very grateful to Upashi Goswami for making my tenure at IIT Guwahati a memorable one. I am also thankful to her for boosting my self-confidence and optimism during hard times. I would like to thank Ujjwol Barman for his perseverance throughout our collaborations, as well as for being a great friend and partner-in-crime. I extend my gratitude to my childhood buddies- Rim, Senty and Suzie for never letting the child in me die. I would like to thank Mridusmita, Anamika Kalita, Anushree Di and Aditi Di for being a part of my life at IIT Guwahati. I would also like to mention my hostel mates: Jumi, Megha, Prerona, Nimisha, Gaurangi and Angana for being like a family away from home. A warm thank you to Larionette, Somorjit and Abhilasha for including me in their midnight tea breaks whenever I was working late in the lab.

I would like to acknowledge the significant contributions of my TT family: Dr. Bishan Roy Sir, Needhi, Abhiram, Ankur, Deepak, Aman, Tejas, Uddipana, Juthika, Tarang, Vishal C., Karthik, Vishal G., Arooshi, Aditi, Sudipta, Abhishek, Saurav, Atman, Samarth, Preetham, Sumanth, Avinesh and Akash for keeping me both physically and mentally fit throughout my IIT Guwahati years. I hope to keep in touch with these wonderful people in the future.

I extend my heartfelt gratitude to my parents, Dr. Jeetendra Goswami and Dr. Nilima Devi for being the pillars of support in every decision I take. I thank them for bringing me up in the best possible way and for the sacrifices they have made to ensure that I have a life that is more privileged than theirs. I thank my parents-in-law, Dr. Binode Kumar Baruah and Aparajita Devi from the bottom my heart, for making me a part of their family and for showering me with so much love and affection. A special thanks to my brothers Gaurav and Rheetwik for always being there for me.

Last but not the least, heartfelt thanks to my husband, Mr. Ashish Baruah for being the wind beneath my wings in every endeavour I undertake. No amount of words can justify my gratitude to him for his unflinching love and support over the years.

Sincerely
Namami Goswami

ABSTRACT

The reliable use of Micro-Electro-Mechanical-Systems (MEMS) for biological applications, generally termed as Bio-MEMS, is one of the fastest growing fields today. Research in this field has attracted much attention and commercialization of reliable point of care sensors have also been successfully accomplished. For accurate diagnosis of a disease, the biomarker needs to be detected in very low concentrations. Hepatitis B surface antigen (HBsAg) is one such biomarker that can be used to efficiently detect Hepatitis B, which is one of the major diseases in need of improvement in its detection methods. It causes the inflammation of liver called cirrhosis or hepatocellular carcinoma which ultimately leads to death.

The method most commonly used in diagnostic centres for HBsAg detection is chemiluminescence immunoassay, with a detection limit as low as 0.05 ng/ml. However, there is a possibility of shift in the trend of the detection method used, with research on mass-sensitive sensors gaining ground. Of the various mass-sensitive label-free sensors developed, the surface acoustic wave (SAW) based sensors have shown great promise in the recent years for detection of biomolecules. Numerous advantages are offered by SAW sensors, of which portability, availability of multiplexed detection and electrical readout are a few.

In this work, we present a SAW-based dual delay line immuno-biosensor for successful in vitro detection of HBsAg. The device works in dual delay line configuration, with one delay line used for the measurement of the sample and the other for reference. As such, the effect of common factors like noise and humidity on the output characteristic of the system is avoided. The reason for choosing a delay line configuration is that the space between the input and output electrodes can be used as the sensing area. The work is based on numerical simulation of the device using a finite element analysis tool, and its design and fabrication for optimum performance. Devices with three different interdigitated electrode widths are fabricated on two different piezoelectric substrates. The recombinant antibody used for the capture of the target biomolecule, Hepatitis B Surface Antigen is produced. The immobilization of the antibody to the sensing surface is achieved using a linker molecule. Samples of HBsAg of varying concentrations (0.0818 IU/ml to 818000 IU/ml) were used for measurements, whereby the detection of HBsAg in the sample was confirmed by the change in S_{21} parameter of the system in real-time whenever the antigen-antibody reaction took place on the system platform. The sensitivity and selectivity of our proposed piezoelectric device are remarkable for liquid medium detection. A limit of detection, as low as 0.139 IU/ml is achieved. Also, a comparison has been made among the six devices, and a label-free detection method has been proposed.

Contents

List of Figures

List of Tables

List of Acronyms

AFM	Atomic Force Microscopy
BAW	Bulk Acoustic Wave
bp	Base pair
BNC	Bayonet Neill–Concelman
BSA	Bovine Serum Albumin
DNA	Deoxyribonucleic acid
EDC	1-ethyl-3-(3-dimethylamino-propyl)carbodiimide
EDTA	Ethylene Diamine Tetraacetic Acid
ELISA	Enzyme-linked immunosorbent assay
FESEM	Field Emission Scanning Electron Microscopy
FE	Finite Element
FEM	Finite Element Method
ATR-FTIR	Attenuated total reflection Fourier-Transform Infrared spectroscopy
HBsAg	Hepatitis B Surface Antigen
HBV	Hepatitis B Virus
HMDS	Hexamethyldisilazane
HRP	Horseradish Peroxidase
IDT	Inter-digitated Transducer
IPTG	Isopropyl β-D-thiogalactopyranoside
k_D	Dissociation rate constant
kDa	Kilodalton
LB	Luria-Bertani
$LiNbO_3$	Lithium Niobate
$LiTaO_3$	Lithium Tantalate
MBP	Maltose Binding Protein
NHS	N-hydroxysuccinimide
PMSF	Phenylmethylsulfonyl Fluoride
OPD	O-Phenylenediamine Dihydrochloride

PBS	Phosphate Buffered Saline
PCR	Polymerase Chain Reaction
RDT	Receptor-binding domain of Diphtheria Toxin
RT	Room Temperature
SAW	Surface Acoustic Wave
scFv	Single chain variable fragment
SDS-PAGE	Sodium Dodecyl Sulfate Polyacrylamide Gel Electrophoresis
SH	Shear Horizontal
SMA	SubMiniature version A
SPR	Surface Plasmon Resonance
SV	Shear Vertical
STW	Surface Transverse Wave
TCD	Temperature Coefficient of Delay
VNA	Vector Network Analyzer

Chapter 1

Introduction and Literature Survey

1.1 Introduction

THE past few decades have witnessed vast advancements in electronic devices for use in the field of biosensing. With rapid advancements in sensor technology, efficient detection of diseases like diabetes and cancer has become possible. Although high sensitivity has been achieved for detecting certain diseases owing to extensive research, there are quite a few diseases that still require attention in terms of fast and reliable detection. For this purpose, a lot of researchers are looking into efficient ways for the use of different types of electronic devices as biosensors. Out of many such devices, mass sensitive devices like microcantilevers and surface-acoustic wave (SAW) based devices are gaining ground. SAW sensors are sensitive to both mass and elastic constants. They are shown to be extremely useful for the analysis of both small and large molecules as well as whole cells interacting with an immobilized binding molecule. The output signal gives information about the pure mass loading, intrinsic properties of bound materials, or viscoelastic effects like structural rearrangements. In this thesis, we will look into the prospects of using a SAW device for the detection of a clinical biomolecule: hepatitis B surface antigen (HBsAg).

This thesis highlights the attempt that has been made to develop a point of care surface acoustic wave device using a recombinant antibody for hepatitis detection. It can be used as an alternative to chemiluminiscense assays, which are conventionally employed for such detection. The disadvantages of the conventionally used assays are that they are costly, time-consuming and require a lot of expertise in handling. Moreover, they cannot be used as point of care diagnostic devices, which enable quick detection. Employing electronic systems for disease detection could open new avenues for future applications not only for Hepatitis B, but numerous other diseases which are in need of early detection. Rapid diagnostics and point of care systems is what can contribute to the advancement of detection methods for early diagnosis of numerous diseases, and the current work has widespread application potential in this field.

1.2 Literature Survey

1.2.1 Hepatitis B

There are a large number of diseases which require urgent attention in terms of easy and fast detection methods. One such disease is Hepatitis B, which is in need of improvement in its detection methods. It causes the inflammation of the liver, and the patient eventually develops cirrhosis, end-stage liver disease or hepatocellular carcinoma, leading to death [1] . Hepatitis B virus (HBV) has infected more than 300 million people worldwide and over 2,50,000 people die annually [2]. HBV is a DNA virus, which is a member of the Hepadnaviridae family [3], and its structure is shown in Figure 1.1.

Serological and virological markers of HBV infection include hepatitis B surface antigen (HBsAg), Antibody to surface antigen (Anti-HBs), Antibody to hepatitis B core antigen, Anti-HBcAg(IgM), Antibody to hepatitis B core antigen, Anti-HBcAg(IgG), hepatitis B e antigen (HBeAg), Antibody to e antigen (Anti-HBe) and HBV DNA [4, 5]. Symptoms of hepatitis B can be nausea, abdominal pain, vomiting, fever, jaundice, dark urine and changes in stool colour [3].

HBsAg is the surface antigen of the HBV and the first marker to appear in the serum following infection. It is present on the envelope protein of HBV virion [4]. It has

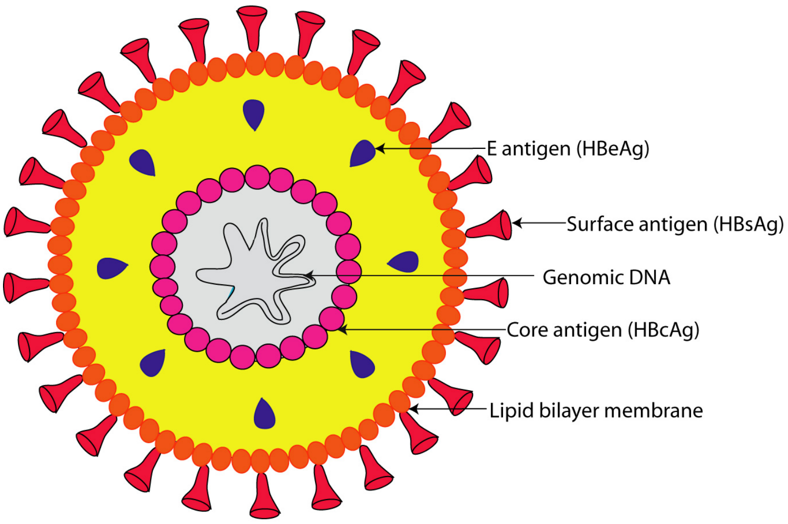

FIGURE 1.1: Structure of Hepatitis B virus (HBV)

been reported that HBsAg carriers have manifold increased chances of developing PHC (Primary Hepatocellular Carcinoma) than HBsAg negative individuals occupying the same geographical region [6]. In many cases, the immune system of the person affected with HBV clears off HBsAg completely from the body. Only in some patients, it develops into a chronic infection. Usually, a serum sample from the patient is used for detection. If detection is negative, HBV infection is ruled out. But if positive, the patient is infected with HBV. A repeat test after six months determines if the infection has resolved or is chronic. The detection period for HBsAg in the serum is different for acute and chronic infections. For acute infection, HBsAg can be detectable between 2 to 12 weeks, while the presence of HBsAg for more than six months indicates the chronic infection [1, 2, 4].

1.2.2 Current Methods for detection of HBsAg

The traditional methods adopted by diagnostic centres for HBsAg detection include chemiluminescence immunoassay, electrochemical immunoassay, polymerase chain reaction, enzyme-linked immunosorbent assays (ELISA) and PCR assays. These methods are both time-consuming and expensive.

All immunoassays use the specific antigen-antibody interaction for analytic purposes. Chemiluminescent immunoassay is a technique in which the label, or indicator, of the antigen-antibody interaction, is a luminescent molecule. This molecule may be luminophore markers or enzyme markers. The electrochemical assay uses the same principle of antigen-antibody interaction, but it is a solid phase system, with the antigen-antibody reaction and electrochemical detection occurring in the same device. ELISA, a very reliable immunoassay, uses various antigen-antibody combinations. It always includes an enzyme-labeled antigen or antibody, and enzyme activity is measured colorimetrically by using a substrate that changes color when modified by the enzyme. The light absorption of the product formed after substrate addition is measured. PCR assays, when used for immunosensing, involves the specificity of an ELISA with signal amplification of polymerase chain reaction.

The method most commonly used for HBsAg detection is chemiluminescence immunoassay, with a detection limit as low as 0.05 IU/ml [7]. Both antigen and antibody-based assays are used for the diagnosis of HBV infection [8–14]. Attempts to detect HBsAg with novel techniques have been tried by a lot of researchers. In 2005, Valanne *et al.* [8] developed a fluorescent nanoparticle label-based rapid and sensitive HBsAg immunoassay. An immunochromatographic assay for the detection of hepatitis B surface antigen (HBsAg) was developed using Fe_3O_4 nanoparticles as signal materials by Oh *et al.* [14] in 2014. A rapid diagnostic test (RDT) based on an immunochromatographic test developed by Chevaliez *et al.* [15] in 2014 also showed remarkable results. Such outstanding developments in research led way to the availability of a large number of commercially available kits for detection of HBsAg, which are shown in Table 1.1.

TABLE 1.1: Commercial kits available for HBsAg detection

Name of the kit (Manufacturer)	**Principle of detection**	**Limit of detection**	**Single use/ Multiple use**	**Ref**
Advia Centaur HBsAg (Bayer)	Magnetic microparticle enzyme immunoassay	0.12 ng/ml	Multiple	[16]
Monolisa HBsAg Ultra (Bio-Rad)	Direct sandwich chemiluminescence immunoassay	0.08 ng/ml	Multiple	[17]

Continued on next page

Table 1.1 – continued from previous page

Name of the kit (Manufacturer)	**Principle of detection**	**Limit of detection**	**Single use/ Multiple use**	**Ref**
Liaison HBsAg (Dia-Sorin)	Direct sandwich chemiluminescence immunoassay	0.050 IU/mL	Multiple	[18]
Vikia HBsAg Ultra (bioMe´rieux)	Enzyme immunoassay	0.09 ng/ml	Single	[19]
AxSYM HBsAg V2 (Abbott)	Enzyme immunoassay	0.16 ng/ml	Multiple	[20]
ICT-CLEIA	Semiautomated immune complex transfer chemiluminescence enzyme immunoassay	0.2 mIU/mL	Multiple	[21]
Architect HBsAg QT assay (Abbott)	Chemiluminescent microparticle immunoassay (CMIA)	0.130 IU/mL	Multiple	[22]
Advanced Quality One Step HBsAg Test (InTec)	Colloidal gold enhanced immunochromatographic assay	0.5ng/ml	Single	[23]
CobasAmpliprep/ CobasTaqMan assay (Cobas)	Molecular techniques	6.25 IU/mL	Single	[24]
Determine (Abott)	In vitro qualitative immunoassay	95.16%	Single	[25]

1.2.3 Mass-sensitive Sensors

Although the use of chemical and optical methods have continued for a long time now, there is a possibility of shift in the trend of the detection method used as research on mass-sensitive sensors is gaining ground and favourable results have been obtained [9–12]. Dominant among the mass sensitive sensors are cantilevers and surface acoustic wave (SAW) based sensors. To highlight the major developments in this field, a few honourable mentions can be made from the historical background of mass-sensitive sensors. Cantilevers were used by Moulin *et al.* [26] in 2000 to differentiate lipoproteins and their oxidised form by measuring the surface stress involved. The use of affinity cantilevers for applications related to cardiac diagnostics by Rao *et al.* [27] in 2007 was another groundbreaking work in this field. By 2012, diverse applications like detection of *E. coli*, *B. anthracis*, *B. subtilis*, Human Anti-IgG, streptavidin, egg albumin, BSA and HBV DNA were accomplished [28]. Various geometry optimisations and integrations with other technologies were also done to improve the efficiency of microcantilevers [29–31], but it still faced issues related to selectivity. The other mass-sensitive sensor that came to the forefront was the SAW device. Long after Lord Rayleigh proved in 1885 that mechanical waves similar to water waves travel on the surface of a solid, devices supporting these acoustic waves came to be used for sensing applications since the late 20th century. The applications of SAW sensors vary from chemical analysis, film detection, gas sensor, pressure sensor and temperature sensor [32–35].

1.2.4 Surface Acoustic Wave Devices

In this section, we summarize the basics of piezoelectricity, SAW generation, interdigitated transducers and types of SAW devices.

Piezoelectricity

The term "Piezoelectricity" is derived from the Greek word "piezo", which means pressure, thus referring to electricity generated by means of pressure. The name was first proposed by Hankel in 1881, while the phenomenon was discovered by Pierre and Jacques

Curie in 1880 [36]. Piezoelectric crystal consists of dipoles arranged in a particular fashion, where the centre of gravities of both the positive and negative charges are located and neutralized at the same point. When an external force is exerted on the crystal surface, the center of gravities shift due to the applied force, and it results in the development of charges along the surface [37], as shown in Figure 1.2. The reverse effect is called converse piezoelectricity. When a voltage is applied to the surface of a piezoelectric material, deformation of the material, either compression or elongation occurs. The polarity of the voltage signal determines whether the material becomes compressed or elongated.

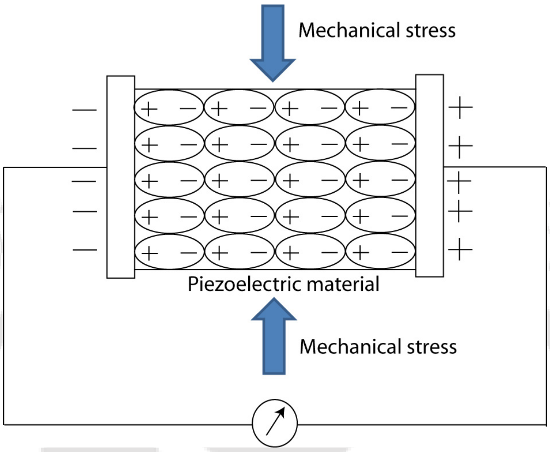

FIGURE 1.2: Transformation of mechanical stress into electrical energy

Surface Acoustic Wave and its Generation

Surface acoustic waves are elastic waves that travel along the surface of the piezoelectric substrate, typically within 1-2 wavelengths from the surface, and is sensitive to any modifications on its path of propagation. Anisotropic substrates like lithium niobate, lithium tantalate, quartz and langasite are the commonly used substrates for SAW generation. Parameters like crystal orientation, SAW velocity (v), coupling coefficient (k^2), permittivity and temperature coefficient of delay (TCD) determine the generation of SAW in these substrates [38]. Table 1.2 below lists the properties of commonly used substrates [38].

Table 1.2: Table for comparison of piezoelectric substrates for SAW generation

Material	**SAW Velocity (m/s)**	**Δv/v (%)**	**TCD (ppm/°C)**
$LiNbO_3$,Y-Z	3488	2.4	94
$LiNbO_3$, 128°Y-X	3979	2.7	75
Quartz, SiO_2, ST-X (42.75°Y-X)	3159	0.06	0
$LiTaO_3$ X-112°Y	3300	0.35	18
$LiNbO_3$, 64°Y-X	4742	5.5	80
$LiNbO_3$, 41°Y-X	4792	8.5	80
$LiTaO_3$, 36°Y-X	4112	2.4	32
SiO_2/$LiNbO_3$, 128°Y-X	3990	3	0

In 1885, Lord Rayleigh put forward the theory that mechanical waves similar to water waves travel on the surface of a solid and these waves came to be known as Rayleigh waves [38]. There are two types of acoustic waves that exist based on how particles move respective to their equilibrium position [39]:

1. Longitudinal wave, in which the displacement is parallel to the propagation direction.
2. Shear wave, where particles move orthogonally to the direction of propagation. Shear waves can again be classified into two, shear vertical (SV) wave and shear horizontal (SH) wave.

Interdigitated Transducer (IDT)

The heart of a SAW device is the interdigitated transducer, or IDT. White and Voltmer in 1965 proposed the idea of the first IDT, which went on to revolutionize the applications of SAW devices. An IDT is nothing but a pair of comb structures arranged in alternating fashion, which acts as the port for the generation and detection of SAW [38].

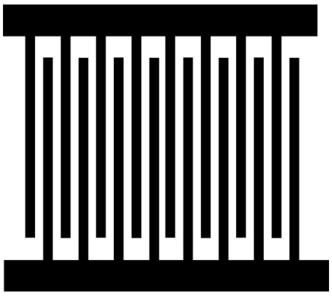

FIGURE 1.3: Structure of IDT

Application of a continuous periodic voltage to the IDT generates surface perturbations due to the converse piezoelectric effect, and are enhanced by the consecutive pair of electrodes, thus launching a surface wave perpendicular to IDT structure. IDT is generally bidirectional, i.e., it generates the surface wave of equal amplitude in both the directions and its efficiency is maximized when the input and output IDTs are electrically matched.

Based on the application, the IDT structure can be modified to obtain different devices such as band pass filters, resonator, oscillator, sensor, etc [37]. SAW devices generate and detect acoustic waves by the transduction of electrical energy to mechanical energy via the IDTs fabricated on the surface of a piezoelectric material.

Types of SAW Devices

SAW devices can be broadly classified into two types:

1. Resonators: The resonators are either one-port or two-port devices, having either one or two IDTs deposited on a piezoelectric substrate, between a pair of reflection gratings, as shown in Figure 1.4 [37]. In a resonator, the acoustic waves are launched within a resonant cavity, thus causing the signal to be reflected back to the generating IDTs.

2. Delay Lines: Delay-lines are two-port devices. It consists of two IDTs, one that generates the wave by converting the applied electrical signal to an acoustic wave, and the other that detects the wave and converts it back to an electrical signal. The space between the IDTs, across which the surface acoustic wave will propagate, is

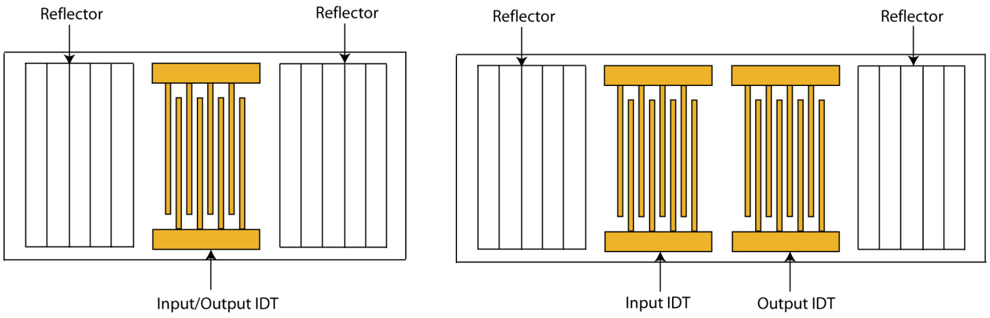

(A) (B)

Figure 1.4: (A) One-port, and (B) Two-port SAW resonator

known as the delay line. The schematic of a delay line configuration of the SAW device is shown in Fig.1.5

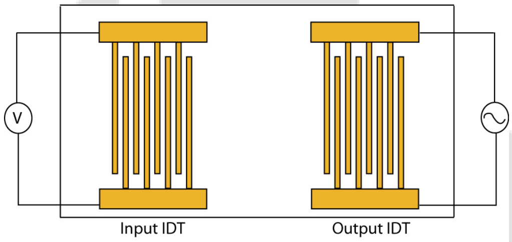

Figure 1.5: SAW delay line

1.2.5 Surface Acoustic Wave (SAW) Sensors

As discussed in the previous section, SAW devices use piezoelectric materials to generate an acoustic wave. Coupling to any medium contacting the surface strongly affects the velocity and/or amplitude of the wave [38]. The factors affecting the increase in sensitivity of the sensor are the substrate material, velocity of SAW, the transducer geometry, surface modifications and the presence or absence of a guiding layer. Confinement of the wave's energy near the surface makes them sensitive to surface changes and perturbations, thus making them ideal for sensing applications [39]. The earliest uses of SAW devices as sensors were to detect changes in pressure and temperature [40–42]. Wohltjen was one of the pioneers in this field, reporting the use of SAW sensors for gas sensing. After this, Rayleigh SAW devices have been used in numerous sensing applications, as varied as dew-point sensing, humidity sensing and chemical vapour sensing [43–47]. In

1983, Roerderer et al. did immunosensing in liquids to detect the binding of goat anti-human IgG and human IgG using a Rayleigh SAW wave [48]. But they suggested that Rayleigh waves are not suitable for liquid sensing as it showed poor sensitivity and limit of detection. As applications like bio-sensing typically require detection in a liquid environment, it is here that Shear Horizontal Surface Acoustic Wave generating substrates came into play. The use of SAW devices for biosensing purposes is discussed in detail in the next section.

1.2.6 Surface Acoustic Wave (SAW) Biosensors

Biosensors are a result of the multidisciplinary adventure between physics, biochemistry, surface chemistry, materials science and electronics. It is one of the fastest-growing and most impactful fields in global scientific research. One of the hallmark features of this field is early detection, which remains the holy grail in the fight against medical diagnostics. Recent advances in medical diagnostics require the development of platforms capable of early detection of disease-causing agents. Hence, the need of the hour is point-of-care (POC) devices that can mimic the in-vivo situations on in-vitro platforms. SAW biosensors allow the label-free detection of an antigen in real-time by monitoring changes in frequency and amplitude of a wave that results from changes in the physiochemical properties (mass density, temperature, viscosity, pH, etc.) in the area where sensing takes place. Acoustic wave bio-sensing by direct analyte detection was done using quartz crystal microbalances (QCMs) as early as 1988 [49]. However, these devices were operated at frequencies as low as 50 MHz. By Saurbrey's equation [49], this in turn meant low sensitivity. Hence, to increase sensor sensitivity, attempts were made to increase the operating frequency. Focus then shifted to Acoustic Plate Mode (APM) sensors that relied on the transmission of bulk waves to operate in a liquid environment [43]. More advancements in the field of acoustic devices led to SAW resonators and delay lines to be used for detection of microorganisms and pathogens for use in medicine, food safety and environmental monitoring [50–81]. In particular, SAW sensors have been used to detect bacteria [55, 80], DNA [65, 79], viruses [81] and cancer biomarkers. In 1997, Harding *et al.* [82] utilized a love wave acoustic device to monitor antigen-antibody interactions in aqueous environments. The love wave sensor was robust, reliable and reusable. Another biosensor designed by Jun Kondoh *et al.* [77] had an urease membrane immobilised on the surface to detect any pH change associated with enzyme reaction. In 2003, Kourosh Kalantar-Zadeh et.al. [78] developed a novel Love mode surface acoustic wave based immunosensor based on ZnO/90° rotated ST-cut quartz crystal structures and it was possible to detect IgG concentrations as low as 500 pg/ml. Darren W. Branch *et al.* [55], in 2004, achieved detection of a *Bacillus anthracis* simulant using love-wave biosensors on 36°YX $LiTaO_3$. Their work demonstrated that Love-wave biosensors are promising for low-level detection for whole-cell biological pathogens. In the same year, Marc D. Schlensog *et al.* [55] designed a biosensor array by coupling aptamers to the surface of a SAW sensor chip, that demonstrated the versatile applicability of the sensor by immobilizing single-stranded DNA (ssDNA) for the detection of the corresponding counter-strand. In 2009, Dae-Sik Lee *et al.* [66] fabricated a SAW-based immunosensing device, that employed biospecific interaction between a 6-(2,4-dinitrophenyl) aminohexanoic acid (DNP) antigen and its antibody, demonstrating the shifts of resonant frequencies on SAW immunosensing device. In 2012, Lothar Schmid *et al.* [83] demonstrated a novel SAW-driven closed PDMS flow chamber driven by surface acoustic waves. It successfully pumped a red blood cell suspension at a physiological rate of 60 beats/min. F. Di Pietrantonio *et al.* [84] in 2013 presented an array of biosensors for vapour phase detection of odorant molecules based on surface acoustic wave (SAW) resonators coated with odorant-binding proteins (OBPs). The sensing capabilities of three different OBPs, as sensitive layers for SAW devices, are studied and compared. Another major application of SAW sensors in biosensing was seen when in 2015, Marina Cole *et al.* [85] designed a novel two-port resonator-based shear-horizontal surface acoustic wave (SH-SAW) sensor, with which they achieved the successful identification of six different tastes: saltiness, sweetness, sourness, bitterness, umami and metallic tastes. In 2016, Young Wook Kim *et al.* [86] achieved the detection of biofilms using a SAW sensor that monitors the total biomass by measuring the resonant frequency of the system. Other novel approaches in SAW device geometry has been achieved by researchers, utilisation of microcavities to minimise insertion loss [87–93] and integration with microfluidics [94–99] being some of them.

1.2.7 SAW Sensors Employing Shear Horizontal Waves

Shear Horizontal-SAW (SH-SAW) devices provide an attractive platform for the design of biosensors that operate in a liquid medium. As SH-SAW devices yield shear horizontal surface waves instead of the Rayleigh waves, hence these devices operate more efficiently in liquid media, where propagation at the solid/liquid interface can be achieved with minimal energy losses. The reason Rayleigh waves are unsuitable for liquid sensing is that its longitudinal component generates a compression wave which releases energy into the fluid, consequently causing a loss of energy. In order to successfully conduct sensing in liquids, a piezoelectric material with the appropriate crystal cut that supports SH-SAWs must be selected. Of the materials listed in Table 1.2, 41°YX $LiNbO_3$ and 36°YX $LiTaO_3$ are suitable for the generation of SH-SAW, and the wave propagates with minimal attenuation when in contact with liquid.

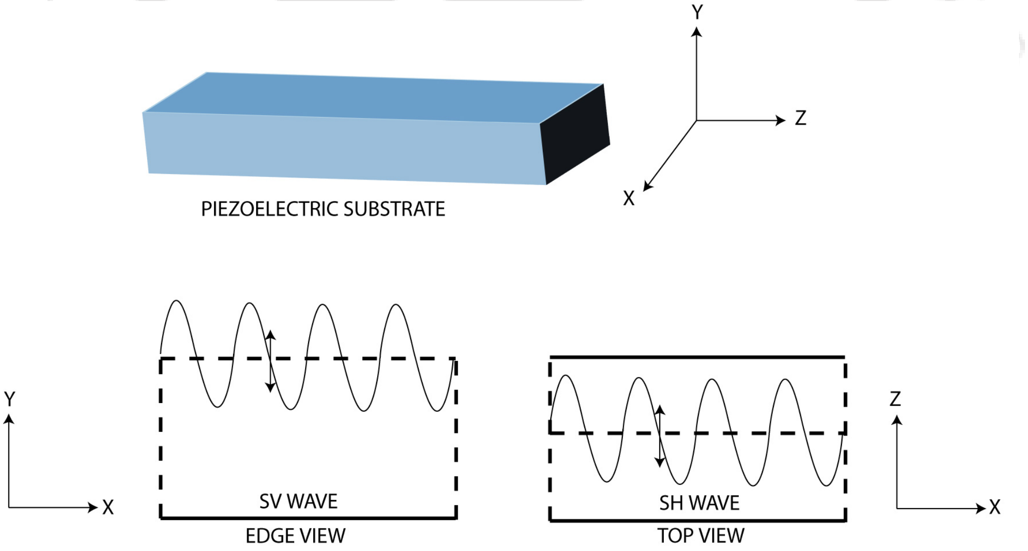

FIGURE 1.6: Difference between SV and SH waves

The use of SH-SAW delay lines is found extensively in the field of biosensing. In 1993, Jun Kondoh *et al.* [77] described a delay line biosensor to detect an enzyme reaction in liquid using SH-SAW. Later, Y. Kwon *et al.* [100] detected protein molecules in liquid solutions applying a particular antibody thin film on the delay line of transverse SAW devices. In 2004, Eric Berkenpas *et al.* [57] reported an SH SAW delay line designed and fabricated on langasite. The biotinylated sensor was exposed sequentially to biotin-binding deglycosylated avidin, biotin-modified rabbit IgG, and goat anti-rabbit IgG antibody. As each protein was bound to the sensing surface, marked changes in the delay line phase were recorded. The following year, the successful development of an SH-SAW sensor for the detection of DNA hybridization was done by Youngjune Hur *et al.* [79]. Taste sensors and sensors to detect whole *E. coli* bacteria were the next successful use of SH-SAW delay lines for biological sensing [80, 101]. The year 2008 saw further development in this field as M. Bisoffi et.al. [81] detected viral bioagents the SAW biosensor was capable of selectively detecting SNV agents in complex solutions, such as naturally occurring bodies of water without analyte pre-processing. Another novel high sensitivity ZnO/SiO_2/Si surface acoustic wave (SAW) biosensor working in delay line configuration for the detection of interleukin-6 (IL-6) was reported by Soumya Krishnamoorthy *et al.* [82] in 2008. Again, in 2016, F. Di Pietrantonio *et al.* [102] achieved rapid and specific detection of D-serine, an amino acid that has an important role in the regulation of N-methyl-d-aspartate (NMDA) signalling in the central nervous system. It had more advantages respect to existing methods of detection and in terms of speed and simplicity of analysis. Since the presence of negative control is essential for measurements related to detection, a study was done into the possibility of dual delay line devices to be used in our work. In 2005, J. Hechner *et al.* [103] designed a SAW dual delay line on 41°YX $LiNbO_3$ with an SiO_2 protective layer and presented the results of liquid viscosity and conductivity measurements. Najla Fourati *et al.* [65] in 2009 had immobilized a 27-mer DNA-probes on the SH-SAW gold sensitive layer and subsequent hybridization was investigated with 36-mer complementary DNA-targets. Apart from these, SAW dual delay lines have also been used for gas as well as humidity sensing.

From this section, we can conclude that SAW sensors are sensitive to both mass and elastic constants. They are shown to be extremely useful for the analysis of both small and large molecules as well as whole cells interacting with an immobilized binding molecule. The output signal gives information about the pure mass loading, intrinsic properties of bound materials, or viscoelastic effects like structural rearrangements. The technology of SAW devices is compatible with planar integrated circuit technology, and hence have a promising future in the field of biosensors. Table 1.3 compares the currently existing biosensors based on SAW devices.

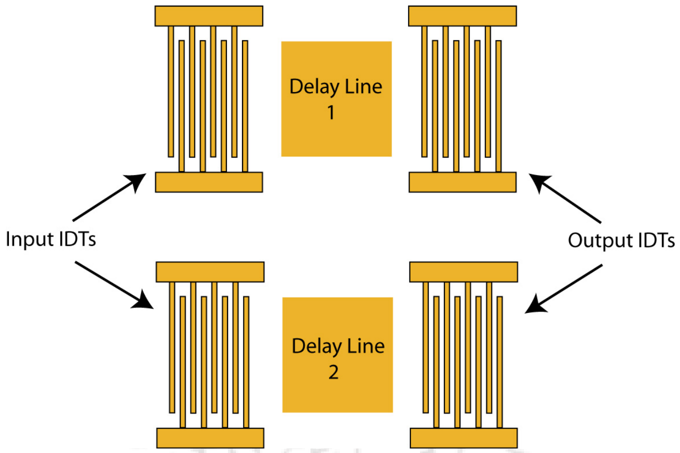

FIGURE 1.7: Schematic of SAW Dual delay line

TABLE 1.3: Table for comparison of existing biosensors based on SAW devices

Type of SAW Sensor	**Substrate material**	**Target**	**Operating Frequency (MHz)**	**LoD**	**Ref**
Love Wave Immunosensor ; Dual delay line	ST-cut quartz	Anti-sheep IgG	110	380 cm^{2}g^{-1}	[76]
SH-SAW ; Delay line	36°YX $LiTaO_3$	Urea (pH change)	50.8	3 µM	[77]
Guided SH-SAW; Dual delay line	36°YX $LiTaO_3$	Organic compounds	103	20 pg/mm^2	[53]
Love mode immunosensor; Delay line	ZnO layer over ST-cut quartz	Anti-rat IgG	89	500 pg/ml	[78]
Love-wave biosensor; Delay-line	36°YX cut $LiTaO_3$	Bacillus anthracis	103	1.0–2.0 ng/cm^2	[55]
Love-wave biosensor array	ST-cut quartz	Human thrombin	142	75 pg/cm^2	[56]

Continued on next page

Table 1.3 – continued from previous page

Type of SAW Sensor	Substrate material	Target	Operating Frequency (MHz)	LoD	Ref
Pure SH-SAW Biosensor; Delay line	$La_3Ga_5SiO_{14}$ (Langasite)	Rabbit IgG	92	25 nM	[57]
SH-SAW ; Dual delay line	36°YX $LiTaO_3$	DNA	100	1.55 ng/ml/Hz	[79]
Love wave immunosensor; Delay line	AT-cut quartz	E. coli bacteria	118	106 bacteria/ml	[80]
Love Wave Immunosensor ; Dual delay line	ST-cut quartz	Anti-sheep IgG	110	380 cm^2g^{-1}	[76]
SH-SAW biosensor	36°YX $LiTaO_3$	Coxsackie virus B4	325	3.6×10^6 viruses/ μl	[81]
SH-SAW; Delay line	ZnO thin films grown on SiO_2	Interleukin-6	747.7	0.165 fg/ml	[82]
SH-SAW; Dual delay line	36°YX cut $LiTaO_3$	DNA	104	6.3 Hz/ng	[65]
SAW immunosensor; Delay line	Nanocrystalline ZnO Film on Si	6-(2,4-DNP) amino-hexanoic acid	176	20 ng/ml	[66]
Love wave immunosensor; Delay line	ZnO/36°YX cut $LiTaO_3$	Human immuno-globulin G	130	2 μg/ml	[104]

Continued on next page

Table 1.3 – continued from previous page

Type of SAW Sensor	Substrate material	Target	Operating Frequency (MHz)	LoD	Ref
SAW-driven chamber; Microfluidic setup	128°Y-Cut $LiNbO_3$	Red blood cell	142	60 beats/min	[83]
Immunosensor array; SAW resonator	Quartz (ST-cut)	Odorant-binding proteins	392	9.2 Hz/ppm	[84]
SAW electronic tongue	36°YX cut $LiTaO_3$	6 different taste solutions	434	0.1 M	[85]
SAW sensor using biofilm; Delay line	ZnO film	*E. coli*	400	166 pg	[86]

1.2.8 Functionalisation of Sensor Surface

Surface morphology can have a profound effect on acoustic wave propagation and subsequently on sensor properties. Selectivity is a parameter that decides the performance of a sensor. To achieve high selectivity, the device surface needs to be properly functionalized for protein immobilization. There are numerous ways in which a sensor surface can be functionalized. In 1992, Folker *et al.* [105] did a study on self-assembled monolayers of alkanethiols on gold. They also discussed in detail the effect of short and long-chain constituents. J.Spinke *et al.* [106] used sulfur-based molecules containing biotin and hydroxyl groups to create a wide variety of self-assembled monolayers on gold surfaces. Surface plasmon resonance was used to study in situ the binding of streptavidin to these monolayers from solution. The self-assembled monolayers allowed a high degree of control over the surface properties. In 2002, Peng Jiang et.al.

[107] studied in detail about the growth of monodispersed PbS nanoparticles on self-assembled monolayers of 11-Mercaptoundecanoic Acid on Au(111) substrate. They suggested that the arrangement of the PbS nanoparticles reflects the structure of the thiol outer surface. Again, Tlili *et al.* [108] designed the steps of surface functionalization to develop a robust biosensor based on quartz crystal microbalance technique for antigen detection, thus establishing the fact that mass-based techniques could be used for antigen detection. The gold electrode was functionalized with the self-assembled monolayer technique. The modified surface was activated with N-hydroxysuccinimide (NHS) and 1-(3-(dimethylamino)propyl)-3-ethylcarbodimide hydrochloride (EDC) cross-linker for antibody coupling. The non-specific sites were blocked with bovine serum albumin molecules. Different concentrations of antigen could be detected with good reversibility in real-time. J. Christopher Love *et al.* [109] in 2005 did an exclusive study and gave important insights into the formation, patterning, functionalization and applications of SAMs. In the same year, Francesca Cecchet *et al.* [110] investigated quantitatively the mechanism of electron transfer (ET) through densely packed and well-ordered SAMs of 11-mercaptoundecanoic acid on gold. In 2007, E. Briand *et al.* [111] did a combined FT-RAIRS, AFM and QCM investigation into the functionalisation of gold surfaces with thiolate SAMs. One interesting finding of their work is that the lowest amount of antibody was immobilised on the MUA-containing base layers but their bioefficiency was better. In 2008, Dae Jung Kim *et al.* [112] devised a simple method for the removal of thiols on gold surfaces using an $NH_4OH–H_2O_2–H_2O$ solution. Zhengjian *et al.* [113] in 2009 showed how 16-mercaptohexadecanoic acid (MHA) film and rat anti-human IgG protein monolayer were fabricated on gold substrates using the SAM method. The surface of the gold substrate was modified with a long carbon chain thiol, namely, 16-mercaptohexadecanoic acid (MHA), because sulfur-containing molecules (thiols, sulfides and disulfides) have a strong affinity for gold and interact with it, yielding an Au–S bond. He again probed the specific interaction forces between Human IgG and Rat Anti-Human IgG by SAM and Atomic Force Microscopy [114]. In 2011, Myungok Yoon *et al.* [115] established that orientation of antibody was retained by protecting the antigen-binding site of the antibody prior to immobilization to ω-functionalized mixed SAM of 12-mercaptododecanoic acid and 1-heptanethiol. The number of immobilization bonds

formed between each antigen-binding site protected antibody molecule and the solid surface was controlled by optimizing the mole fraction of the activated carboxyl group of the linker molecules in the mixed SAM. Another important study done by P. Bhadra *et al.* [116] in 2015 looked into n-alkanethiol chain lengths on a gold-coated surface and their effect on antibody-antigen binding efficiency. SAMs of different chain lengths of n-alkanethiol were covalently immobilized on 1 cm X 1 cm gold-coated surfaces to form well-packed monolayers. Alkanethiol with chain lengths, n = 2, 3 has less antibody immobilized on SAM surface due to the loosely packed nature of SAM. Antigen estimation revealed that antigen-binding efficiency greatly increased upto n = 11 SAM. Beyond n = 11, no increase in antigen binding was observed.

1.2.9 Outcome of Literature Survey

1. Of the various diseases that are in need of urgent attention in terms of point of care detection, Hepatitis B is one of the most prominent. To develop an efficient immunobiosensor, Hepatitis B Surface Antigen (HBsAg) will be the target molecule of choice.

2. To avoid the complexity of charge-based detection, the requirement was an in-vitro platform that can mimic the in-vivo interactions between the target antigen and its corresponding antibody. Hence, a mass-based sensor working in SAW delay line configuration was used for detection.

3. The quality of detection in liquid medium is affected by insertion loss, which is taken care of by shear-horizontal SAW. Hence the substrates chosen for SH-SAW generation are 41°YX $LiNbO_3$ and 36°YX $LiTaO_3$.

4. Surface functionalisation plays a crucial role in antibody immobilisation on the sensor surface. A thin gold film is required on the sensing surface so that an 11-MUA linker molecule can be used for the attachment of the anti-HBsAg antibody by the EDC-NHS method.

1.3 Objectives of the Work

Based on the literature survey, the problem formulation has been done and the following objectives have been set for the thesis work:

1. Design and finite element simulation of the SAW delay line using the COMSOL Multiphysics Tool.
2. Fabrication and characterization of SAW delay line devices.
3. Production of Anti-HBsAg antibody as recombinant scFv.
4. Immobilisation of the recombinant scFv on the sensing surface.
5. Detection of Hepatitis B Surface Antigen (HBsAg) using the SAW dual delay line.

1.4 Novelty of the Work

The succesful development of a point of care Surface Acoustic Wave (SAW) based system for in-vitro sensing of HBsAg is encompassed in the work described in this thesis. It is capable of detecting HBsAg, both in PBS and human serum. A method is also described for the regeneration of the sensing layer, using a buffer of a particular pH, thus introducing a method to reduce the cost of operation of the device.

1.5 Thesis Outline

The thesis has been organized into 7 chapters, and their contents are briefly outlined as follows:

Chapter 1 introduces the objective of the thesis work, which is to develop a surface acoustic wave device, working in a dual delay line configuration for the efficient detection of Hepatitis B disease. The motivation behind the objective and the brief summary of the literature survey are presented. The scope and salient features of the work done have been discussed.

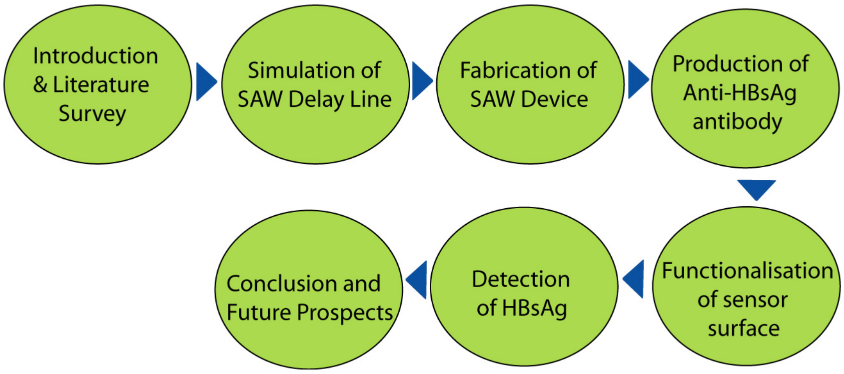

In Chapter 2, the design and simulation of a SAW delay line are described which was done using finite element analysis tool COMSOL Multiphysics. Six different devices were simulated, varying the IDT widths and the piezoelectric substrate. Eigen value analysis under the piezoelectric devices module was implemented in order to evaluate the resonant frequencies of the structures under varying conditions. A comparison of the displacement and voltage profiles at the input and output IDTs was then done for the devices. The maximum and minimum element sizes of 20 μm and 1 μm respectively were adopted for meshing. Simulations were done to evaluate the resonant and antiresonant frequency, admittance variations and the shear horizontal wave generation for a sinusoidal input voltage. The IDT parameters like aperture and number of finger pairs were calculated using MATLAB for an optimum design. The mask layout was finally designed in Clewin software.

In Chapter 3, the results related to the fabrication and characterization of the SAW devices are shown. The fabrication was done in the National Nanofabrication Centre, IISc Bangalore. The piezoelectric substrates chosen for the generation of shear horizontal surface acoustic wave (SH-SAW) were 41°YX $LiNbO_3$ and 36°YX $LiTaO_3$. On each of these, IDTs and a sensing region made of gold metal with a chromium adhesive layer were fabricated. After successful lift-off, the devices were separated using a wafer dicing machine to get the dual delay lines, which could then be used as a reference channel and a measuring channel. The s-parameters of the devices were measured using Vector Network Analyzer, and matching networks were designed.

Chapter 4 discusses the synthesis of recombinant Anti-HBsAg. Serological markers of HBV infection include hepatitis B surface antigen (HBsAg), Antibody to surface antigen

(Anti-HBs), hepatitis B core antigen (HBcAg), Antibody to core antigen (Anti-HBc), hepatitis B e antigen (HBeAg), Antibody to e antigen (Anti-HBe) and HBV DNA. HBsAg is the first marker to appear in the blood of an infected person. To efficiently detect HBsAg in the blood of infected patients, we aim at the expression and purification of the recombinant Anti-HBsAg antibody, expressed as a fusion protein MBP-scFv.

In Chapter 5, immobilisation of the antibody on the sensing surface on the device is discussed. To achieve high selectivity, the device surface needs to be properly functionalized for protein immobilization. There are numerous ways in which a surface can be functionalized. For the proposed SAW-based sensor, 11-Mercaptoundecanoic acid was used as the linker molecule, and then the reliable EDC/NHS method was used for protein immobilisation. EDC (1-Ethyl-3-(3-dimethylaminopropyl)-carbodiimide) is a crosslinking agent used to couple carboxyl or phosphate groups to primary amines, while N-hydroxysuccinimide (NHS) increases the stability of the active ester. Mouse Anti-HBsAg antibody and the MBP-scFv was then immobilised on the sensing surface. EDX, AFM, FESEM and ATR-FTIR were done in every step, which confirmed the immobilization of Anti-HBsAg on the sensor surface.

In Chapter 6, the detection of HBsAg using functionalized devices is discussed. The s-parameters were measured for each device using a Vector Network Analyzer (VNA) and were then connected via appropriate matching circuits to obtain maximum power transfer. Out of the two delay lines, one is used as the sample channel, while the other was used as the reference channel. For the detection purpose, two different sets of immobilization were done: one with the commercially available Anti-HBsAg and the other with the recombinant Anti-HBsAg antibody. A comparison between the two was done. Apart from the sensitivity, time-based experiments were also done and successful detection of HBsAg was achieved.

Chapter 7 lists the conclusion of the research work and recommendations for future work. It contains an overview of the thesis and enlists the vital findings reported in the thesis.

Chapter 2

Finite Element Simulation of SH-SAW Delay Line

THIS chapter outlines the 3D-Finite Element simulation of a shear horizontal surface acoustic wave (SH-SAW) generating delay line. Fabrication of piezoelectric devices is crucial, owing to the brittleness of the piezoelectric substrates and sensitivity of SAW generation to parameters like crystal orientation, electrode width, and substrate thickness. As such, a thorough study of the behavior of the SAW devices using a simulation tool is beneficial to reduce the risk of wastage of resources in fabricating dysfunctional SAW devices. Also, the nature of the SAW varies, depending on the choice of piezoelectric substrates and the electrode design parameters. Hence, all six proposed devices were simulated using the simulation tool COMSOL Multiphysics. Three delay lines with Interdigitated Transducer (IDT) widths, viz. 4 μm, 8 μm and 12 μm, on two piezoelectric substrates, namely 41°YX $LiNbO_3$ and 36°YX $LiTaO_3$ were considered, giving a total of six devices. This study includes the resonant and anti-resonant frequency determination using eigenmode analysis, computation of admittance values using the frequency analysis, and the time-dependent simulation to check the generation of SH-SAW on all six devices. Finally, the aperture widths of the IDT designs are calculated for the efficient design of the IDT geometry. These parameters, obtained by FE simulation, were then used for designing the mask layout for microfabrication of the SAW devices.

2.1 Components of a SAW Delay Line

A SAW delay line consists of three main parts: the piezoelectric substrate, interdigitated transducers and a sensing film, both made of gold. These components are shown in Figure 2.1 and are discussed in detail.

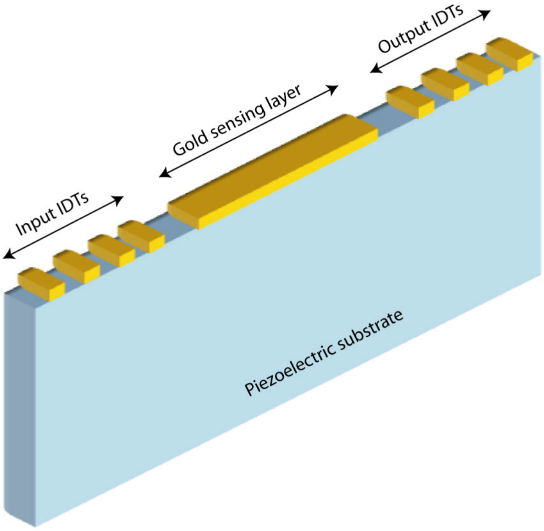

FIGURE 2.1: Components of a delay line

The main components of the SAW delay line sensor are as follows [37, 38, 117]:

1. **The piezoelectric substrate**: Piezoelectric materials are inherently anisotropic, so the properties of elastic waves are dependent upon both the cut angle and the direction of SAW propagation The main function of the substrate is to facilitate the passage of the acoustic wave. Materials with higher velocity are preferred to reduce propagation loss. The nature and frequency of the acoustic wave generated in a piezoelectric substrate is determined by the following factors:

1. Piezoelectric crystal orientation
2. Thickness of the piezoelectric substrate used
3. Geometry of the metal IDTs

Since our aim is to design a SAW delay line that will be used for detection in liquid medium, a shear-horizontal wave generating substrate is the most preferred one, due to the low losses involved. Through proper selection of the specific substrate materials, the particle displacements on the SH-SAW device can be polarised to be parallel with the sensing surface. Because there is no normal displacement on the surface, energy dissipation into the liquid is not severe. Two substrates were chosen for generating the SH-SAW, namely 41°YX $LiNbO_3$ and 36°YX $LiTaO_3$, with SAW velocity of 4379 and 4112 m/s respectively on a metallized surface. A 41°Y-cut indicates that the crystal is cut at the plane 41° rotated from the Y-plane about the X-axis. Similarly, a 36°Y-cut indicates that the crystal is cut at the plane 36° rotated from the Y-plane about the X-axis.

Another important parameter is the electromechanical coupling constant k^2, which is defined as twice the magnitude of the short-circuit velocity change, i.e.

$$k^2 = 2\frac{\Delta v}{v_\circ} \tag{2.1}$$

In physical terms, k^2 gives the fraction of the total potential energy of the wave that appears as ϕ, the potential generated at the surface by the SAW, the remainder being used to produce the elastic deformation of the piezoelectric substrate. The efficiency with which RF voltage applied to the IDT couples to the mechanical deformation depends on the piezoelectric substrate material used. 41°YX $LiNbO_3$ exhibits almost four times higher value of k^2 than 36°YX $LiTaO_3$. The temperature coefficient of delay (TCD) gives an idea of the temperature stability of the substrate. 36°YX $LiTaO_3$ shows a better temperature stability than 41°YX $LiNbO_3$. The material properties of the two substrates are shown in Table 2.1 [37, 38, 117].

TABLE 2.1: Material properties of piezoelectric substrates

Type of substrate	**Euler angles (degree)**			**SAW velocity (m/s)**	**k^2 (%)**	**TCD (ppm/°C)**
	ϕ	θ	ψ			
41°YX $LiNbO_3$	0	41	0	4379	17.2	80
36°YX $LiTaO_3$	0	36	0	4112	4.7	32

If one of the material properties can be properly modulated by the quantity to be measured, the effect of sensing can be created.

2. **Interdigitated Transducers (IDTs)**: A delay line consists of two sets of IDTs, which serve as the input and output ports for the electrical signals. An IDT consists of a pair of overlapping interspersed finger arrays, made of conducting material. The IDTs are placed at opposite ends of the piezoelectric material. The input transducer generates a spatially periodic electric field with a periodicity determined by the spacing of the adjacent electrodes. This field generates surface waves through the piezoelectric effect with maximum efficiency at frequency f_0 where the acoustic wavelength equals the periodicity, L of the transducer. Other frequencies will have reduced SAW generation efficiency due to cancellation of waves generated at one end of the transducer with those at the opposite end. The generated surface wave propagates to the output transducer. The output IDT then senses the electric fields which accompany the wave due to piezoelectric effect.

   The acoustic wavelength, λ is determined by the IDT geometry and spacing, d as shown in the following equation:

$$\lambda = 4\mathrm{d} \tag{2.2}$$

   The fundamental frequency of the device, is the frequency f_0 of the generated surface acoustic wave in a neutral environment, and is given by:

$$f_0 = \frac{v_0}{\lambda} \tag{2.3}$$

High frequency of operation results in more sensitive devices because sensitivity is proportional to square of the operation frequency. It is known that increasing the number of IDT pairs could reduce insertion loss at the centre frequency. As the number of IDTs increases, the magnitude at the center frequency increases and the bandwidth of the centre lobe decreases. However, the ripples around the centre frequency increases.

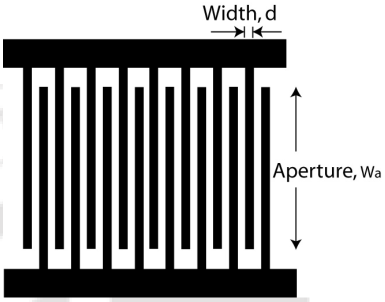

FIGURE 2.2: An IDT structure, showing the width and aperture

3. **A gold thin film**: A thin metallic film of gold can be sputter coated between the two electrodes, to be used as the sensing area. The reasons why gold was chosen are listed below:

    a. Gold is least reactive towards other elements

    b. Because of its electrical conductivity, it enhances the electromagnetic feedthrough between the transucers.

    c. Provides the necessary foundation for the thiol-surface chemistry used to attach biomolecules.

    d. Least stable chemisorption rate

The thickness of the sensing area is an important factor in measuring the frequency change of the SAW device. Due to relatively lower shear acoustic velocity of gold, thin films on top of piezoelectric layers provide strong waveguiding.

2.2 Finite Element Simulation

Finite Element Method (FEM) is a widely used numerical technique for solving partial differential equations governing natural phenomenons. This versatile technique takes into account the effects of piezoelectric perturbation, diffraction, backscattering, energy storage caused by non-radiating bulk waves, and electric flux leakage from the substrate surface. Using the vastly popular simulation tool COMSOL Multiphysics, finite element simulation of a particular device can be done from the designed geometrical structure using the constituent material properties, and for a set of applied boundary conditions, response of the device to an excitation source can be visualised. To simulate SAW sensors, the complete set of fundamental equations related to piezoelectricity that relate the mechanical and electrical domains need to be solved. This approach requires discretization of the domain under study into smaller areas called elements, which are connected at specific points called nodes. The wave equations are discretized and solved to generate displacement profiles and voltage profiles at each node. The use of FE simulations to model wave propagation characteristics and SAW response are available extensively in literature [115, 116, 118–121].

For our device simulation, COMSOL Multiphysics Version 4.4 was used. Modal analysis was carried out to analyse the freely propagating eigenmodes and eigen-values, followed by harmonic analysis to analyse the time-dependent behaviour of the generated acoustic waves. 3D geometry of the devices was utilized, which contributed to more precise simulation results considering that the acoustic wave generated was of a shear-horizontal nature. However, the use of a 3D geometry instead of a 2D geometry increased the computation time and system memory usage manifold. A system with 8 GB RAM was used for the computation. However, any computation involving a mesh of more than 30,000 elements led to issues of shortage of memory. Hence, the number of elements was limited to 30,000 in all the simulations.

2.3 Results and Discussion

The input parameters provided for the simulations are listed below:

1. Geometry of the SAW device structure to be simulated
2. Co-ordinate systems with rotation angles for the piezoelectric substrate
3. Material properties
4. Boundary conditions

The steps in the simulations carried out for the SAW delay line are as follows:

1. The eigen mode analysis was performed, in which no voltage was applied to the structure. This analysis gives us the resonance and anti-resonance frequencies, where the constructive and destructive interference occurs respectively. In terms of displacement profile, the displacement was maximum at the ends of the structure in resonant frequency, while the displacement was maximum at the middle of the IDT in anti-resonant frequency.
2. Admittance values were plotted for the delay line using frequency analysis, and the maximum and minimum values were obtained at the resonance and anti-resonance values.
3. Time-response simulation was carried out to calculate the displacements and voltages at the output IDTs. To avoid mass loading effects, massless IDTs were used for simulation.

2.3.1 Rotation Angle of Piezoelectric Substrates

In the first step, SAW velocity of the substrates for different crystal rotations from 0° to 180° was checked using eigen mode analysis for the proper optimization of rotation angle. Here, "free" and "short" indicate the absence and presence of ground applied to the substrate surface. The value of SAW velocity was calculated using the equation:

$$v_{SAW} = f_0.\lambda \tag{2.4}$$

The values obtained were in consonance with those obtained from literature [37,38], thus indicating that a particular rotation can be used to obtain the proper conditions for SAW propagation. In our case, for generating the SH-SAW, 41°YX $LiNbO_3$ and 36°YX $LiTaO_3$ showed a SAW velocity in accordance with the theoretical values of 4379 and 4112 m/s respectively on a shorted surface [38].

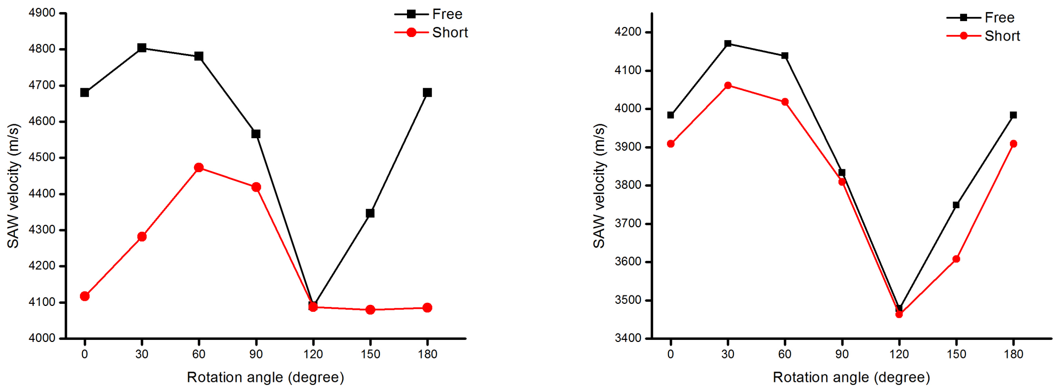

(A) (B)

Figure 2.3: Velocity of SAW on rotated Y-cut substrates: (A) 41°YX $LiNbO_3$ substrate, (B) 36°YX $LiTaO_3$ substrate

2.3.2 Eigenmode Analysis

The eigenmode analysis was carried out for the two substrates with three different IDT widths. Figure 2.4 show the deformation of the substrates at the resonant frequency for all six devices. It can be observed that maximum deformation occurs at the area under the IDT at the resonant frequency, which is desired for confirmation of the value of operating frequency.

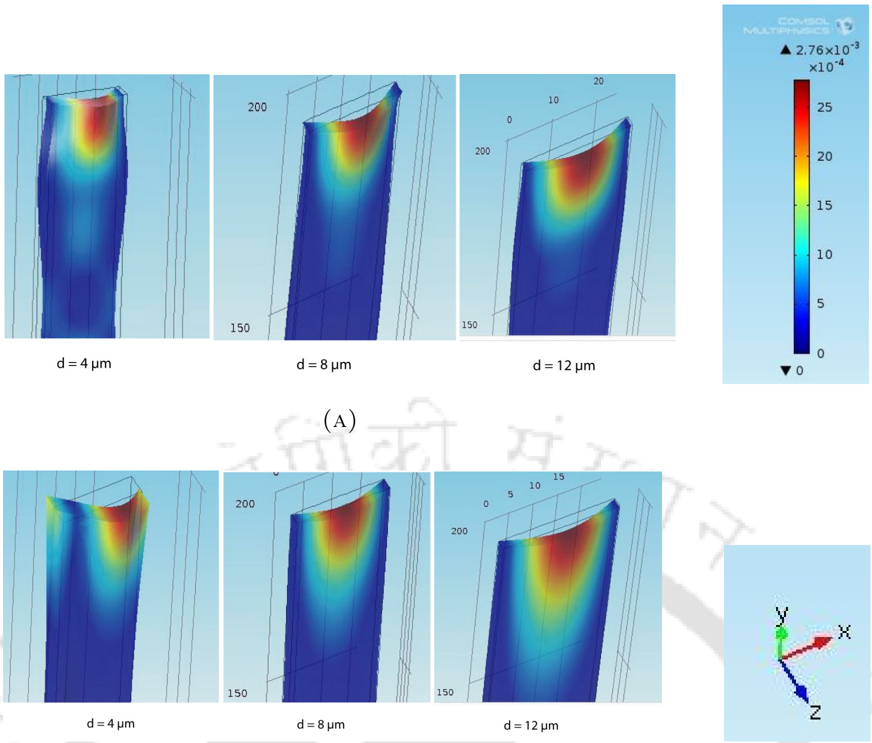

(A)

(B)

FIGURE 2.4: Eigenmode analysis showing maximum deformation at the resonant frequency for: (A) 41°YX $LiNbO_3$ substrate, (B) 36°YX $LiTaO_3$ substrate

Table 2.2 shows the different values of resonant and anti-resonant frequencies obtained for the six devices. All devices exhibit a behaviour that agrees with the theoretical values for that particular substrate and the width of the IDT.

TABLE 2.2: Resonant and anti-resonant frequencies from eigen mode analysis

Type of substrate	**IDT width (μm)**	**Resonant frequency (MHz)**	**Anti-resonant frequency (MHz)**
41°YX $LiNbO_3$	4	274.141	274.175
	8	137.033	137.037
	12	91.156	91.248
36°YX $LiTaO_3$	4	254.715	254.734
	8	127.347	127.352
	12	84.898	84.904

2.3.3 Frequency Analysis

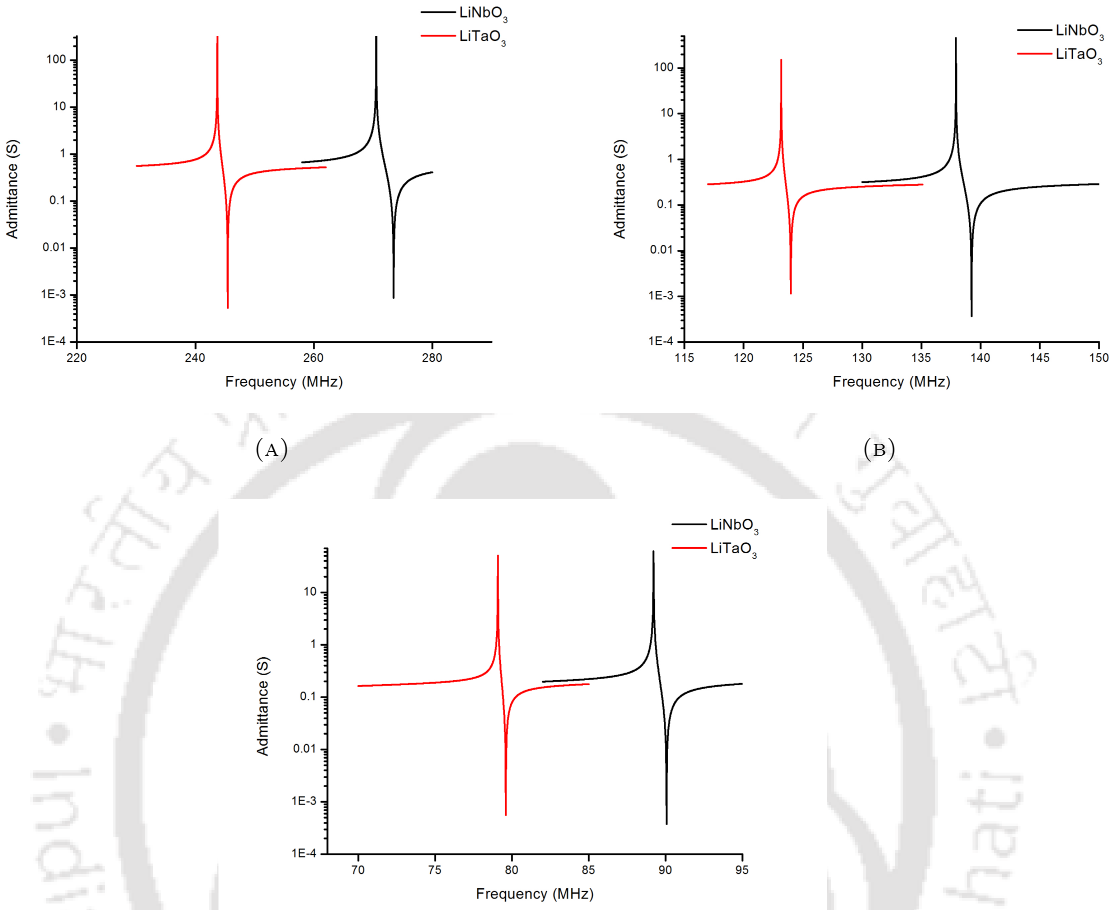

(A) (B)

(C)

FIGURE 2.5: Variation of admittance values for IDT widths of (A) 4 μm , (B) 8 μm, and (C) 12 μm

The computation of admittance values by frequency analysis gave us the maximum and minimum admittance at the resonant and anti-resonant frequency respectively. Figure 2.5 give us an idea of the variation of admittance for a particular range of applied frequencies of input signal. As observed from the eigenmode analysis, a peak was observed at the resonant frequency, indicating maximum admittance of approximately 100 siemens, while a dip was observed of about 10^{-3} siemens at the anti-resonant frequency, showing minimum admittance.

2.3.4 SH-SAW Generation

To check the nature of the SAW generated, periodic boundary conditions were kept along Z-axis, which effectively makes the IDTs of infinite aperture and keeps the simulation geometry small. The desired orientation of the substrates were obtained by using the Euler angles in the rotated coordinate system. The mesh was limited to 30000 elements in each case due to computational constraints. A critically damped region of size one lambda was made on the left of the input IDT, right of the output IDT and below the substrate, to eliminate spurious reflections that occur at the edge of the device. A sinusoidal input voltage of 5.sin(2πft) V, was given to the input IDT to activate the inverse piezoelectric effect, where the applied potential difference induced mechanical deformations in the crystal. Figure 2.6 shows the 3D geometry used for COMSOL simulation alongwith the dimensions.

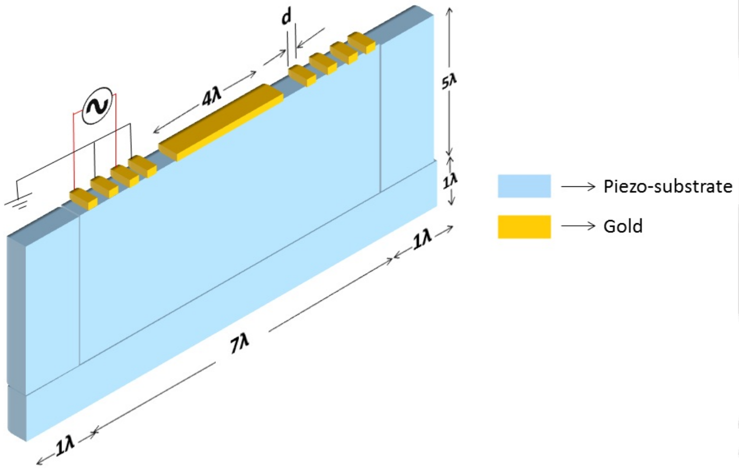

FIGURE 2.6: Geometry of simulated structure with dimensions

The propagation of shear-horizontal SAW propagating through the device surface of a delay line is shown in Figure 2.7. The generation and propagation of the SH-SAW proves that the various material properties and boundary conditions were appropriate.

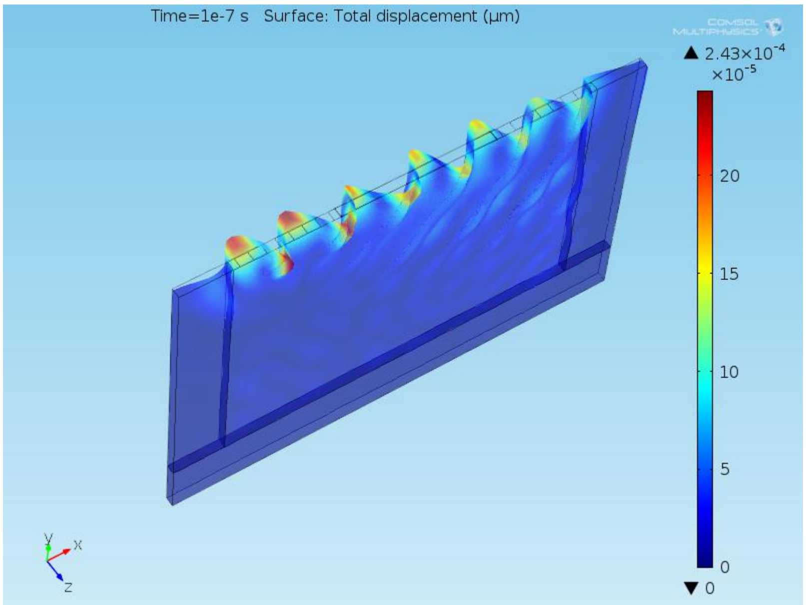

FIGURE 2.7: Generation of SH-SAW on the delay line structure

2.3.5 Displacement and Voltage profiles

The generation of SH-SAW was checked for all six devices, and a comparison was done for the displacement profiles and voltage profiles at the output electrodes. As mentioned in the earlier section, a sinusoidal input voltage of 5.sin(2πft) V was applied at the input port, and a point evaluation was done at a particular point on the output port of the delay line. The simulations were carried out for 100 ns with a time step of 0.01 ns from the time of application of electric signal to the input IDT. Figure 2.8(A) and 2.8(B) shows the displacement profiles for three different IDT widths on 41°YX $LiNbO_3$ and 36°YX $LiTaO_3$ respectively.
Similarly, Figure 2.9(A) and 2.9(B) shows the voltage profiles for three different IDT widths on 41°YX $LiNbO_3$ and 36°YX $LiTaO_3$ respectively. The voltage at the output IDT starts to rise in about 18, 38 and 50 ns for 41°YX $LiNbO_3$ and 22, 42 and 52 ns for 36°YX $LiTaO_3$.

Finally, a comparison is shown between the voltage profiles for IDTs of same width on the two substrates considered, as shown in Figure 2.10. As it can be clearly observed, for a input voltage of peak value 5 V, the output voltage is seen. Also, there is more delay in the propagation of the wave in the devices on 36°YX $LiTaO_3$ wafer, owing to the slower velocity of SAW on that substrate compared to 41°YX $LiNbO_3$ substrate.

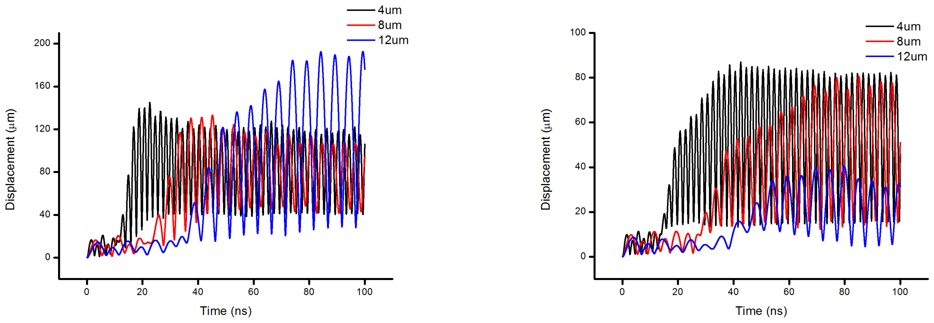

(A) (B)

FIGURE 2.8: Comparison of displacement profile for different IDT widths on: (A) 41°YX $LiNbO_3$ substrate, (B) 36°YX $LiTaO_3$ substrate

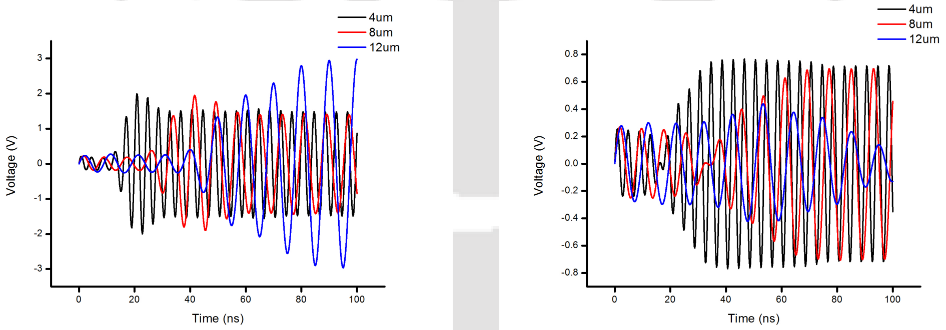

(A) (B)

FIGURE 2.9: Comparison of voltage profile for different IDT widths on: (A) 41°YX $LiNbO_3$ substrate, (B) 36°YX $LiTaO_3$ substrate

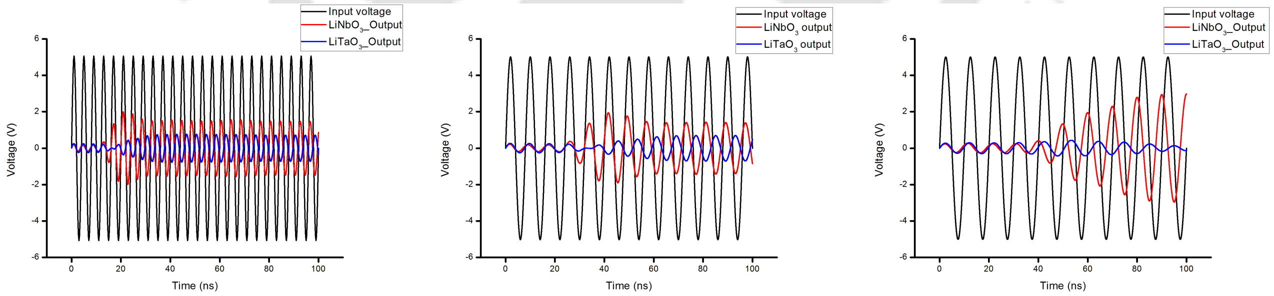

(A) (B) (C)

FIGURE 2.10: Comparison of voltage profile for IDTs of same width on different substrates for IDT width: (A) 4 μm, (B) 8 μm, and (C) 12 μm

2.4 Determination of IDT Parameters

An optimal design for an IDT must match the real impedance, i.e. IDT resistance to the source resistance (considered 50 Ω). The number of finger pairs in our case was kept fixed at 40. The IDT finger overlap or aperture width (W_a) was then adjusted so that the IDT design achieves the correct IDT resistance. Equation 2.5 [37] was used to optimize the aperture for the different devices.

$$W_a = \frac{1}{50\Omega} . \frac{1}{f_0 2 C_s N_p} . \mathrm{Re}\left(\frac{1}{4k^2 N_p + j\pi}\right) \tag{2.5}$$

Here, C_s represents the capacitance per unit length for a pair of fingers, while N_p is the number of finger pairs. The value of C_s for 41°YX $LiNbO_3$ and 36°YX $LiTaO_3$ are 4.6 pF/cm and 4.4 pF/cm respectively [37, 38, 117]. The number of finger pairs were fixed at 40. Table 2.3 shows the values of different parameters used in IDT optimization.

TABLE 2.3: Parameters for IDT optimisation

Type of substrate	C_s (pF/cm)	IDT width (μm)	f_0 (MHz)	Aperture width (mm)
41°YX $LiNbO_3$	4.6	4	274.14	2.3
		8	137.03	4.6
		12	91.15	7
36°YX $LiTaO_3$	4.4	4	254.71	1.5
		8	127.34	3.1
		12	84.89	4.6

2.5 Summary

The finite element simulation of six SAW devices with different device dimensions have been achieved. The resonant and anti-resonant frequencies were checked, followed by the plotting of the admittance curves. The delay line structure for each device was simulated and the generation of Shear-Horizontal SAW tested. The displacement profile and voltage profile of all delay line devices have been compared. Finally, the IDT parameters were obtained to achieve the maximum efficiency of the fabricated devices. The importance of the simulations carried out and the parameters calculated, discussed in length in this chapter, is in the microfabrication of efficient SAW devices, which will be described in the next chapter. The mask layout design, which is necessary for the lithography process, is created using the IDT width, aperture width and crystal orientation that were validated using the 3D Finite Element simulations.

Chapter 3

Fabrication of SAW Devices

This chapter outlines the process followed to fabricate the Surface Acoustic Wave based dual delay line devices for the detection of Hepatitis B Surface Antigen (HBsAg). The SAW devices were fabricated using the Indian Nanoelectronics Users Programme (INUP) facility at the National Nanoelectronics Fabrication and Characterisation (NNfC) facility in the Centre for Nanoscience and Engineering (CeNSE), IISc Bangalore. The fabrication steps are discussed in detail, followed by the characterisation of the devices and design of matching circuits, which were done using the facility in the Centre for Nanotechnology, IIT Guwahati.

3.1 Fabrication Process Flow

The aim of the fabrication was to create SAW dual delay lines on two substrates, namely 41°YX $LiNbO_3$ and 36°YX $LiTaO_3$. As discussed previously in Chapter 2, three IDT widths were considered, so three device designs were included in the mask layout. The substrates used were purchased from University Wafer. The fabrication was carried out in a class 100/1000 clean room, the process flow of which is shown in Figure 3.1.

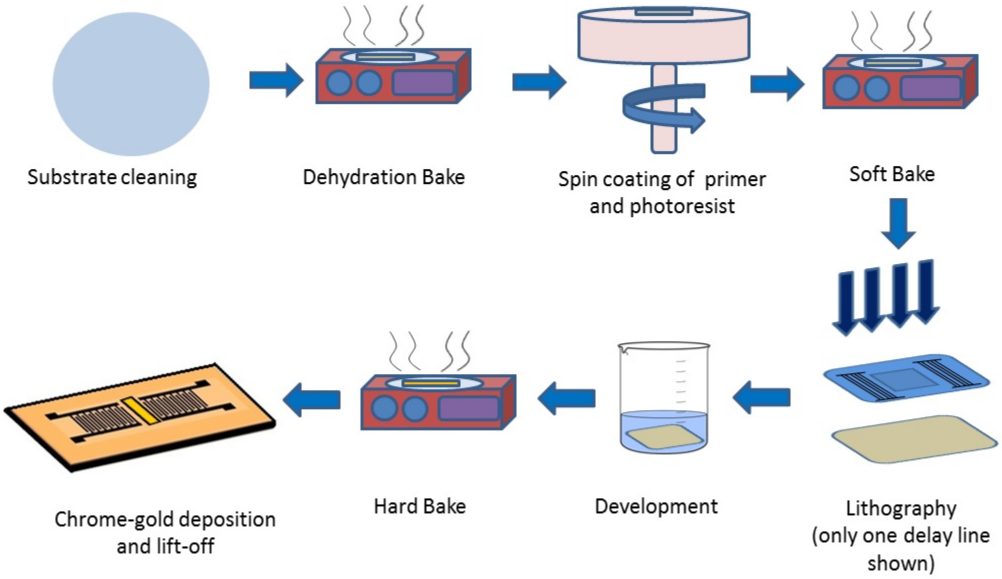

FIGURE 3.1: Process flow of microfabrication

3.2 Details of Microfabrication Steps

The steps followed in the microfabrication are discussed in detail in the following section:

1. **Cleaning of wafer**: Two piezoelectric wafers, one each of 41°YX $LiNbO_3$ and 36°YX $LiTaO_3$, were cleaned using acetone, isopropanol and deionized (DI) water. After that, the wafers were dried using nitrogen stream. The diameter of both the wafers were 3 inch and thickness 500 μm.

2. **Dehydration bake**: Dehydration bake was done for 10 minutes at 110 °C to remove any residual liquid on the substrate surface.

3. **Spin coating of primer**: Some substrates are naturally hydrophilic due to water on the surface layer because of ambient humidity. Unless it is removed before the coating of photoresist, this layer of water can be the cause of etch undercutting or complete removal of the photoresist film. Thus, to ensure adhesion of PR during developing and wet etching, it was necessary to convert the surface to a hydrophobic one, which was achieved using a primer. Hexamethyldisilazane (HMDS) was used as the primer for our wafers. It was spin coated at 6000 rpm for 1 minute.

4. **Spin coating of photoresist**: AZ5214E was used as our photoresist of choice. It was dispensed on the substrates and spin coated at 4000 rpm for 1 minute over the HMDS primer.

5. **Soft bake**: Soft bake was done for 1 minute at 110 °C to ensure proper adhesion of the photoresist to the substrate surface.

6. **Lithography**: Lithography is the process of transferring an image from a photographic mask to a substrate. Direct writing was done to define the device designs onto the photoresist on the wafers using Heidelberg μPG-501 Machine. The mask designs for the two wafers were done using Clewin software, and are shown in Figure 3.2.

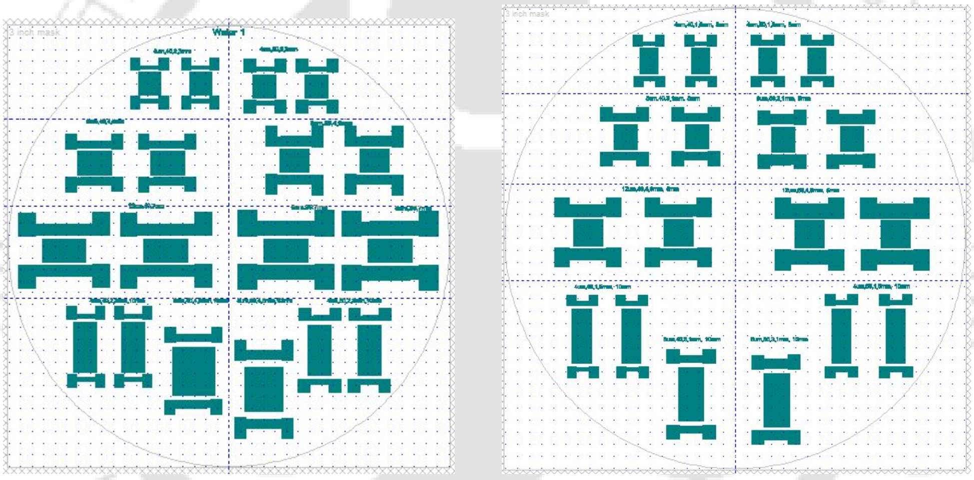

(A) (B)

FIGURE 3.2: Layout of mask design using Clewin software for: (A) 41°YX $LiNbO_3$ substrate (B) 36°YX $LiTaO_3$ substrate

The resolution of the design was 4 μm, which is the minimum feature size in the design. The bond pads, shown in the designs are required for electrical connection.

7. **Development**: The development of the wafers post-lithography was done to remove the exposed resist using MF26A developer solution for 1 minute. The wafers were then observed under an optical microscope to check if the devices were free from any fabrication defects. The images in Figure 3.3 show the devices with different IDT widths after development.

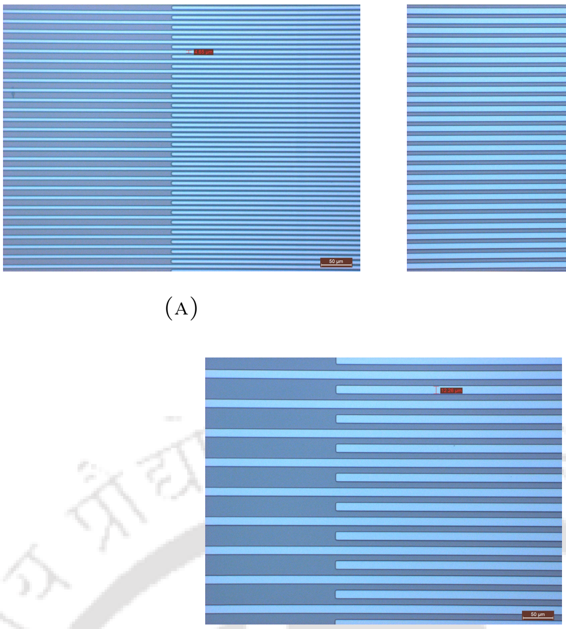

(A) (B)

(C)

FIGURE 3.3: Devices after development with IDT width: (A) 4 μm, (B) 8 μm, and (C) 12 μm

8. **Chrome-gold deposition**: Proper development of the photoresist was confirmed by observing the patterns on the substrate surface under an optical microscope (LEICA). Then we went ahead with the deposition of an adhesion layer of 10 nm chrome and 90 nm gold, which was carried out by an RF-sputtering unit. The base pressure and deposition pressure were maintained at 5 x 10^{-6} Torr and 6 x 10^{-3} Torr respectively. The pump down time was 60 minutes, and the deposition was carried out at room temperature. The gas flow of Argon was maintained at 130 SCCM. The process parameters for chromium and gold are given in Table 3.1.

TABLE 3.1: Sputtering parameters

Parameters	**Chromium**	**Gold**
Thickness (nm)	10	90
DC Power (V)	100	25
Deposition time (secs)	20	200
Deposition rate (A/s)	4	4

9. **Lift-off**: Lift-off is the penultimate and most crucial step in the proper fabrication of a device in microfabrication. In our case, a PG-developer solution was used at 60°C for 30 minutes to achieve proper lift-off of the deposited metal.

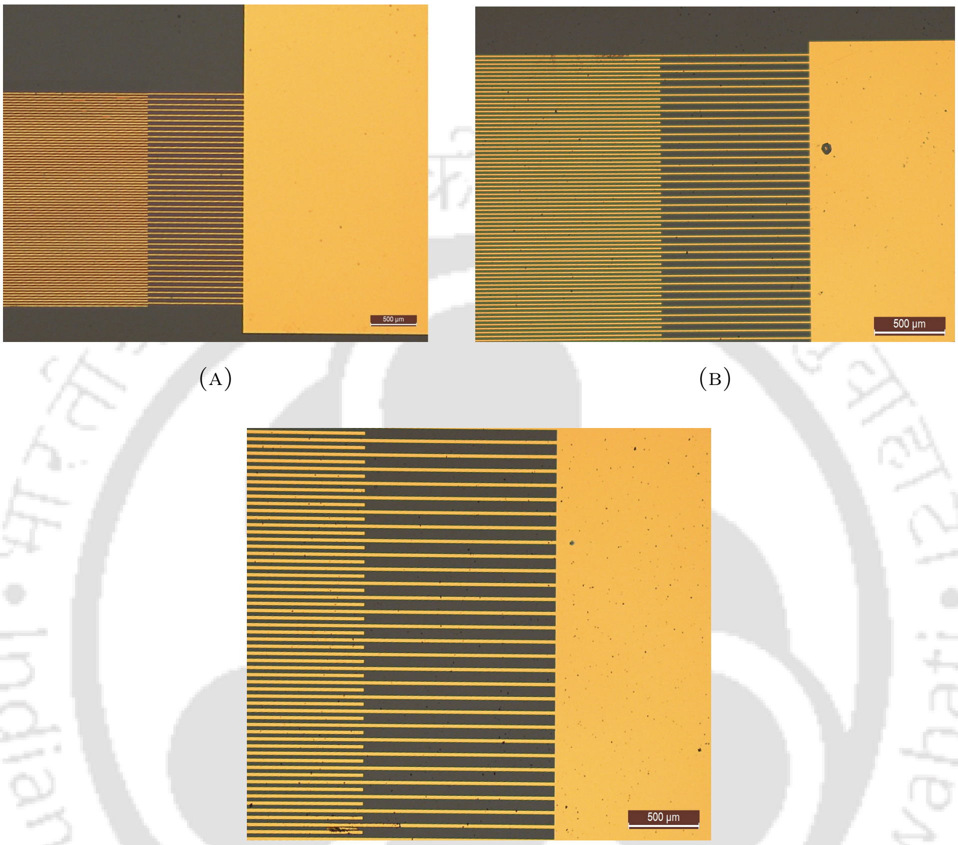

(A) (B)

(C)

FIGURE 3.4: Devices after lift-off with IDT width: (A) 4 μm, (B) 8 μm, and (C) 12 μm

The height of the deposited metal was then checked using the Dektak XT surface profiler, an advanced thin and thick film step height measurement tool. The height of the chrome-gold layer was found to be 83 nm.

The final devices on the two wafers after lift-off are shown in Figure 3.5. These wafers were then taken out of the clean room and the subsequent step of dicing was done in the packaging laboratory.

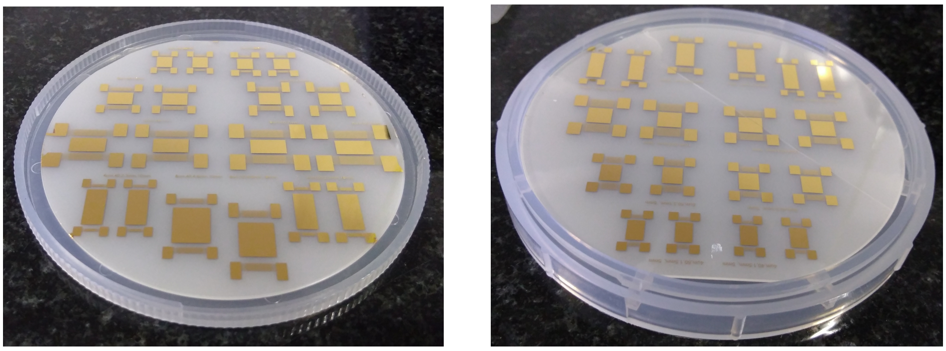

(A) (B)

FIGURE 3.5: Final devices after lift-off on: (A) 41°YX $LiNbO_3$, (B) 36°YX $LiTaO_3$

10. **Dicing**: Since the microfabrication was done on a piezoelectric wafer, proper conditions should be maintained in the process owing to its brittle nature. The instrument used for this purpose was a semi-automatic MTI-cut wafer dicing machine, as shown in Figure 3.6.

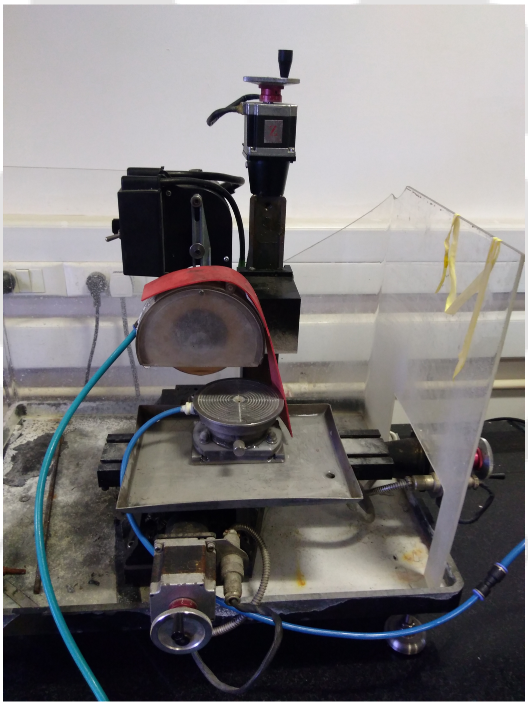

FIGURE 3.6: Wafer dicing machine

The various stages of dicing are shown in Figure 3.7. A glass plate was first mounted on a chuck and heated to 125 °C. Wax is then melted on top of the glass plate so that the wafer can be firmly secured on it. Then, the setup was left to cool down for 15 minutes. Once the desired temperature was obtained, the chuck with the substrate on it was mounted onto the dicing machine, the blade width of which was 0.35 mm. The cutting speed and moving speed of the blade were set to 4 mm/min and 50 mm/min, while the cut depth was set at 0.5 mm, which was equal to the thickness of the wafer. Throughout the dicing process, water supply was kept on so that it keeps the surface of the blade and wafer cool. Once the dicing process was completed, the individual devices were dipped in acetone and sonicated to remove the wax stuck to it. Figure 3.7 shows the various stages in the dicing of the piezoelectric wafers. After sonication, the devices were free of any residual wax and ready for characterisation.

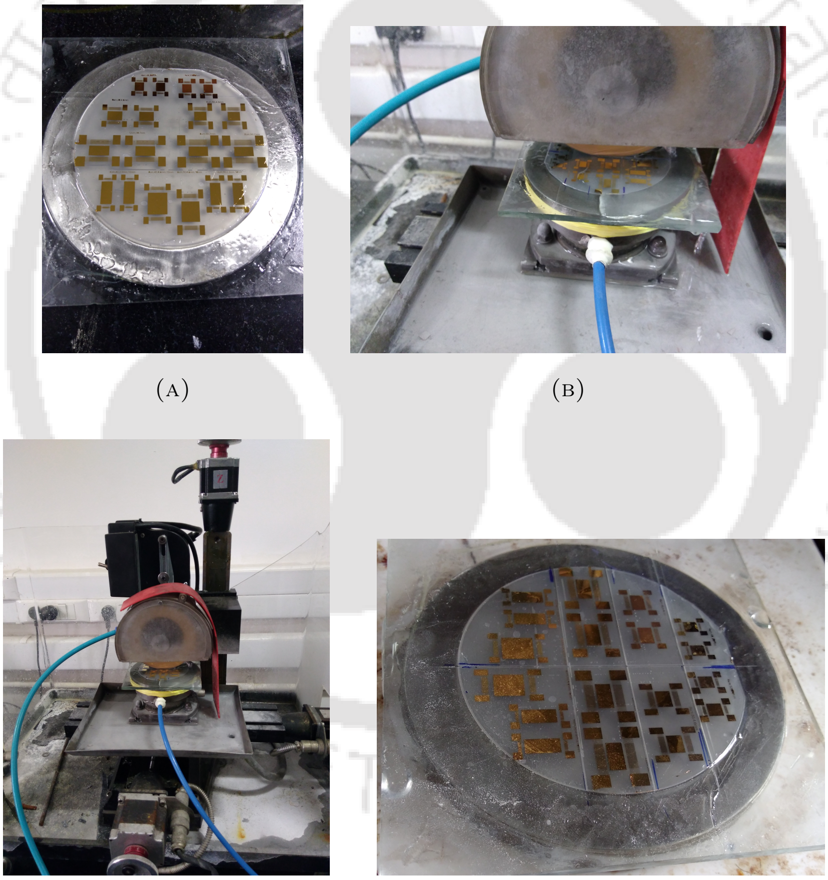

(A) (B) (C) (D)

FIGURE 3.7: Various stages in the dicing of the wafers, (A) Fixing the wafer on the glass, (B) Mounting the glass plate with wafer onto the chuck, (C) Dicing in progress, and (D) After completion of dicing

At the end of the microfabrication process, we had SAW dual-delay lines of three varying

IDT widths, viz. 4 μm, 8 μm and 12 μm on two different substrates, namely 41°YX $LiNbO_3$ and 36°YX $LiTaO_3$. One such dual delay line is shown in Figure 3.8.

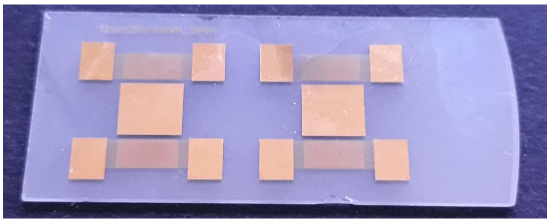

FIGURE 3.8: One SAW dual-delay line

3.3 Characterisation of the SAW Dual-Delay Lines

For a two-port device with input and output ports, scattering parameters, or S-parameters in short, are the the best means to check the efficiency of the device. S-parameters can be defined as the ratio of the output power to input power. For a two-port device, if a signal is incident on one port, part of the signal will reach the other port and a part of it will be reflected back. The four S-parameters, shown in Figure 3.9 measures the following parameters:

S_{11} : The ratio of reflected signal to the signal incident on Port 1

S_{12} : The ratio of the signal reaching Port 1 to the signal generated at Port 2

S_{21} : The ratio of the signal reaching Port 2 to the signal generated at Port 1

S_{22} : The ratio of reflected signal to the signal incident on Port 2

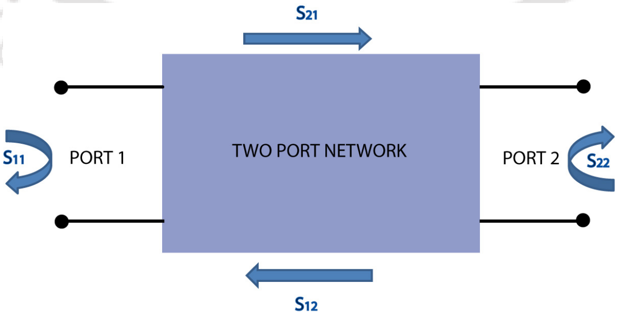

FIGURE 3.9: S-parameters for a two port network

A SAW delay line is a two-port device, with the two sets of IDTs acting as the input and output ports. To check the individual ports of all six devices, the S_{11} and S_{22} parameters are measured using Vector Network Analyzer (VNA). In a SAW delay line, the signal is transmitted from Port 1 and received at Port 2, so S_{21} measured as a function of frequency helps us to measure acoustic wave transmission [117]. In network analyzer measurements, insertion loss (IL) can be calculated from the S_{21} parameter, using the following equation:

$$\mathrm{IL} = 20 \log_{10} |S_{21}| \tag{3.1}$$

As the device under consideration is a dual delay line, we have two input ports and two output ports, as shown in Figure 3.10. Hence, a four-port Vector Network Analyzer is the instrument of choice to measure frequency responses, and to do the complete characterisation of the SAW device.

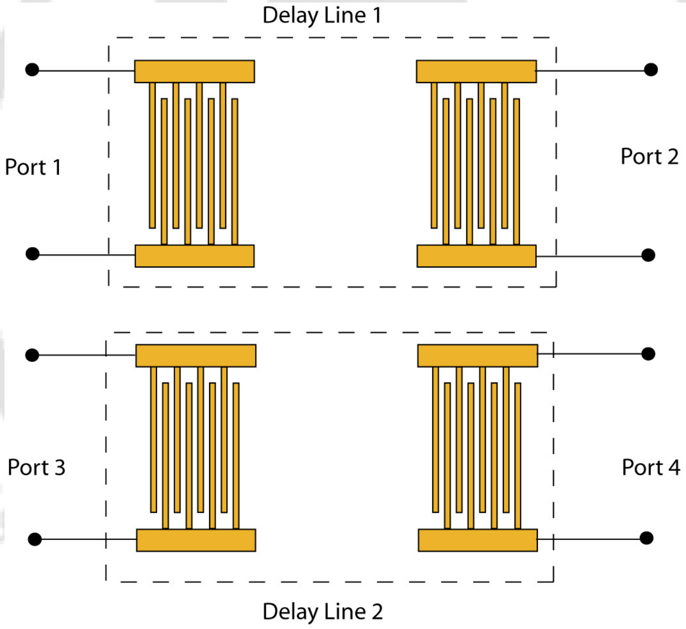

FIGURE 3.10: A four port SAW dual-delay line

3.3.1 Design of Matching Networks

To make a SAW device function efficiently, matching network is one of the most important design considerations. For maximum power transfer, the input and output impedances of the device should have a common value of 50 ohm. The final fabricated SAW device may not have 50 ohm impedance, as the presence of metal film and IDTs make it a capacitive type load to the voltage source electrically. Hence it should be externally matched. The matching network design for the SAW delay line is done by first taking the impedance value at the resonant frequency from the Smith chart for the unmatched device. The Smith chart is an effective tool to confirm that both the input (S_{11}) and the output impedances (S_{22}) are matched at the operating frequency, which is critical to the efficiency of the SAW device. The matching circuit is designed depending on the value of the load resistance, Z_L of the SAW device, which consists of a small real part and a high capacitative imaginary part. As the source impedance of 50 Ω is higher than the load impedance, the matching network arrangement is shown in Figure 3.11. It is built using an inductor in series and a capacitor in parallel in an L-type network. Using the appropriate network, the impedance as seen from the source at the operating frequency becomes equal to 50 Ω, thus reducing unwanted reflections of the acoustic wave and improving the frequency response of the SAW device.

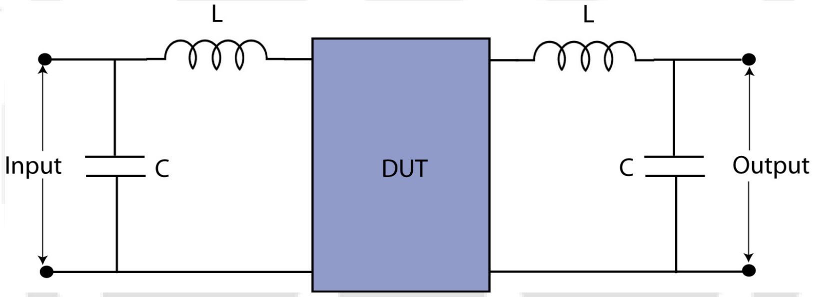

FIGURE 3.11: Matching LC-network

Since the device under test (DUT) in our work is a dual delay line, the matching network design is shown in Figure 3.12.

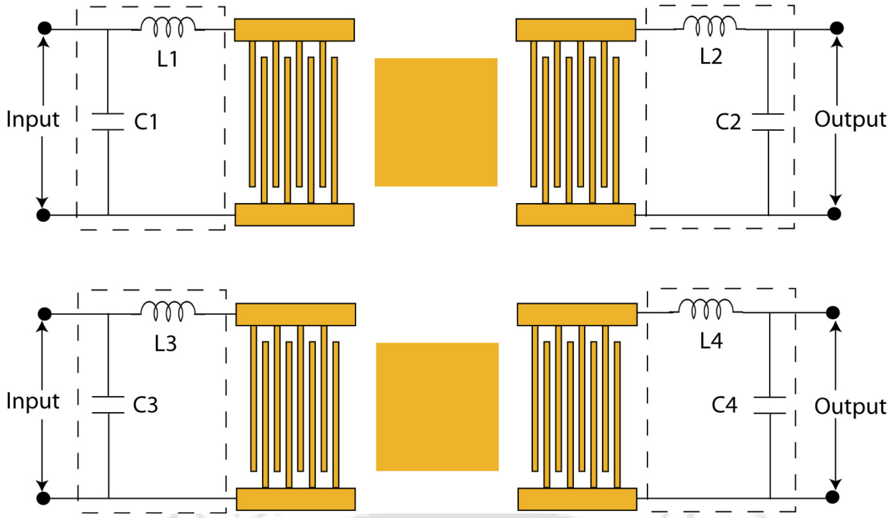

FIGURE 3.12: Matching networks in a dual delay line

3.3.2 Experimental results

The S-parameters are measured using a VNA (Model: PNA-L, Make: Keysight). The dips for the S-parameters are observed around the expected resonant frequencies after using a matching network.

The impedance of the setup was measured at the expected resonant frequency, and then the matching network was designed based on these values. Table 3.2 shows the values of the components in the LC-matching networks for all six devices.

TABLE 3.2: Matching network parameters

Substrate	IDT width	Impedance (ohm)		Matching Network			
	(μm)	Port 1	Port 2	L1 (nH)	C1(pF)	L2(nH)	C2(pF)
41°YX	4	1-j3.68	18-j15	6.21	81.42	22.68	15.51
$LiNbO_3$	8	2-j11.5	4-j14	24.77	114	32.06	78.8
	12	9-j38	12.8-j44	99.82	74.48	114.8	59.49
36°YX	4	6-j20	26.9-j36	22.45	33.54	37.73	11.48
$LiTaO_3$	8	1.7-j13	15-j8.6	27.32	132	39.03	37.84
	12	2.6-j46.9	15.2-j5.8	107.8	158.7	53.51	56.23

As shown in the Figure 3.13 and Figure 3.14, without impedance matching, transmission (in dB) at the resonant frequency was lower when the matching network was not used. The S-parameters (S_{11} and S_{22}) were measured for each device, and the use of a properly designed matching network led to a large increase in the power transmitted from the input port to the output port at the resonant frequency.

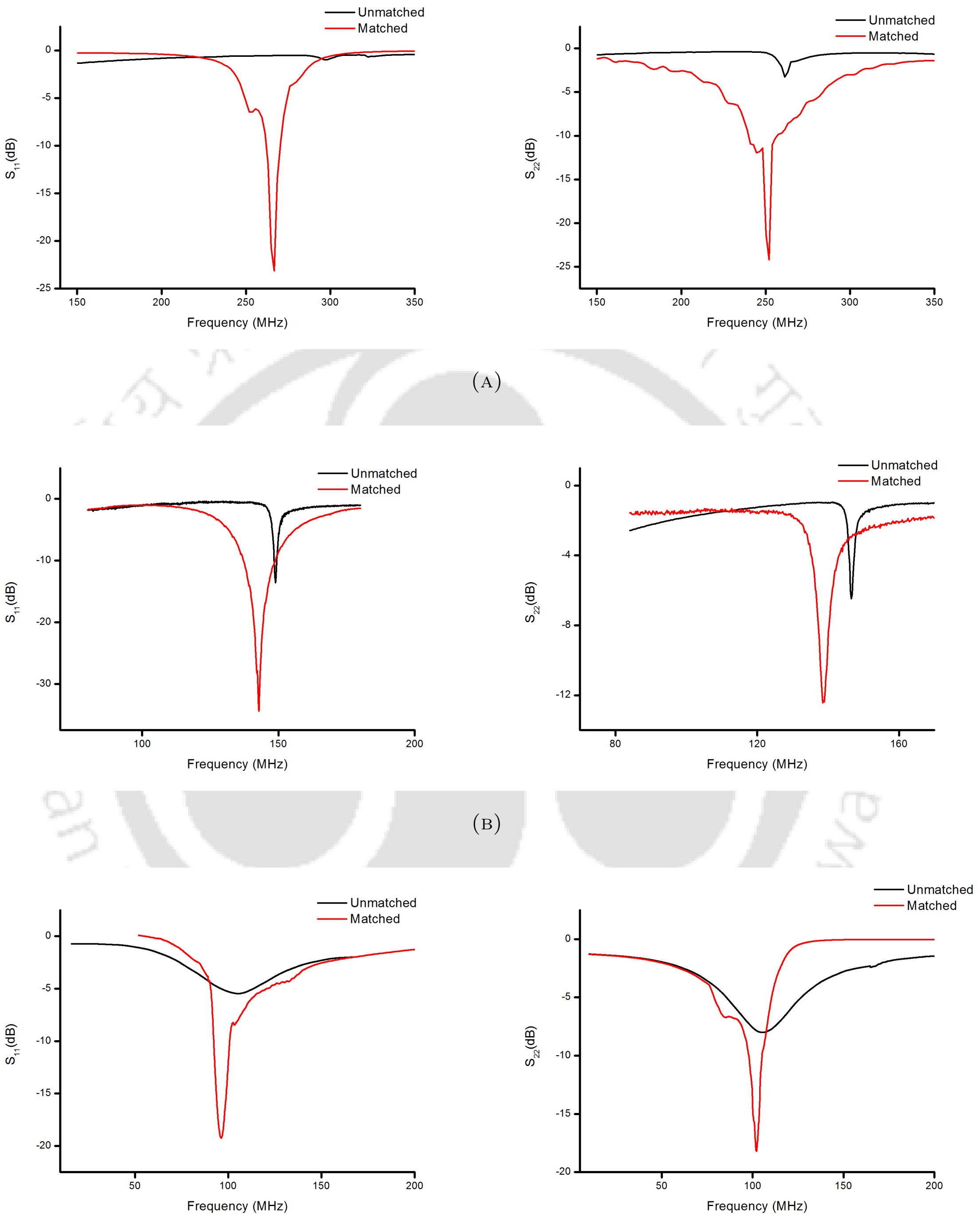

(A)

(B)

(C)

FIGURE 3.13: S$_{11}$ and S$_{22}$ parameters of delay lines on 41°YX LiNbO$_3$ substrate with and without matching networks for IDT width: (A) 4 μm, (A) 8 μm, and (C) 12 μm

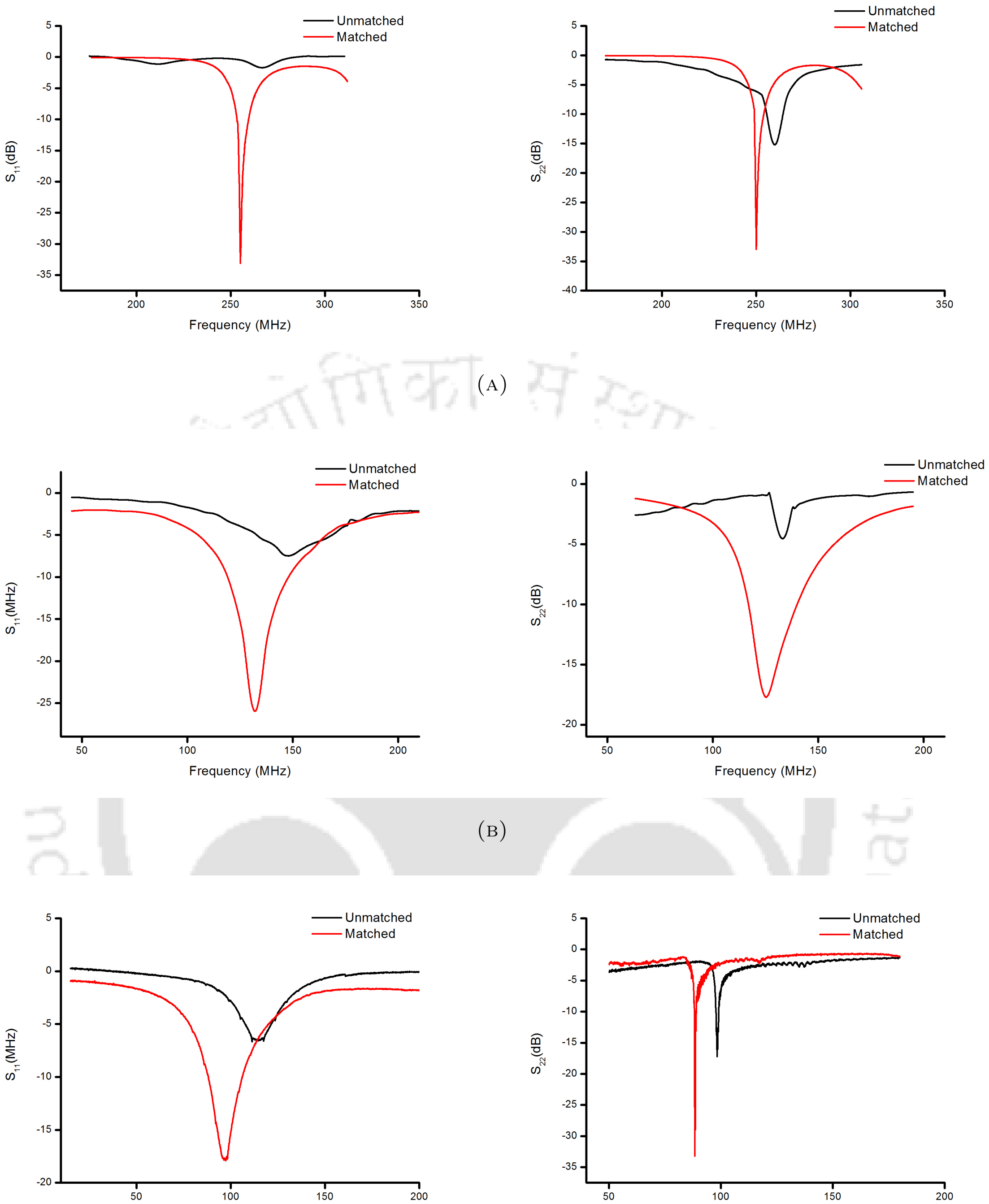

(A)

(B)

(C)

FIGURE 3.14: S_{11} and S_{22} parameters of delay lines on 36°YX $LiTaO_3$ substrate with and without matching networks for IDT width: (A) 4 μm, (A) 8 μm, and (C) 12 μm

3.4 Summary

From the results obtained in this chapter, it can be concluded that the resonant frequency obtained after using matching networks for the fabricated devices are in consonance with the expected theoretical as well as the simulated values. Table 3.3, shown below compares the values of resonant frequencies obtained for the different devices.

TABLE 3.3: Comparison of resonant frequency values

Substrate	IDT width (μm)	Resonant frequency (MHz)			
		Theoretical	Simulated	Experimental	
				Without MC	With MC
41°YX $LiNbO_3$	4	273.68	274.14	298	266.8
	8	136.84	137.03	146.9	140.5
	12	91.22	91.15	102.9	95.1
36°YX $LiTaO_3$	4	257	254.71	262	250.45
	8	128.5	127.34	132.5	125.7
	12	85.66	84.89	90.1	88.28

Chapter 4

Cloning, Expression and Purification of Anti-HBsAg scFv

THIS chapter discusses the cloning, expression and purification of the recombinant antibody for capture of the target molecule, HBsAg. In our work, we have generated a recombinant antibody against HBsAg and expressed it in *E. coli*. This protein is used on the sensor surface of the fabricated SAW device. The materials and methods are discussed in the first section, while the results obtained are shown in the subsequent section.

4.1 Materials and Methods

Bacterial cell culture

The glycerol stock of *Escherichia coli* strains and recombinant clones were stored in -80 °C. These were cultured in LB or 2xTY medium, with or without ampicillin as per requirement.

Plasmid Isolation

Plasmid was isolated using HiPurA plasmid DNA miniprep purification kit (HiMedia). 3 ml *E. coli* culture grown overnight was taken into a tube and centrifuged at 12,000 rpm for 1 minute. The bacterial pellet was resuspended in 250 μl resuspension solution (HP1) and then 250 μl lysis solution (HP2) was added. Then it was mixed thoroughly by gently inverting the tube 4-6 times. Subsequently, 350 μl neutralization solutions were added and mixed thoroughly by gently inverting the tube 4-6 times. Samples were centrifuged at 12,000 rpm for 10 min at room temperature to obtain compact white pellet. Supernatant was carefully transferred into HiElute miniprep spin column and then centrifuged at 12,000 rpm for a min at room temperature. Column was washed twice with 500 μl wash solutions (HPB) and centrifuged at 12,000 rpm for 1 minute at room temperature. Flow through liquid was discarded and the empty tube was centrifuged to remove the excess wash solution. Water (30 μl) was added in column and allowed to stand for 2 min at room temperature, followed by centrifugation at 12,000 rpm for 1 minute. Eluted plasmid was stored at -20 °C.

Agarose gel electrophoresis

DNA samples were resolved by agarose gel electrophoresis. Agarose gel (0.8-1%) was prepared containing ethidium bromide (0.5 μg/ml) in 1X TAE buffer. After loading samples, gel was run at 80 V for 1 hour at room temperature. The DNA fragments were visualized using gel documentation system (Bio-Rad, ChemiDoc XRS+). Composition of the buffer and staining solutions are given in Appendix A.

Polymerase chain reaction (PCR)

PCR was performed using a thermal cycler (Bio-Rad, C1000). The standard PCR program was followed which involved initial denaturation for 5 minutes at 95 °C, followed by 30 cycles of 30 s at 95 °C, 30 s at 60 °C, 30 s at 72 °C, and the final extension was performed for 5 minutes at 72 °C. Sequence of primers used are given in Appendix A.

Reaction mixture:

2X Master mix (HiMedia)	50.0 μl
Forward Primer	4.0 μl (Conc.= 100 μM)
Reverse Primer	4.0 μl (Conc.= 100 μM)
Template	8.0 μl
Water	34.0 μl
Total volume	**100.0 μl**

Restriction digestion

PCR amplified product and plasmid were digested with restriction endonucleases like SalI, BamHI and XhoI (NEB) as per the requirement. The reaction mixture was incubated at 37 °C for 2 hours. The reaction was terminated by heat inactivation at 65 °C for 20 minutes. The restriction digested product was resolved by agarose gel electrophoresis. The composition of reaction mixture is given below:

DNA sample	20.0 μl (Conc. = 90 ng/μl)
10X CutSmart buffer	4.0 μl
Enzyme I	1.0 μl
Enzyme II	1.0 μl
Water	14.0 μl
Total reaction volume	**40.0 μl**

Quantification of DNA

The UV-Vis spectrophotometry was used to quantify DNA. The spectrophotometric measurements were made at 260 nm and 280 nm using the spectrophotometer. The concentration of DNA was estimated from the absorbance at 260 nm considering $A_{260} = 1$ for a solution of 50 µg/ml of dsDNA when the path-length is 1 cm. The ratio of A_{260}/A_{280} was used to detect contamination by protein. Values near 2 for this ratio was considered as good. UV-Vis spectrophotometry was done using the DU 730 [Model] UV/Vis Spectrophotometer, manufactured by Beckman Coulter, USA.

Preparation of competent cell

Competent *Escherichia coli* cells were prepared by the $CaCl_2$ method. A single colony was inoculated in 5 ml LB media and incubated overnight at 37 °C with shaking. 500 μl of primary culture was inoculated into 25 ml of LB media and grown till its OD_{600} reached 0.4-0.5. The pellet was resuspended uniformly in 12.5 ml of chilled sterile 50 mM $CaCl_2$ and kept on ice for 45 minutes. The cells were harvested at 3,000 rpm for 10 minutes at 4 °C and pellet was re-suspended in 2 ml chilled 50 mM $CaCl_2$. Sterile glycerol (20% of final volume) was added to the cell suspension and aliquots of 100 μl each were made in sterile vials and stored in -80 °C for further use. The composition and preparation of sterile $CaCl_2$ and glycerol is given in Appendix A.

Transformation in bacterial cells

The plasmid was transformed into chemically competent *Escherichia coli* cells by the standard heat shock method. Plasmid (50 ng) or ligation mixture (10 μl) was added in 100 μl competent cells and incubated in ice for 45 minutes. The cells were subjected to heat shock at 42 °C in water bath for 60 s and chilled on ice immediately afterwards. 900 μl of LB media was added and the cells were incubated for 1 hour at 37 °C with shaking. Cells were harvested by centrifugation at 5000 rpm for 8 minutes at 4 °C and resuspended in 100 μl LB media. The cells were plated on LB agar (LBA) plate containing ampicillin followed by incubation at 37 °C for 12-16 hours. Subsequently, the colonies were picked and inoculated in 5 ml LB media containing ampicillin. Further, plasmid was isolated using HiPurA plasmid DNA miniprep purification kit (HiMedia).

Expression and purification of recombinant protein

The recombinant plasmid constructs, scFv-pET-22b(+) and scFv-pMAL-p5x were transformed into competent E. coli cells (100 μl) by the standard heat shock method. Transformed cells were plated on LB agar plate containing ampicillin (100 μg/μl). A single colony was inoculated in 5 ml 2xTY media containing ampicillin (100 μg/μl) and 1% glucose. It was incubated overnight at 37 °C with shaking (180 rpm). Then, it was further sub-cultured (1:200 dilution) into 100 ml 2xTY media containing ampicillin. It was incubated at 37 °C with shaking (180 rpm) till its OD_{600} reached 0.6-0.8. The expression of recombinant protein was induced by Isopropyl β-D-thiogalactopyranoside (IPTG). Cells were harvested by centrifugation and re-suspended uniformly in PBS (pH 7.4). The whole cell lysate was prepared by sonication for 5 cycles each of 60 s, at 25% amplitude on ice using ultrasonic processor (Hielscher). Homogenate was clarified by centrifugation at 10,000 rpm for 15 minutes at 4 °C. The supernatant was saved and stored at -20 °C for further processing. In case of periplasmic extract, the harvested cells were resuspended in 10 ml of buffer containing 30 mM Tris-HCl, 1 mM EDTA and 20% sucrose. After 20 minutes incubation on ice, centrifugation was done at 4000 rpm for 20 minutes at 4 °C. The supernatant is removed, and the pellet is resuspended in 5 ml of ice-cold 5 mM $MgSO_4$. Another 30 minutes incubation was done on an ice bath, followed by centrifugation at 10000 rpm for 20 minutes at 4 °C. The supernatant obtained is the periplasmic extract. The precipitate is referred to as the insoluble fraction in this work.

Protein estimation by Bradford's assay

The concentration of purified protein samples were estimated by Bradford assay using Bradford reagent (Sigma). Solutions of BSA (HiMedia) with known concentrations were prepared to generate a standard curve. Bradford reagent (200 μl) was added to each sample and incubated for 10 minutes at room temperature. Subsequently, absorbance was measured at 595 nm.

SDS-PAGE

The protein samples as well as standard protein marker were resolved using Sodium Dodecyl Sulfate Polyacrylamide Gel Electrophoresis(SDS-PAGE). The 4% stacking and 12% separating gels of thickness 0.75 mm was prepared. The electrophoresis was run at constant voltage of 120 V for both stacking and separating gel in a MiniVE vertical electrophoresis system (GE Healthcare). The electrophoretic run was monitored with tracking dye, bromophenol blue present in sample buffer. After the completion of electrophoresis, the gels were stained with the coomassie brilliant blue (CBB). The buffer composition of SDS-PAGE is given in Appendix A.

Enzyme-linked immune sorbent assay (ELISA)

The recombinant protein was detected by ELISA. Recombinant scFv having His-tag was detected using mouse anti-His antibody (1:1000 dilution, Calbiochem), while MBP-scFv was detected using Anti-MBP antibody (1:1000 dilution, Sigma-Aldrich). HRP (Horse Radish Peroxidase) tagged secondary antibody (Sigma) (1:1000 dilution) was used as the secondary antibody. The wells of ELISA plate were washed with PBS after every step of immobilisation. Reaction was stopped by adding 50 μl of 8 N H_2SO_4, and absorbance was measured at 492 nm. The composition of substrate solution is given in Appendix A.

Western blotting

Protein lysate were separated by 12% SDS-PAGE and transferred to polyvinylidene fluoride (PVDF) membranes (FloroTrans, PALL). Nonspecific binding was blocked with 3% bovine serum albumin in PBS (pH 7.4) (Sigma Aldrich) containing 0.1% Tween 20 (HiMedia) for 2 hours at room temperature. The membrane is incubated with primary antibody (1:1000 dilution) overnight at 4 °C, followed by incubation with HRP-tagged secondary antibody (1:2000 dilution). Protein was detected using Super Signal West Dura kit (Thermo scientific). The detailed compositions of buffers are given in Appendix A. The blots were imaged using ChemiDoc XRS+ (Bio-Rad).

Surface Plasmon Resonance

The kinetics of binding study was estimated using SPR-based biosensor (Biacore X100 system from Biacore, GE). The HBsAg was covalently immobilized on CM5 chip by using an amine coupling kit according to manufacture's protocol. Briefly, immobilization involves activation of carboxymethyl groups on a dextran-coated chip by reaction with N-hydroxysuccinimide, followed by covalent bonding of the ligands to the chip surface via amide linkages and blockage of excess activated carboxyl with ethanolamine. The sensor chip was equilibrated with 10 mM phosphate buffer (pH 7.4). The surface was activated by passing 1:1 mix of 0.4 M EDC and 0.1 M NHS, at a flow rate of 10 μl/min for 7 min. Recombinant HBsAg in PBS was added to 10 mM sodium acetate coupling buffer and immobilized for 10 min with default flow rate. Excess activated groups were blocked using a 7 minute injection of 1 M ethanolamine, pH 8.5, at a flow rate 10 μl/min. The compositions of buffers are given in Appendix A. The analyte was injected with varying concentration at 25 °C. To remove non-specific interaction, the assay channel was subtracted by control channel. The kinetic constant was determined by BIAevaluation 3.1 software and the 1:1 binding model was used.

Data Analysis

SigmaPlot was used to create graphs for all analysis. Error bars represent standard deviation in the data.

In the next section, the experimental results obtained are discussed in detail.

4.2 Cloning of scFv in pET-22b(+) vector

The recombinant antibody is a single chain variable fragment (scFv) molecule having the variable regions of an anti-HBsAg antibody. The original antibody was generated using hybridoma technology [122]. The authors of that paper [122] cloned the scFv in pHEN1 vector. This vector does not allow expression of the scFv with any additional tag. Therefore, it is difficult to purify the scFv from bacterial extract.

Hence, in our present work, we have used the scFv cloned in pHEN1 [122] as the starting material. We subcloned the scFv in another bacterial protein expression vector for expression and purification.

The primers for the recombinant scFv fragment were designed as shown below:

Forward primer (HBSF) : 5'-TAATACGACTCACTATAGGG-3

Reverse primer (BSR) : 5'-GCTAGTTATTGCTCAGCGG-3

The scFv was amplified by PCR using the scFv cloned in pHEN1 (pHEN1-scFv) as template. After amplification, scFv was sub cloned in pGEM-T Easy vector (Promega) through T/A cloning as per the manufacturer's protocol and transformed into *E. coli* DH5α. This is explained in Figure 4.1.

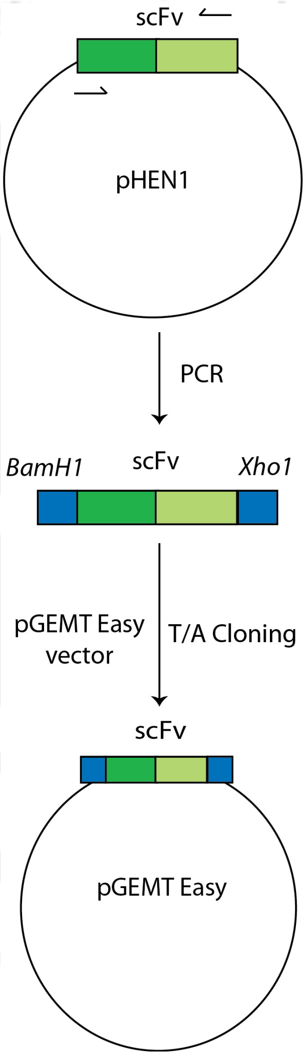

FIGURE 4.1: Sub-cloning of the anti-HBsAg scFv in pGEM-T Easy vector through T/A cloning

The transformed colonies were distinguished from the untransformed colonies by blue-white screening. The sequence of the insert after the cloning was confirmed by DNA sequencing, which was performed at the DNA sequencing facility at University of Delhi. The sequence of the insert is shown in Figure 4.2.

GAGGTGCAGCTGCAGCAGCCCGGGGCTGAGCTGGCGACGCCTGGGGCC
TCATTGAAGATGTCCTGCAAGGCTTCTGGCTACTCATTTAGCACCTACAAC
ATTCACTGGGTAAAGCAGACACCTGGACGGGGCCTGGAATGGATTGGAA
CTATTTATCCAGGAATTGGTGATACCTCCTACAATCAGAAGTTCAAAGGCA
AGGCCACATTGACTGCAGACAAATCCTCCAGCACAGCCTATTTGCACCTCA
ACAGCCTGACATCTGAGGACTCTGCGGTCTATTACTGTGCAAGAAGTGAC
ATCTACTATGGTAACTACAATGCTTTGGACTACTGGGGTCAAGGAACCTC
AGTCACTGTCTCTTCAAGTGGTGGTGGGAGCGGTGGTGGCGGCACTGGC
GGCGGCGGATCTATTGTGATGACCCAGACTCCACTCTCCCTGCCTGTCAG
TCTTGGAGATCAAGCCTCCATCTCTTGCAGAGCTAGTCAGAGCATTGTCCA
CAGTTATGGAGACACCTATTTGGAATGGCACCTGCAGAAACCAGGCCAGT
CTCCAAAGCTCCTGATCTACAAAGTTTCCAACCGATTTTCTGGGGTCCCAG
ACAGGTTCAGTGGCAGTGGATCAGGGACAGAATTCACACTCAAGATCAG
CAGAGTGGAGGCTGAGGATCTGGGAGTTTATTTCTGCTTTCAACGTTCAT
ATGTTCCGTGGACGTTCGGTGGAGGCACCAAGCTGGAACTCAAACGG

FIGURE 4.2: Sequence of 5s scFv

The sequencing results for the scFv insert in pGEMT-Easy vector were found to be correct. Subsequently, the scFv was cloned in the bacterial expression vector pET-22b(+), as explained in Figure 4.3.

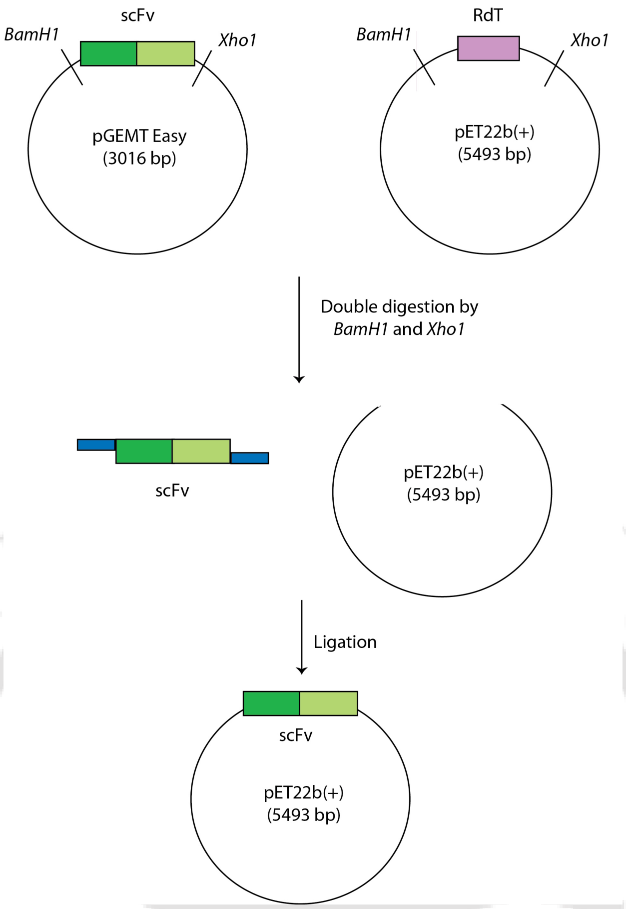

FIGURE 4.3: Cloning of the anti-HBsAg scFv in the bacterial protein expression vector pET-22b(+)

4.2.1 Restriction Digestion of pGEM-T Easy and pET-22b(+)

The bacterial expression vector, pET-22b(+) was chosen as our vector for cloning since it is a high expression vector. It contains the pel B leader sequence at N-terminal end which directs the protein to periplasm space and has a His-tag that makes the purification of protein easier. The expression vector pET-22b(+) carrying the RDT gene and the pGEMT Easy vector containing the scFv insert were digested with restriction enzymes *BamHI* and *XhoI*. The digested products were verified by agarose gel electrophoresis, as shown in Figure 4.4.

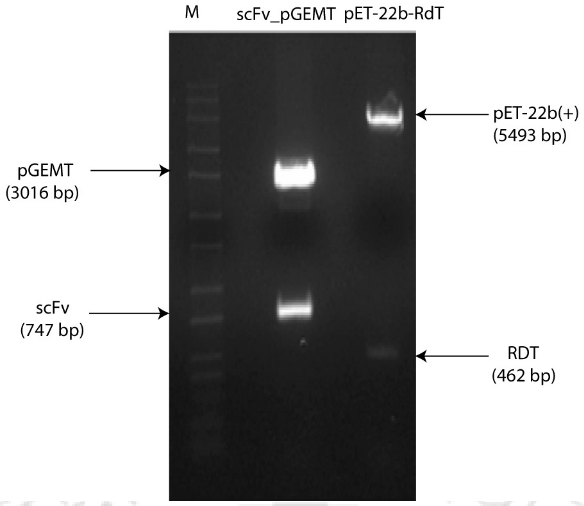

FIGURE 4.4: Restriction digestion of pGEM-T Easy vector carrying scFv and pET-22b(+) carrying RDT gene. Both were double digested with restriction enzyme *BamHI* and *XhoI* at 37 °C overnight. M=DNA ladder

4.2.2 Gel Elution

After double digestion by *BamHI* and *XhoI*, the digested vector backbone and scFv were eluted out of the gel. The eluted products were checked again by agarose gel electrophoresis, shown in Figure 4.5.

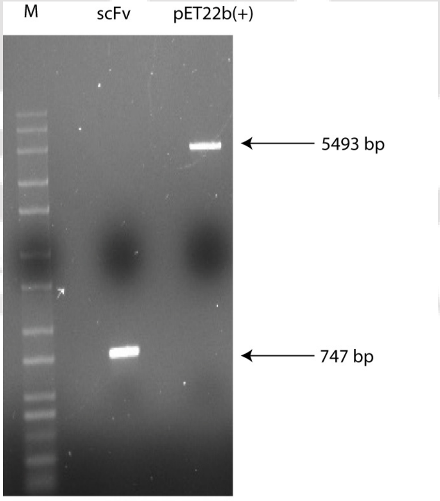

FIGURE 4.5: Agarose gel electrophoresis of eluted double digested pET-22b(+) vector backbone (5493 bp) and the scFv (747 bp). M= DNA ladder

4.2.3 Ligation Reaction for Cloning into Expression Vector

The gel eluted products, namely the anti-HBsAg scFv insert and pET-22b(+) vector were ligated using T4 DNA ligase. The ligated product was transformed into *E. coli* DH5α and spreaded over Agar-ampicillin plate, as shown in Figure 4.6.

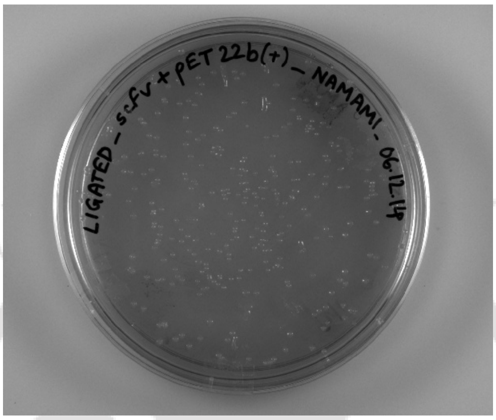

FIGURE 4.6: Agar-Ampicillin Plate comprising of colonies obtained after ligation

A master plate was made for colonies selected from transformed clones (Figure 4.7). From this plate, a single colony was picked up and sent for sequencing to the DNA Sequencing Facility of Delhi University. The sequence information is given in Figure 4.8. The DNA sequencing confirmed the clone.

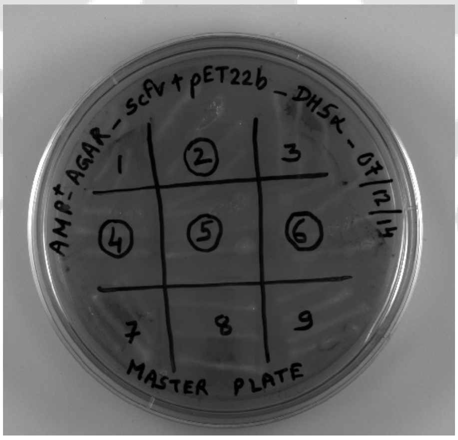

FIGURE 4.7: Master plate of *E. coli* DH5α colonies containing the scFv insert

ATGAAATACCTGCTGCCGACCGCTGCTGCTGGTCTGCTGCTCCTCGCTGCCCAGC
CGGCGATGGCCATGGATATCGGAATTAATTCGGATCCGGAGGTGCAGCTGCAGC
AGCCCGGGGCTGAGCTGGCGACGCCTGGGGCCTCATTGAAGATGTCCTGCAAGG
CTTCTGGCTACTCATTTAGCACCTACAACATTCACTGGGTAAAGCAGACACCTGG
ACGGGGCCTGGAATGGATTGGAACTATTTATCCAGGAATTGGTGATACCTCCTAC
AATCAGAAGTTCAAAGGCAAGGCCACATTGACTGCAGACAAATCCTCCAGCACA
GCCTATTTGCACCTCAACAGCCTGACATCTGAGGACTCTGCGGTCTATTACTGTGC
AAGAAGTGACATCTACTATGGTAACTACAATGCTTTGGACTACTGGGGTCAAGGA
ACCTCAGTCACTGTCTCTTCAAGTGGTGGTGGGAGCGGTGGTGGCGGCACTGGCG
GCGGCGGATCTATTGTGATGACCCAGACTCCACTCTCCCTGCCTGTCAGTCTTGG
AGATCAAGCCTCCATCTCTTGCAGAGCTAGTCAGAGCATTGTCCACAGTTATGGA
GACACCTATTTGGAATGGCACCTGCAGAAACCAGGCCAGTCTCCAAAGCTCCTGA
TCTACAAAGTTTCCAACCGATTTTCTGGGGTCCCAGACAGGTTCAGTGGCAGTGG
ATCAGGGACAGAATTCACACTCAAGATCAGCAGAGTGGAGGCTGAGGATCTGGG
AGTTTATTTCTGCTTTCAACGTTCATATGTTCCGTGGACGTTCGGTGGAGGCACCA
AGCTGGAACTCAAACGGCTCGAGCACC

(A)

MKYLLPTAAAGLLLLAAQPAMAMDIGINSDPEVQLQQPGAELATPGASLKMSCKAS
GYSFSTYNIHWVKQTPGRGLEWIGTIYPGIGDTSYNQKFKGKATLTADKSSSTAYLHL
NSLTSEDSAVYYCARSDIYYGNYNALDYWGQGTSVTVSSSGGGSGGGGTGGGGSIV
MTQTPLSLPVSLGDQASISCRASQSIVHSYGDTYLEWHLQKPGQSPKLLIYKVSNRFS
GVPDRFSGSGSGTEFTLKISRVEAEDLGVYFCFQRSYVPWTFGGGTKLELKRLEH

(B)

Figure 4.8: Sequencing results for the scFv cloned in pET22b(+): (A) DNA Sequence (B)Protein sequence. "ATG" in green bold letters: Start codon; Orange letters: PelB leader; "GGATCC" in green background: *BamHI*; Extra "G" in Yellow; Blue letters: scFv; "CTCGAG" in light blue background: *XhoI*; "CAC" in grey: Histidine

4.2.4 Clone Confirmation by Double Digestion

Plasmid was isolated from the selected clone. The purified plasmid was double digested using the enzymes *BamHI* and *XhoI*. The images of agarose gel electrophoresis are shown in Figure 4.9.

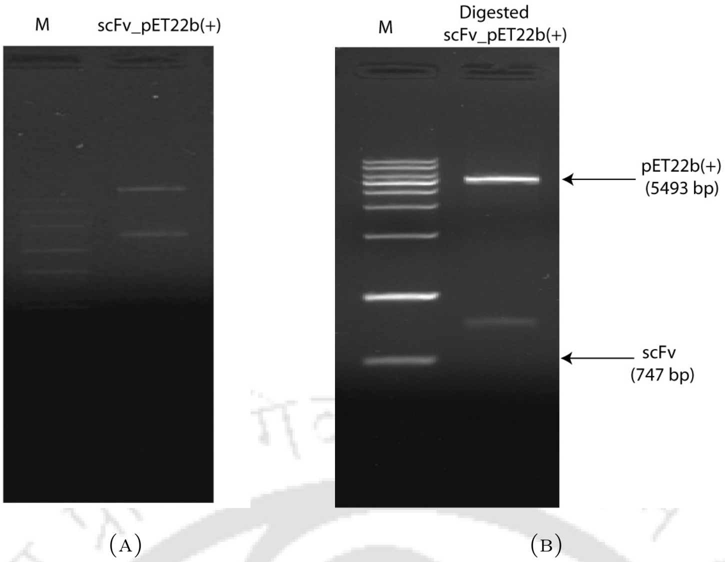

(A) (B)

Figure 4.9: (A) Images of agarose gel electrophoresis of scFv cloned in pET-22b(+), and (B) After digestion with *BamHI* and *XhoI*. M=DNA ladder

4.2.5 Expression of Soluble scFv

Once the clone was confirmed by double digestion and DNA sequencing, the plasmid of scFv-pET-22b(+) was purified and transformed in *E. coli* BL21 cells by heat shock method. The transformed cells were selected on Agar-ampicillin plate and glycerol stock of the same was made for long term storage. Subsequently, we tried different methods to induce this clone to express recombinant His-tagged scFv. The generalised scheme of the work is shown in Figure 4.10.

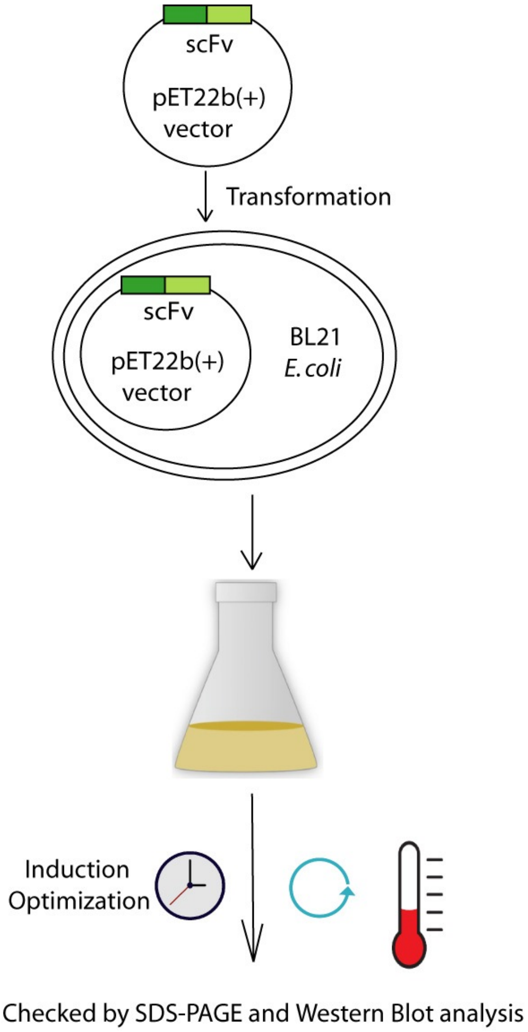

Figure 4.10: Schematic representation of the steps in expression and characteristisation of recombinant scFv

We have tried different induction conditions and level of expression of the scFv was checked by SDS-PAGE analysis. Here, we discuss our observations:

Induction by 0.5 mM IPTG at 30 °C

Here, the clone was induced by 0.5 mM IPTG at 30 °C overnight. Expression of the scFv in whole cell lysate, insoluble fraction and in periplasmic extract was checked by SDS-PAGE analysis. The data is shown in Figure 4.11. The scFv was detected only in the insoluble fraction, not in other fractions.

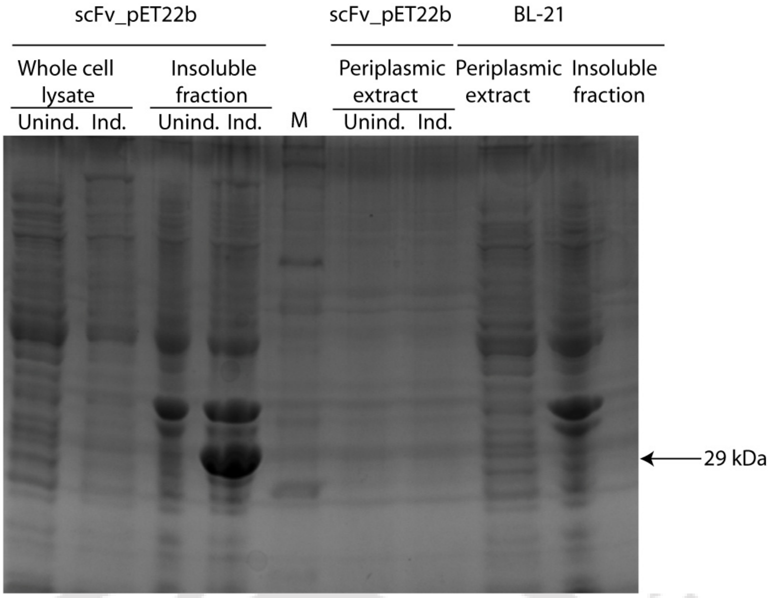

FIGURE 4.11: SDS-PAGE analysis of expression of the scFv in different fractions after induction with 0.5 mM IPTG at 30 °C. Extracts of *E. coli* BL21 clone was used as control. Expected molecular weight of the scFv is 29 kDa. M=Protein marker.

Induction by Varying IPTG Concentration and Temperatures

Subsequently, we tried different concentrations of IPTG (0.5, 1 and 2 mM) and different temperatures (28 °C and 37 °C) for induction of expression of the scFv. Samples were analysed by SDS-PAGE as shown in Figure 4.12. However, we did not observe any induction in expression of the protein in soluble form in these conditions.

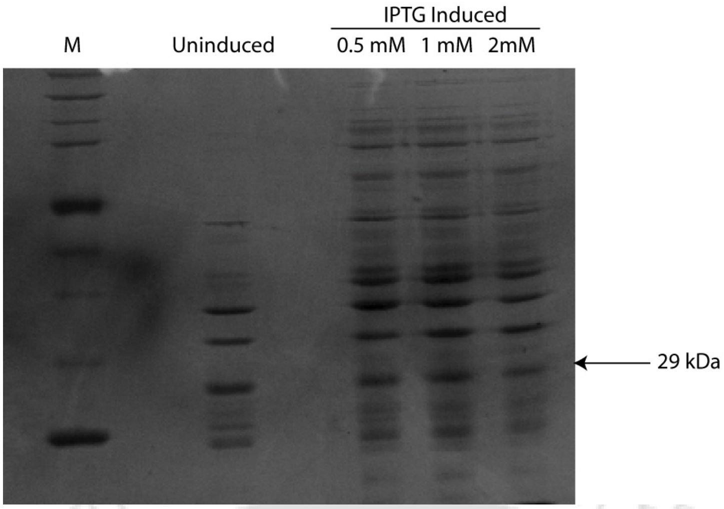

(A)

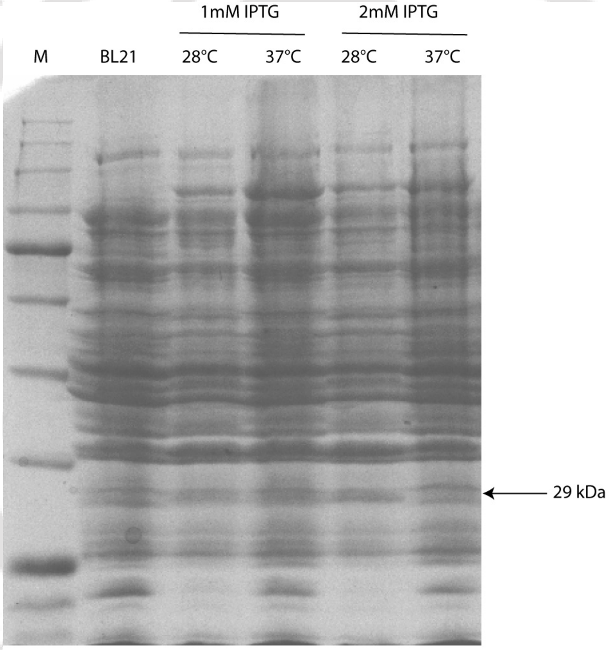

(B)

FIGURE 4.12: SDS-PAGE gel analysis of whole cell lysate samples with different induction conditions: (A) 0.5 mM, 1 mM and 2 mM IPTG at 37 °C and (B) 1 mM and 2 mM IPTG at 28 °C and 37 °C. M=Protein marker.

Induction by Varying IPTG Concentration and Time

We had observed that the scFv production is induced in our system, but the protein is going in the insoluble fraction. One way to circumvent this problem is to reduce the amount of IPTG used and also the duration of induction. Therefore, we reduced the concentration of IPTG (0.2 mM and 0.5 mM) and treated the culture only for 6 hours and 8 hours. Even then, we observed the protein only in the insoluble fraction , as seen in Figure 4.13.

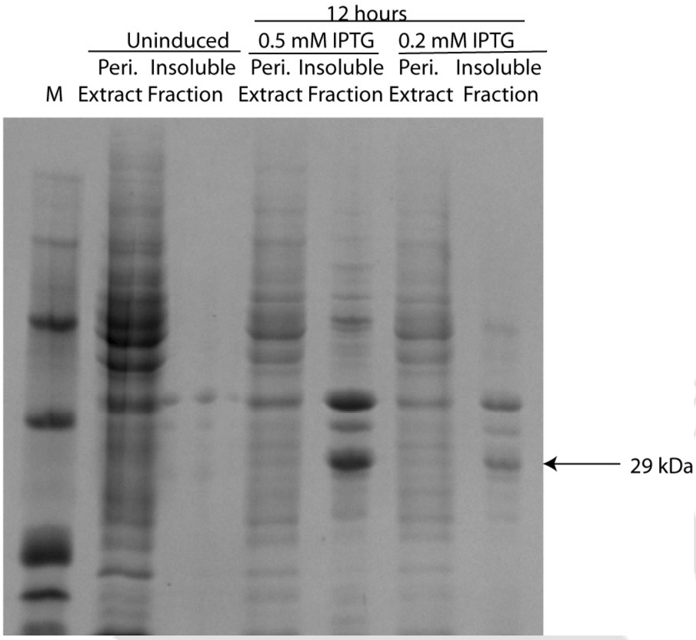

(A)

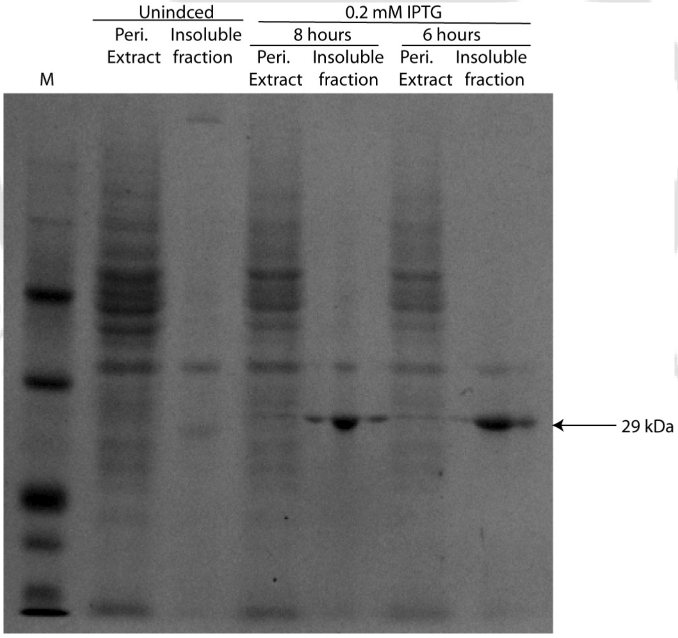

(B)

Figure 4.13: SDS-PAGE analysis of samples induced with lower IPTG concentration and shorter duration: (A) 0.5 mM and 0.2 mM IPTG for 12 hours at 37 °C, and (B) 0.2 mM IPTG for 8 hours and 6 hours at 37 °C. M=Protein marker.

Change in Extraction Technique

Since the protein was expressed only in the insoluble fraction, we tried a change in the extraction protocol by using different concentrations of sarkosyl (0.2% and 2%) in the extraction process. Sarkosyl is an ionic detergent and is known to be useful in resolubilization of protein in the soluble fraction. Figure 4.14 shows the effect of sarkosyl in solubilisation of our target protein. As shown in Figure 4.14, addition of sarkosyl helped in solubilisation of some of the scFv and we could detect that in the soluble whole cell lysate.

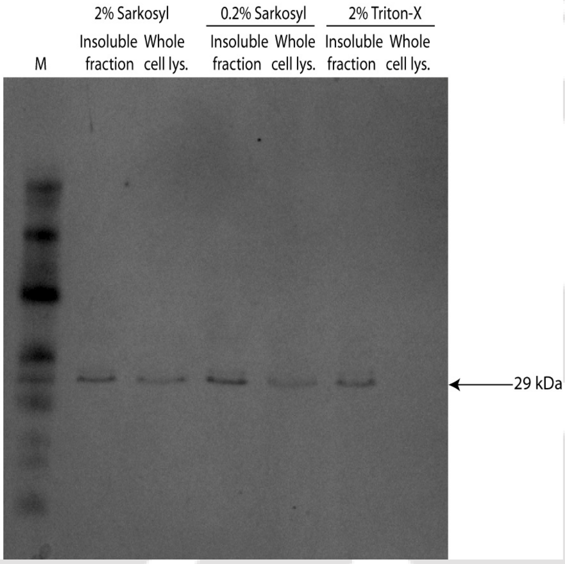

FIGURE 4.14: SDS-PAGE analysis of samples with extraction buffers with different detergents. Both soluble whole cell lysate and insoluble fraction of each sample were resolved in this gel.

We performed ELISA and Western Blot experiments to confirm successful extraction of the scFv in the whole cell soluble fraction.

ELISA showed positive results for the scFv in the sample extracted with sarkosyl. Absorbance of 0.5 a.u. and 0.9 a.u. were observed for 2% and 0.2% sarkosyl extracted soluble fraction, as shown in Figure 4.15. A whole cell lysate of untransformed *E. coli* BL21 cells was used as the negative control. Next, a Western blot was performed, as shown in 4.16. Anti-His antibody (Calbiochem) was used as the primary antibody, and

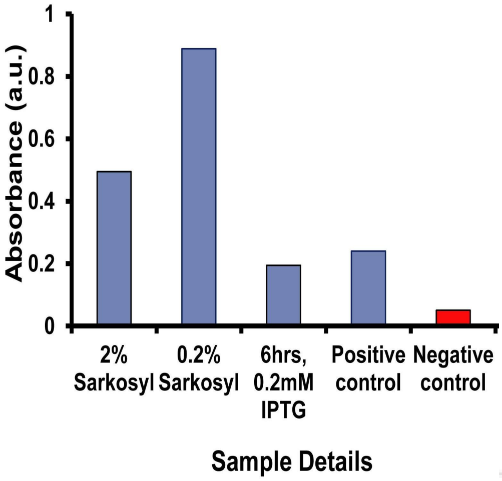

FIGURE 4.15: ELISA confirm successful extraction of the scFv into the soluble fraction by sarkosyl. RDT protein was used as the positive control, while a whole cell lysate of untransformed *E. coli* BL21 cells was used as the negative control.

HRP-conjugated Anti-mouse IgG (Sigma) was used as the secondary antibody. The recombinant RDT protein that has a His-tag was used as the positive control, while the whole cell lysate of *E. coli* BL21 cell was used as the negative control.

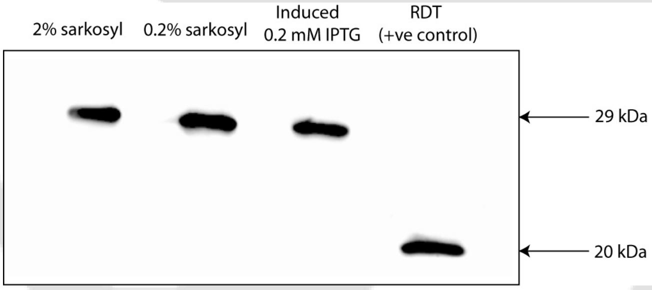

FIGURE 4.16: Western blot to confirm presence of the scFv protein extracted with different concentrations of sarkosyl. RDT protein was used as the positive control

Although we were able to successfully extract the protein in the soluble fraction, we could not purify the same by affinity chromatography. Presence of detergents are known to hinder affinity chromatography. As discussed above, we did several optimization experiments to produce the scFv in soluble form using the pET-22b(+) clone. We were able to express the scFv but failed to get it in the purified soluble form. All the optimization experiments are briefed in Table 4.1.

Table 4.1: Table showing the attempts at expression of Anti-HBsAg scFv

***E. coli* strain**	**Vector**	**Extraction method**	**Induction conditions**	**IPTG conc. (mM)**	**Protein in soluble fraction**	**Protein in insoluble fraction**
Rosetta gami	pHEN1	PBS lysis buffer, sonication	4/6/8 hours, 30 °C	1	No	No
Rosetta gami	pET-22b(+)	PBS lysis buffer, sonication	4/6/8 hours, 30 °C	1	No	No
BL21	pET-22b(+)	PBS+ PMSF+ EDTA buffer, sonication	8 hours, 30 °C	0.5	No	Yes
BL21	pET-22b(+)	PBS+ PMSF+ EDTA buffer	8 hours, 30 °C	0.5, 1, 2	No	Yes
BL21	pET-22b(+)	PBS+ PMSF+ EDTA buffer	12 hours, 28 °C, 30 °C, 37 °C	1, 2	No	Yes
BL21	pET-22b(+)	PBS+ PMSF+ EDTA buffer	6/8 hours, 30 °C	0.5	No	Yes

Continued on next page

Table 4.1 – continued from previous page

***E. coli* strain**	**Vector**	**Extraction method**	**Induction conditions**	**IPTG conc. (mM)**	**Protein in soluble fraction**	**Protein in insoluble fraction**
BL21	pET-22b(+)	PBS+ PMSF+ EDTA buffer	12 hours, 30 °C	0.2, 0.5	No	Yes
BL21	pET-22b(+)	Sarkosyl and β-ME lysis bufer	8 hours, 30 °C	0.2	Yes	Yes

Although we were able to express the scFv in the soluble form using sarkosyl, it could not be purified by affinity chromatography.

4.3 Cloning of scFv in pMAL-p5x Vector

In the pET-22b(+) system, the scFv was cloned to express as a His-tagged protein. As this approach failed to produce soluble scFv, we attempted MBP-based bacterial expression system. pMAL-p5x is a vector that is designed to express a recombinant protein as an MBP-tagged molecule. Maltose binding protein (MBP) is a large molecule. It is known to help soluble expression of other smaller proteins tagged to it. Further, MBP tagged proteins can be easily purified by affinity chromatography. Figure 4.17 shows the scheme of the cloning strategy.

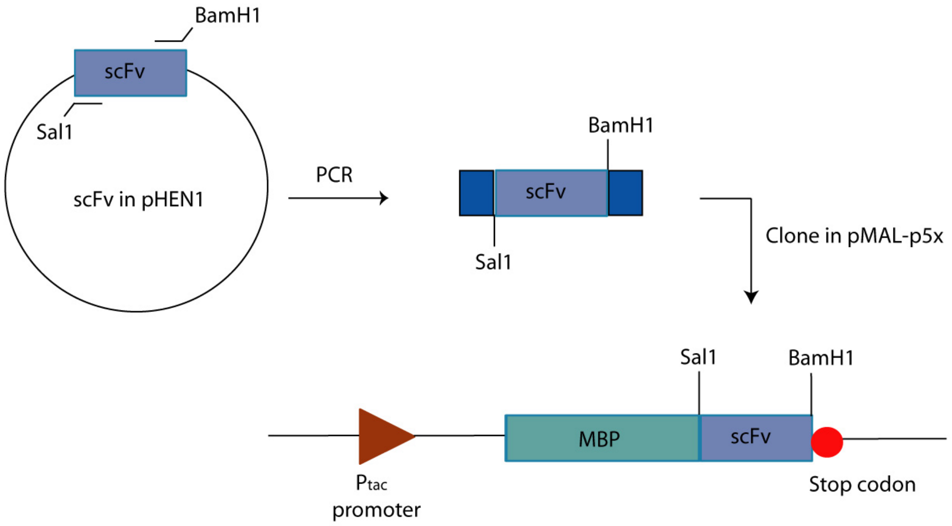

FIGURE 4.17: Schematic diagram of the strategy to clone the scFv in pMAL-p5x to express it as an MBP-tagged protein

4.3.1 PCR Amplification of the scFv

We performed PCR to amplify the scFv using the pHEN1 clone with the following primers:

Forward primer: 5'-GCAAGTCGACGAGGTGCAGCTGCAGCAGC-3

Reverse primer: 5'-GCAAGGATCCTCACCGTTTGAGTTCCAGCTTG-3

These primers were designed to introduce *SalI* and *BamHI* restriction sites in the amplified product. The PCR product was resolved by agarose gel electrophoresis (Figure 4.18) and the DNA corresponding to the scFv was extracted from the gel.

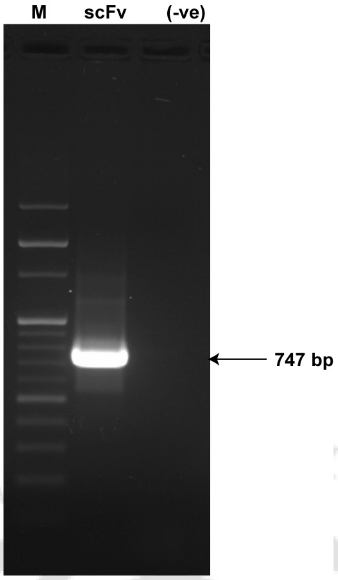

FIGURE 4.18: PCR amplification of the scFv to clone in pMAL-p5x. The pHEN1 clone was used as a template. Primers were designed to introduce *SalI* and *BamHI* sites. (–ve): Negative control of PCR where water was used as template. M=DNA ladder.

4.3.2 Restriction Digestion of the Vector and the scFv

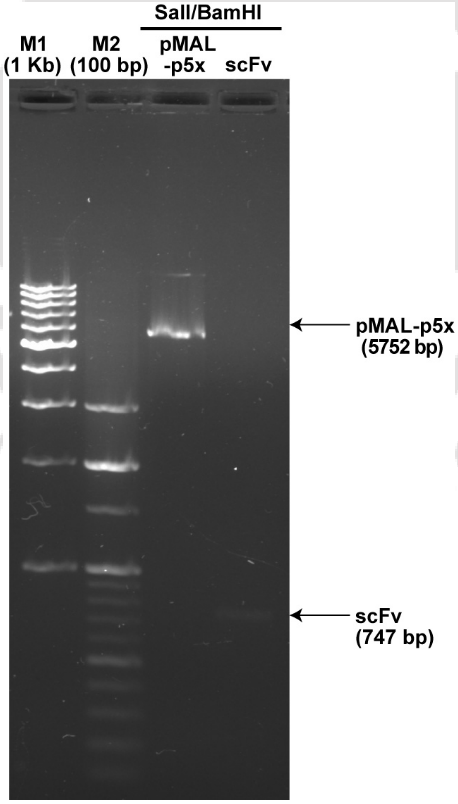

FIGURE 4.19: Agarose gel electrophoresis of pMAL-p5x and the scFv double digested by *SalI* and *BamHI*. M1,M2: DNA ladders

We used *SalI* and *BamHI* for directional cloning of scFv in pMAL-p5x vector. The vector and the PCR amplified scFv were both double digested by these two enzymes. Digested products were resolved in agarose gel by electrophoresis (Figure 4.19). Double digested products were eluted out of the gel and used for cloning.

4.3.3 Cloning of the scFv in pMAL-p5x Vector

Double digested scFv and pMAL-p5x were ligated. Ligation mix was transformed into *E. coli* DH5α. Clones were selected on Agar-ampicillin plate. Subsequently, six colonies were picked up and checked by colony PCR for presence of the insert. Figure 4.20 shows the result of this colony PCR. As shown in Figure 4.20, all colonies except colony A2 were positive.

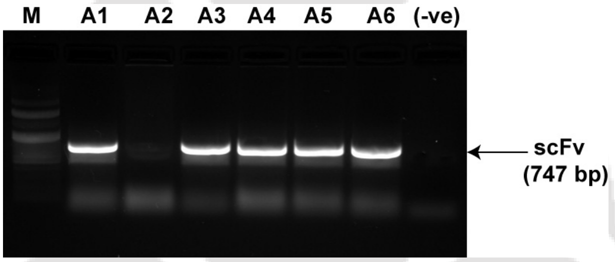

FIGURE 4.20: Colony PCR to check clones after transformation with scFv-pMAL-p5x. PCR was performed using the scFv specific primary.

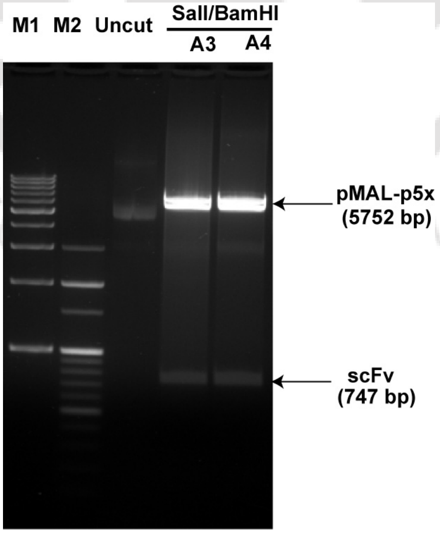

FIGURE 4.21: Clone confirmation by double digestion. Two clones of scFv-pMAL-p5x (A3 and A4) were digested by *SalI* and *BamHI*. In both cases, an insert corresponding to the size of scFv was observed. M1,M2: DNA ladders

After colony PCR, plasmid DNA was isolated from clone A3 and A4. Presence of the insert was checked by double digestion with *SalI* and *BamHI*. As shown in Figure 4.21, both the clones were tested positive in this experiment.

4.3.4 Expression and Purification of MBP-tagged scFv

For expression of the MBP-tagged scFv (MBP-scFv), *E. coli* BL21 was transformed with the plasmid DNA of clone A3 of scFv-pMAL-p5x. Transformed clones were selected over Agar-ampicillin plate and glycerol stock of a selected clone was made for further processing.

For expression of the MBP-scFv, the transformed clone was grown in LB-Agar media and induced with 0.4 mM IPTG at 28 °C for 2 hours. Induction in expression of the protein was checked by SDS-PAGE analysis. As shown in Figure 4.22, we were able to detect an additional band in the SDS-PAGE corresponding to a protein of size 71 kDa in the induced sample. This showed that the MBP-scFv was expressed in the sample.

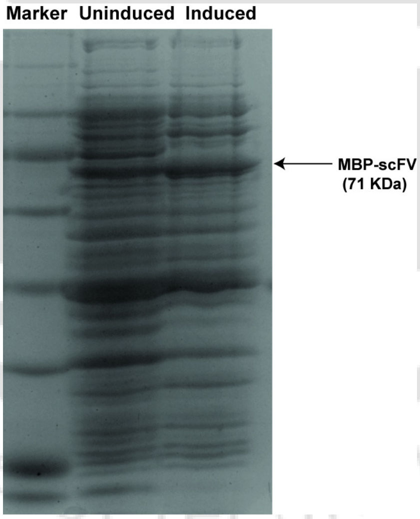

Figure 4.22: SDS-PAGE analysis to check induction by MBP-scFv. MBP-scFv clone was induced by 0.4 mM IPTG at 28 °C for 2 hours. Expected size of the protein is 71 kDa.

The whole cell extract of the induced sample was further processed for purification of the MBP-scFv. The recombinant MBP-scFv was purified from the whole cell extract by affinity chromatography using amylose column (Amylose Resin, NEB). After loading the whole cell extract, the column was washed repeatedly with PBS and the bound MBP-scFv was eluted out using 10 mM maltose. SDS-PAGE analysis of different fractions of samples collected during affinity chromatography are shown in Figure 4.23. As shown in Figure 4.23, we were able to purify the MBP-scFv. The purified protein also had some amount of truncated molecules. However, that does not affect our functional assays as shown later.

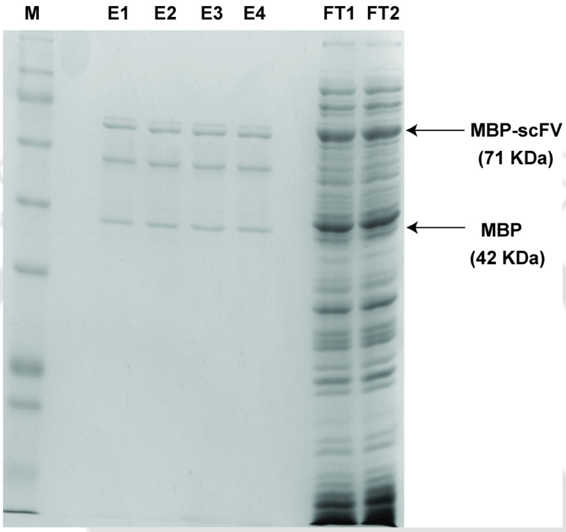

FIGURE 4.23: SDS-PAGE analysis of different fractions collected in affinity chromatography for purification of MBP-scFv. Whole cell extract of induced clone was used. The MBP-scFv was purified by an amylose column. E1 to E4: Eluted fractions. FT1 and FT2 are flowthrough after loading of the extract to the column. Eluted fractions from E1 to E4 were pooled together and used in subsequent experiments. M=Protein Marker.

4.3.5 Functional Assay of the Purified MBP-scFv

The ability of this MBP-scFv to detect the antigen (HBsAg) was checked by ELISA. For this, ELISA plate was coated by HBsAg (100ng/well). After blocking, purified MBP-scFv of concentration 150 ng/μl was diluted (1:10 and 1:50) and added to the ELISA plate. After incubation for 2 hours, bound MBP-scFv was detected using anti-MBP mouse antibody (1:2000 dilution) followed by anti-mouse HRP-conjugated antibody (1:1000 dilution). Subsequently, the ELISA was developed using OPD in substrate buffer (0.5 mg/ml). The result of this experiment is shown in Figure 4.24. The ELISA showed that the MBP-scFv binds to the antigen.

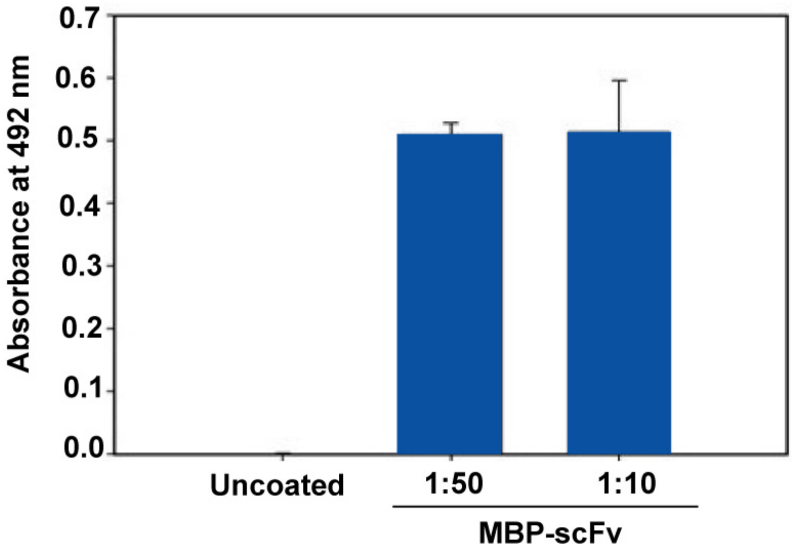

FIGURE 4.24: The purified MBP-scFv binds to HBsAg. ELISA to check binding of purified MBP-scFv to HBsAg. ELISA plate was coated with HBsAg. Two dilutions of MBP-scFv was used. Bound MBP-scFv was detected using anti-MBP scFv. ELISA data was corrected for background reading in uncoated wells. Mean of four wells is shown here.

Further, we used SPR to confirm the binding and to calculate the affinity of MBP-scFv for HBsAg. For SPR, C5 chip was coated with recombinant HBsAg. Purified MBP-scFv, at different concentrations, was used as analyte. As shown in Figure 4.25, the SPR sensogram showed binding of the MBP-scFv to the antigen, HBsAg.

The SPR data was fitted to 1:1 binding model and affinity of MBP-scFv for HBsAg was estimated. The estimated affinity, in terms of dissociation rate constant, k_D was 3.8 x 10^{-8} M. This shows that the MBP-scFv has good affinity for the antigen.

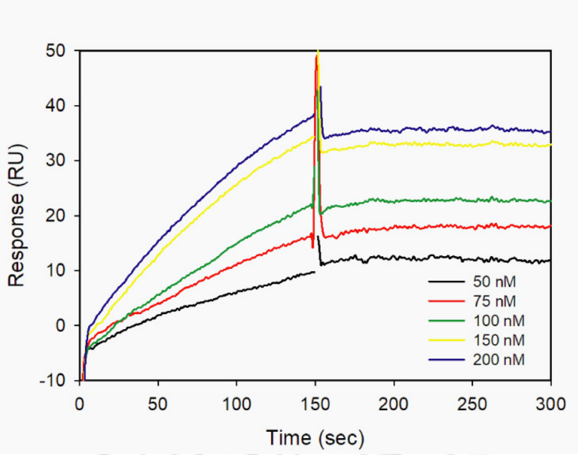

FIGURE 4.25: SPR analysis to check binding of MBP-scFv to HBsAg. C5 chip was coated with HBsAg. Different dilutions of purified MBP-scFv was used as analyte.

4.4 Procurement of commercially available Anti-HBsAg antibody

The commercially available monoclonal Anti-HBsAg antibody (Sigma Aldrich, SAB470-0767) was purchased to validate the working of the SAW sensor with different antibodies. The ability of the Anti-HBsAg antibody to bind to HBsAg (Lab Banaras, Varanasi) was checked by SPR analysis, as shown by the sensogram in Figure 4.26. This shows that the antibody procured binds to the antigen. We have used this antibody along with the recombinant MBP-scFv generated in our laboratory for subsequent works.

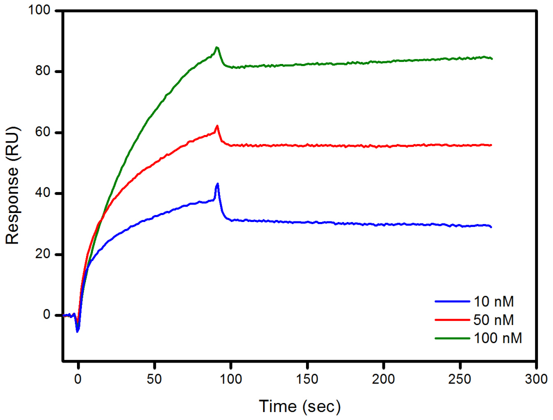

FIGURE 4.26: SPR analysis to check binding of Mouse Anti-HBsAg antibody to HBsAg. C5 chip was coated with HBsAg. Different dilutions of Anti-HBsAg antibody was used as analyte.

4.5 Procurement of hepatitis B surface antigen (HBsAg)

The hepatitis B surface antigen (HBsAg), used for all experiments, was procured from Lab Banaras (Varanasi, India). The concentration of the protein was checked by Bradford Assay. Its estimate concentration was 100 ng/μl. The purity of the protein was checked by SDS-PAGE. As shown in Figure 4.27, the HBsAg sample showed one band of appropriate size in the gel.

In clinics, concentration of HBsAg in a sample is usually measured in terms of IU/ml, using a known standard. We used Enhanced Chemiluminescence Immunoassay (ECI) developed by VITROS Immunodiagnostic System to measure the concentration of the recombinant HBsAg in terms of IU/ml. We diluted our stock HBsAg sample to 50 ng/ml and measured it using the ECI assay. As per this ECI assay, concentration of this diluted sample was 4090 IU/ml. Therefore, the concentration of the stock HBsAg solution used in our work is 81.8 x 10^5 IU/ml.

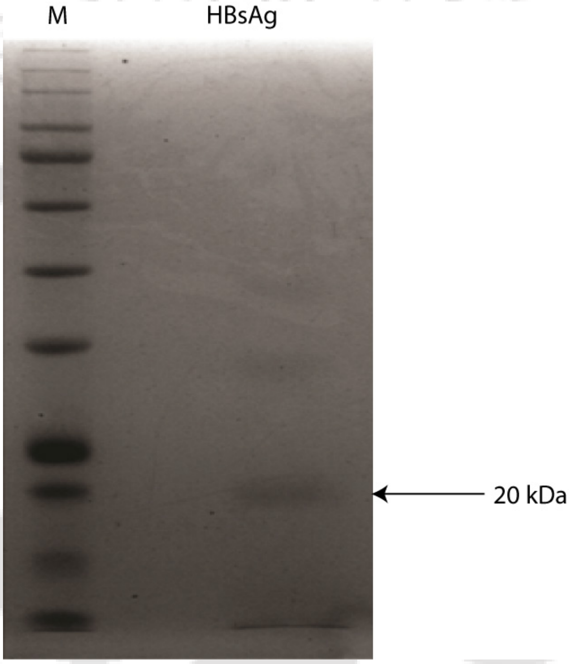

Figure 4.27: SDS-PAGE analysis of recombinant HBsAg. Expected size of the protein is 20 kDa. M=Protein marker.

We performed a sandwich ELISA to find out the detection limit for MBP-scFv, in terms of IU/ml of HBsAg. For this, we coated an ELISA plate with a commercially available anti-HBsAg antibody (Sigma). Seven different concentrations of HBsAg were added to the wells for 1 hour, followed by MBP-scFv (1μg/ml). Anti-MBP (1:1000 dilution) was then added as the primary antibody, followed by the secondary antibody, Anti-mouse HRP (1:1000 dilution). The ELISA was developed using OPD in substrate buffer (0.5 mg/ml).

The result of the ELISA is shown in Figure 4.28. It is evident from the figure that the MBP-scFv has linear binding in a very long concentration range of HBsAg and it can detect the antigen even at HBsAg concentration of 8.18 x 10^{-3} IU/ml.

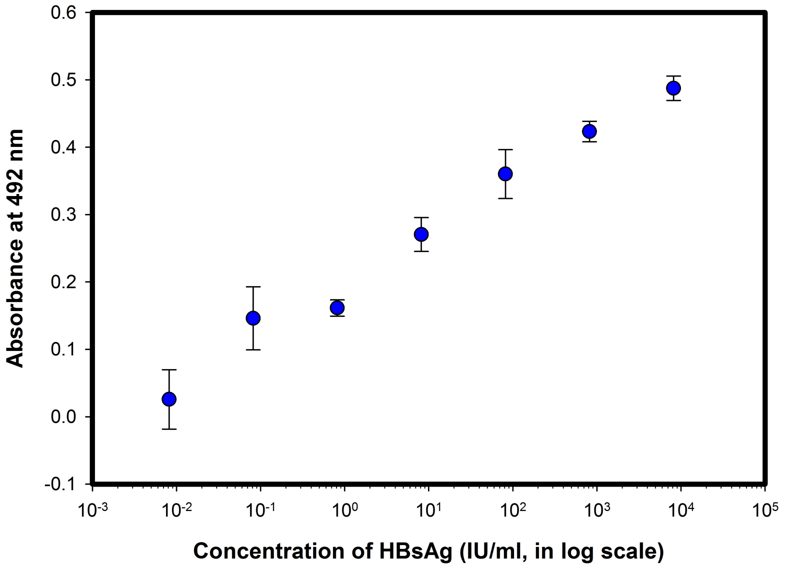

FIGURE 4.28: Sandwich ELISA to check the binding of HBsAg with the MBP-scFv. ELISA plate was coated with a commercially available anti-HBsAg antibody to capture HBsAg added in different concentrations (8.18 x 10^{-3} IU/ml to 8.18 x 10^{2} IU/ml). Bound HBsAg was detected by MBP-scFv followed by anti-MBP antibody. Average value of four independent wells were shown.

4.6 Summary

In this chapter, various attempts to produce the scFv in soluble form using the pET-22b(+) clone were shown. Since this approach failed to obtain the protein in soluble form, cloning was subsequently done in pMAL-p5x vector to express the recombinant protein as an MBP-tagged molecule. Purified MBP-scFv was obtained and then functional assays were done to confirm the binding of the recombinant protein to HBsAg. We have used the purified MBP-scFv, along with the commercially available anti-HBsAg antibody to functionalize the SAW device.

Chapter 5

Immobilization of Antibodies on Sensor surface

In this chapter, functionalization and immobilization of antibodies to the sensor surface on the SAW device is discussed. To achieve high selectivity, the device surface needs to be properly functionalized for biomolecule immobilization. There are numerous ways in which a surface can be functionalized. For our work, 11-Mercaptoundecanoic acid (11-MUA) has been used as the linker molecule, and then EDC/NHS method has been used for covalently linking the mouse Anti-HBsAg antibody. ATR-FTIR, FESEM and AFM imaging was done in the consequent step, which confirmed the immobilization of Anti-HBsAg antibody on the sensor surface.

5.1 Scheme of Functionalization

The proposed SAW dual delay line sensor has a gold thin film in the area between the input and output IDTs. This area is used as the sensor surface to target HBsAg molecule by immobilizing the antibody to the gold surface.

The antibody cannot be directly attached to the gold surface. Now, sulphur exhibits aurophilicity, which is a natural tendency of sulphur to be covalently linked to gold [123]. This property of Au-S interaction led us to choose 11-Mercaptoundecanoic acid (11-MUA) as the linker molecule. The piezoelectric substrate was dipped in a 1 mM ethanolic solution of 11-MUA for 12 hours. This led to the formation of a co-ordinate bond between the sulphur in 11-MUA and the gold in the thin film, as sulphur has a lone pair of electrons and bonds easily with gold. Also, the flexible long carbon chain of 11-MUA serves as a spacer to minimise interference between the protein molecules attached to 11-MUA at the top and the gold film [123].

The next step in the functionalization process was to attach the antibody using the reliable EDC/NHS method. The 11-MUA linker molecule has a -COOH group at the end, which cannot be directly conjugated to the -NH_2 group present in proteins. The -COOH group needs to be activated for this reason. This is acheived using the EDC/NHS method. (1-Ethyl-3-(3-dimethylaminopropyl)-carbodiimide) or EDC, is a crosslinking agent used to couple carboxyl or phosphate groups to primary amines, while N-hydroxysuccinimide (NHS) increases the stability of the active ester. The substrate is dipped in a 1:1 volume mixture of EDC and NHS.

In the final step, the Anti-HBsAg antibody, taken in acetate buffer was immobilized on the activated surface. Thus, the SAW device was ready to be used as a sensor for the capture of the target molecule(HBsAg). The process flow for immobilization of Anti-hepatitis-B surface antigen (Anti-HBsAg) on a piezoelectric substrate is shown in Figure 5.1.

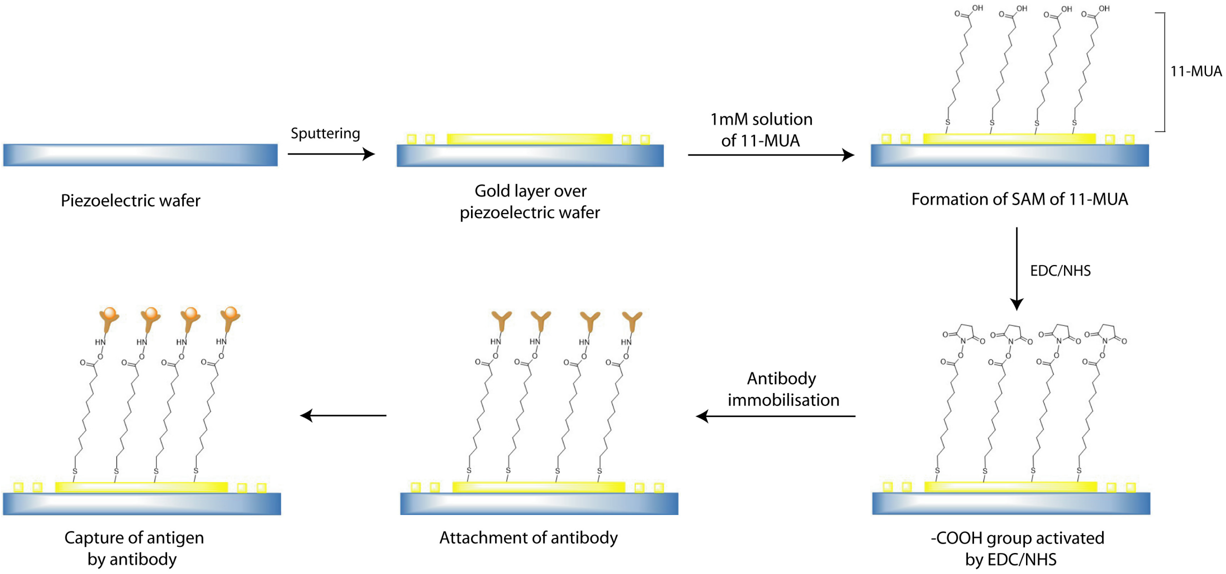

FIGURE 5.1: Schematic representation of the process flow for antibody immobilization on the sensor surface

5.2 Methods for Characterisation

1. **Energy Dispersive X-ray Analysis (EDX)**: EDX works on the fundamental principle that each element has a unique atomic structure and allows a unique set of peaks on its electromagnetic emission spectrum. The elemental composition of the samples during functionalization was observed by an EDX instrument (Model:Sigma, Make: Zeiss, Germany). The samples were mounted on stubs with conductive carbon tape.

2. **Atomic Force Microscope (AFM)**: AFM is a tool that is widely used for imaging and manipulating matter at the nanoscale. In our work, we have used an AFM (Model: Innova SPM, Make: Bruker) for morphological analysis of the sample. The mode used for characterisation was the tapping mode at a resonance frequency of 300 kHz. The cantilever tip used for the purpose had dimensions 125 μm x 30 μm x 4 μm, and a spring constant of 40 N/m.

3. **Field Emission Scanning Electron Microscopy (FESEM)**: The surface of the samples were scanned using an FESEM (Model: JSM-7610F, Make: Jeol). The samples were attached to the stub on the sample holder and scanned at an operating voltage of 15 kV and at 150,000X magnification.

4. **Fourier Transform Infrared Spectroscopy (FTIR)**: FTIR (Model: Frontier, Make: Perkin-Elmer, USA) was done in attenuated total reflection(ATR) mode to analyze the samples during functionalization. The scans were carried out in the wavelength range 4500-500 cm^{-1}, with a resolution of 4 cm^{-1}.

5.3 Experimental Section

5.3.1 Gold Film Deposition

In the first step, a gold coating of 20 nm was deposited in a 41°YX $LiNbO_3$ substrate by using a sputter coater (Quorum Technologies). The deposition was done at a voltage of 1 kV and current 5 mA for 5 minutes. The deposition of the gold thin film was checked by EDX and AFM analysis.

Figure 5.2 shows the EDX analysis before and after the deposition of the gold film. Lithium (atomic number=3) shows no peaks in the spectrum because elements below atomic number 8 cannot be detected easily with EDX. Figure 5.2(B) shows the presence of peaks for gold (Au) in the spectrum, thus indicating the proper deposition of a gold film. The spectra are taken in the range 0 to 10 keV.

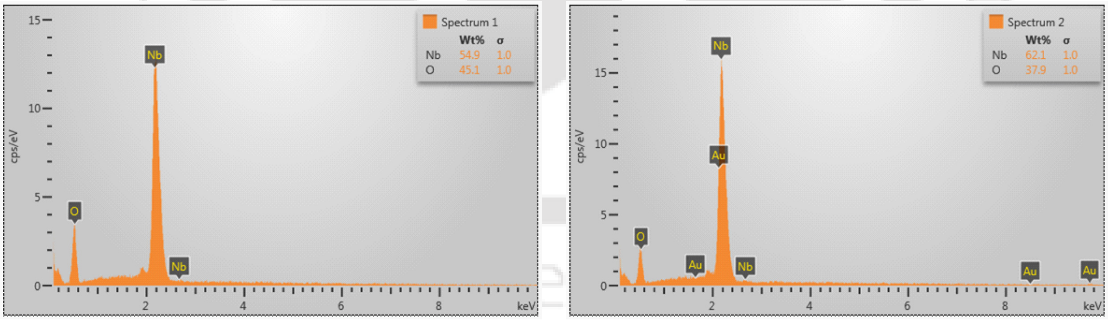

(A) (B)

FIGURE 5.2: EDX analysis of: (A) 41°YX $LiNbO_3$ substrate, and (B) Gold film sputtered over 41°YX $LiNbO_3$ substrate.

The image obtained by AFM after deposition of the gold on the 41°YX $LiNbO_3$ substrate is shown in Figure 5.3. An area of size 5μm x 5μm was chosen for scanning with the AFM tip. As can be seen in Figure 5.3, a layer with negligible roughness can be seen, which indicates the fine quality of gold film deposited by sputtering.

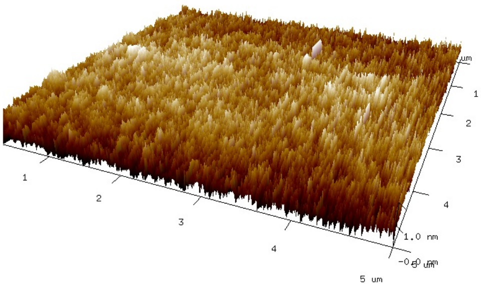

FIGURE 5.3: AFM image of gold film on 41°YX $LiNbO_3$ substrate

5.3.2 Growth of 11-MUA SAM

The gold coated 41°YX $LiNbO_3$ substrate was dipped for 12 hours at 4°C in an ethanolic solution of 1 mM 11-Mercaptoundecanoic acid (Sigma). Then, it was washed with ethanol. To check the development of a self-assembled monolayer (SAM) of 11-MUA on gold, AFM, FESEM and ATR-FTIR analysis were used.

Figure 5.4 shows the AFM image of the surface topology after the growth of a self-assembled monolayer of 11-MUA. On scanning an area of size 5 μm x 5 μm, an average height of 13.6 nm was observed.

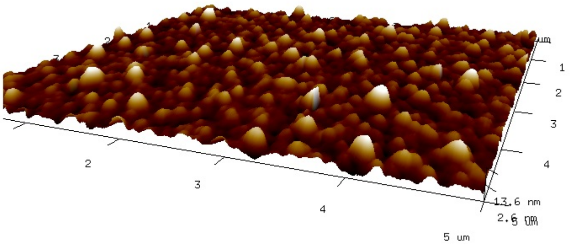

FIGURE 5.4: AFM image of 11-MUA on 41°YX $LiNbO_3$ substrate

The surface morphology of the sample was observed by Field Emission Scanning Electron Microscope (FESEM), as shown in Figure 5.5. No metal coating was done on the sample surface. The image was taken at 15 kV operating voltage and a magnification of 150,000X. Formation of island-like structures are seen on the surface, indicating the possibility of proper SAM formation.

Figure 5.6 shows the ATR-FTIR analysis of the sample. 11-MUA has a chemical formula $HS(CH_2)_{10}COOH$. The spectrum, taken in the wavelength range 4500-500 cm^{-1} with a

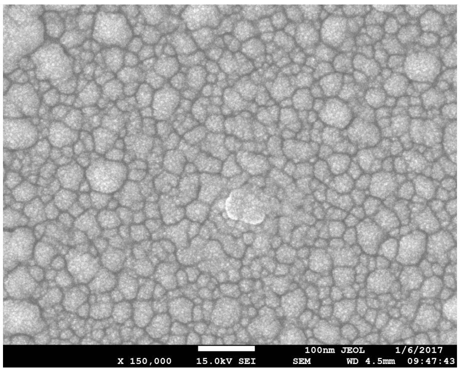

FIGURE 5.5: FESEM image of 11-MUA on 41°YX $LiNbO_3$ substrate

resolution of 4 cm^{-1}, shows absorption dips that indicate the presence of –SH, -COOH and –CH_2 bonds at 2900, 1700 and 1100 cm^{-1} respectively [124]. This indicates the presence of 11-MUA over the gold thin film.

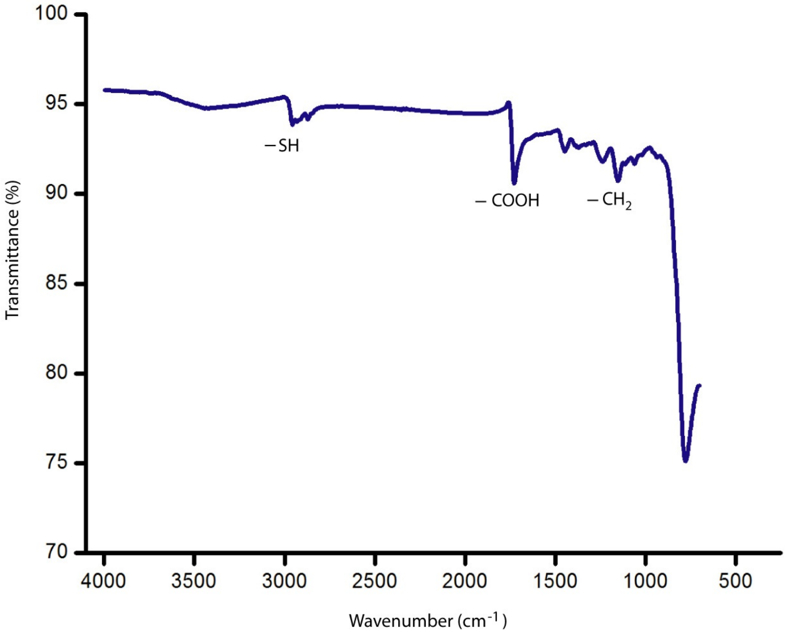

FIGURE 5.6: ATR-FTIR image of 11-MUA on 41°YX $LiNbO_3$ substrate

5.3.3 Immobilization of Anti-HBsAg Antibody

In the next step, the substrate is dipped for 1 hour in 1:1 volume mixture of 0.1 M N-hydroxysuccinimide (NHS) and 0.4 M EDC [Biacore]. This is done to activate the

-COOH group present in 11-MUA.

In the final step, the device with the activated carboxylic group is dipped in Monoclonal Anti-HBsAg antibody (Sigma) in acetate buffer, pH=5.0 (1:1000 dilution) at 4 °C for 12 hrs. The reason for this particular pH selection is because buffering the pH to about 1 pH point below the isoelectric point (pI) of the protein helps to bind the primary amine of the protein to the carboxylic acid on the surface activated with EDC-NHS. This happens because proteins carry a net positive charge below their pI. The pI of the purified MBP-scFv is 5.5. Hence, the same acetate buffer (pH=5.0) can be used for immobilizing it to the sensor surface. AFM, FESEM imaging and ATR-FTIR analysis were done in the subsequent step, which confirmed the immobilization of Anti-HBsAg on the substrate surface.

Figure 5.7 shows the AFM image of the surface topology after the immobilization of antibodies over 11-MUA. On scanning an area of size 5μm x 5μm, an average height of 24.1 nm was observed. Since this average height obtained was more than the average height of 13.6 nm observed after the growth of 11-MUA, it can be said that the immobilization process was successfully done.

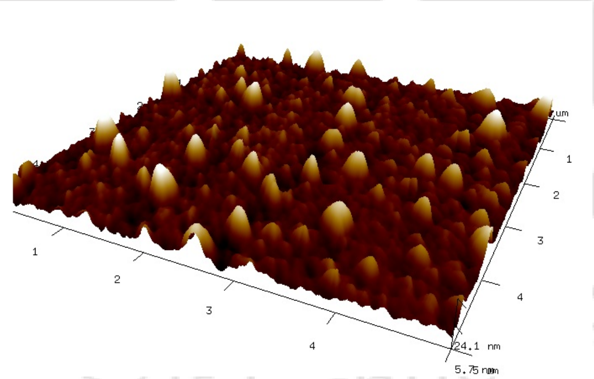

FIGURE 5.7: AFM image of surface after antibody immobilization

The FESEM image in Figure 5.8 shows the surface morphology of the sample after antibody immobilization. The image was taken at 15 kV operating voltage and a magnification of 150,000X. Formation of uniformly deposited island-like structures similar to the ones after 11-MUA SAM formation were observed.

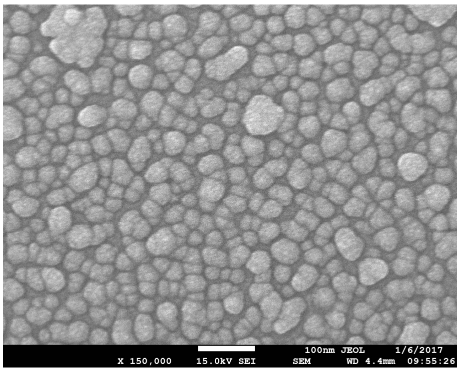

FIGURE 5.8: FESEM image of surface after antibody immobilization

Figure 5.9 shows the ATR-FTIR analysis of the sample after antibody immobilization. The spectrum, taken in the wavelength range 4500-500 cm^{-1} with a resolution of 4 cm^{-1}, shows absorption dips that indicate the presence of Amide A and Amide I bonds at 3300 and 1500 cm^{-1} respectively [148]. This indicates the possibility of successful functionalization of antibody on the piezoelectric wafer surface.

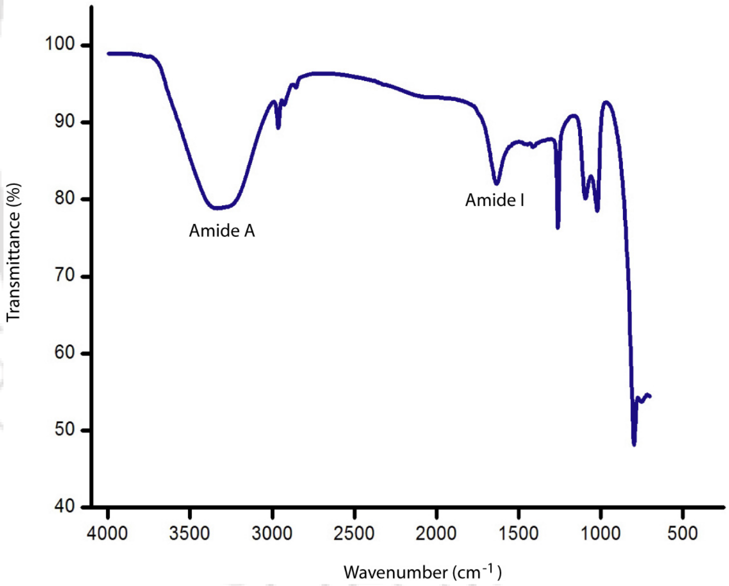

FIGURE 5.9: ATR-FTIR image of surface after antibody immobilization

5.3.4 Quantitative Optimisation of Anti-HBsAg Required for Functionalization

To perform optimisation of the antibody functionalization, Anti-HBsAg antibody in 10 mM sodium acetate buffer, pH=5.0 (Biacore) with different concentrations (1 μg/ml, 10 μg/ml and 100 μg/ml) were immobilized on three EDC/NHS activated substrates and left at 4°C for 12 hrs. Subsequently, an ELISA like method was used to detect the presence of the antibody on the surface. The method is explained schematically in Figure 5.10. The substrate was dipped in anti-mouse HRP-conjugated antibody in PBS with 2% BSA (1:1000 dilution) for one hour at room temperature. This antibody will bind to the Mouse anti-HBsAg antibody immobilized on the sensor surface. Then, the substrate were washed with PBS, after which the ELISA was developed using OPD (0.5 mg/ml) as substrate. For different concentrations of antibody used, different values of absorbance was seen. Plotting these values give us the results of quantitative optimization, as shown in Figure 5.10.

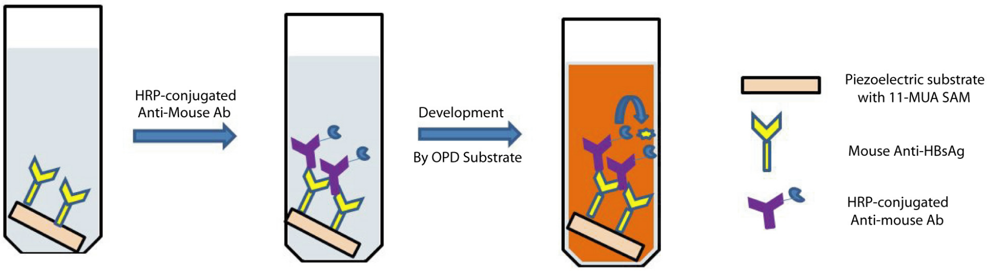

(A)

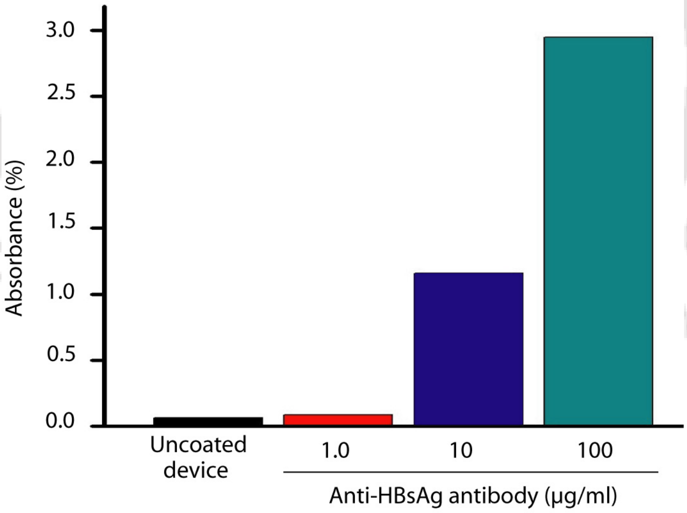

(B)

FIGURE 5.10: Detection of anti-HBsAg antibody immobilized on a 41°YX $LiNbO_3$ substrate. (A) Schematic representation of the ELISA like method used. (B) Results obtained by the method to detect antibody immobilization

The absorbance data indicates that the Anti-HBsAg antibody at the concentration of 10 μg/ml is sufficient for proper immobilization on the sensor surface.

5.4 Summary

From the work carried out, it can be concluded that antibody immobilization on the piezoelectric substrate was successfully obtained by the method followed. The same method was followed for the attachment of MBP-scFv antibody. The EDC/NHS method worked efficiently to attach the protein onto the linker molecule used. Analysis carried out by EDX, AFM, FESEM and ATR-FTIR showed the success of immobilization, and hence, we can proceed to the detection of antigen by the immobilized antibody. Also, the ELISA like method carried out gave us an optimum concentration of 10 µg/ml for proper immobilization. Hence, the surface has been prepared for capture of appropriate antigen, which is Hepatitis B Surface Antigen (HBsAg) in our case.

Chapter 6

Detection of HBsAg using SAW Dual Delay Line

This chapter deals with the utilisation of SAW dual delay line to achieve specific and quantitative detection of HBsAg. The measurement setup used for the detection is explained, alongwith the measurement scheme that is followed. The device consists of a piezoelectric substrate, on which two delay lines, each consisting of two interdigitated transducers (IDTs): a transmitter IDT and a receiver IDT, are separated by a sensing layer. The piezoelectric substrates considered were 41°YX $LiNbO_3$ and 36°YX $LiTaO_3$ to generate Shear horizontal SAW (SH-SAW), while gold was chosen as the IDT metal. The IDTs were fabricated for three different dimensions: 4 µm, 8 µm and 12 µm. Hence, we have six devices in total, working in six different resonant frequencies. A comparison of the detection results of all the devices is done in this chapter.

6.1 Measurement Setup

An aluminium metal plate fabricated in the Central workshop at IIT Guwahati was used for mechanical support of the entire system. On either side of the plate, two holes were drilled to accommodate the straight Bayonet Neill Concelman (BNC) bulkhead jacks for the four ports of the device. A coaxial adapter (SMA-F to BNC-M) was then used to connect to the coaxial cables of the Vector Network Analyzer (Model: PNA-L, Make: Keysight). The SAW dual delay line device to be used as the sensor was placed over a Printed Circuit Board (PCB), and wires were soldered onto the bond pads of the device. As described in Chapter 3, a matching circuit, generally comprising of an inductor (L) and a capacitor (C) is needed for maximum power transfer for all four ports of a delay line. So the matching circuits were connected to the ports, from which connections were made using wires to the BNC connector for electrical connection.

An individual dual delay line and the experimental setup for the quantitative measurement of HBsAg detection is shown in the Figure 6.1.

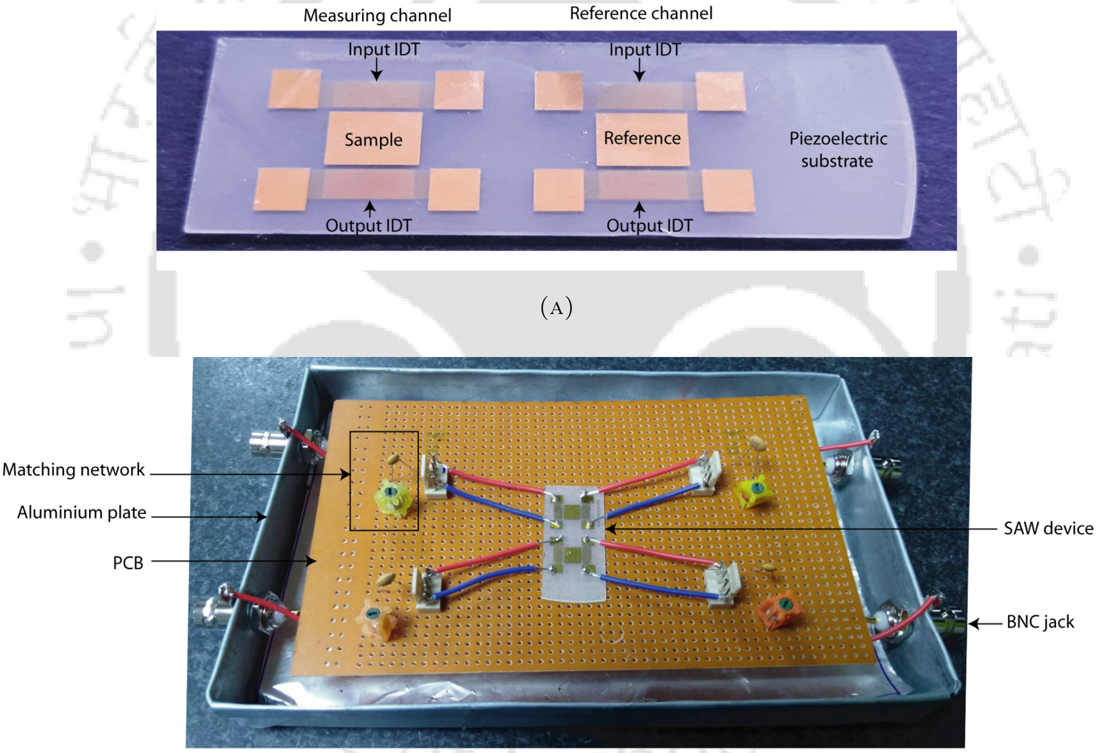

(A)

(B)

FIGURE 6.1: (A) A SAW dual delay line, and (B) Measurement setup used in this work

The connection of the measurement setup to the VNA is shown in Figure 6.2. The BNC jacks attached to the aluminium plate were connected to the coaxial cables of the VNA via a coaxial adapter.

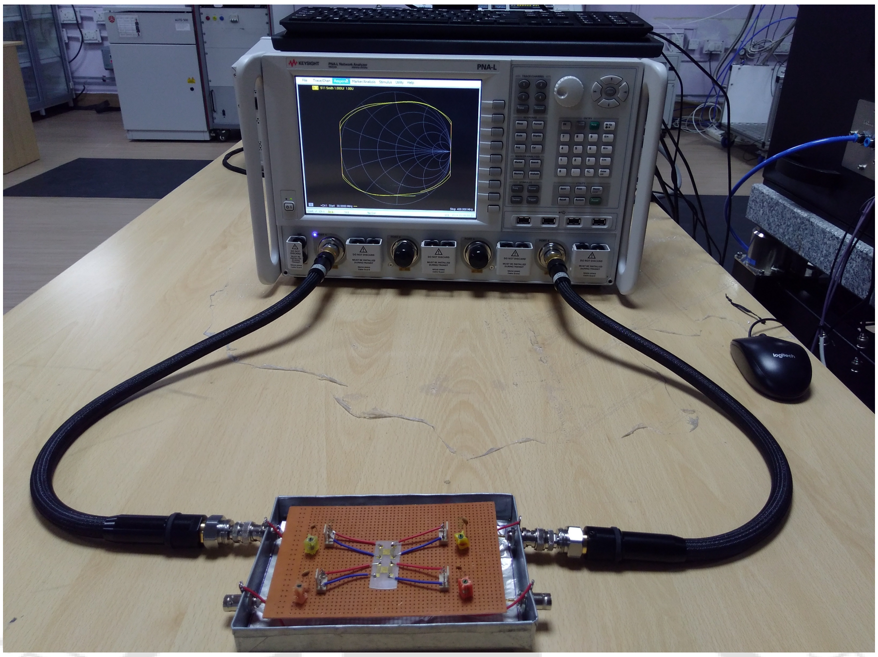

FIGURE 6.2: Connection of SAW dual delay line to VNA

6.2 Measurement Scheme

The dual-delay line relies on the high affinity of antigen-antibody interaction for the precise detection of HBsAg by means of our sensor. Two sets of antibodies were immobilised on the sensor surface for targeting the HBsAg in two separate set of experiments:

1. Commercially available Mouse Anti-HBsAg antibody (Sigma)
2. Anti-HBsAg MBP-scFv produced in our laboratory (as discussed in Chapter 4).

As discussed in the previous chapter, the detection experiments were performed on the gold sensing area formed between the transmitting and receiving IDTs. Both these areas on the sample and reference SAW device were coated with Mouse Anti-HBsAg antibody that can bind with HBsAg. Eight samples of different concentrations of HBsAg, starting from 0.0818 IU/ml to 818000 IU/ml were prepared in Phosphate Buffered Saline (PBS), and used for the sample channel. For the reference channel, PBS was used as the analyte. The resonance frequency shift was monitored for each concentration to detect the specific binding of HBsAg to Anti-HBsAg antibody, which was calculated by the

S_{21} measurements obtained using a VNA. Figure 6.3 shows a schematic to explain the connection and the measurement with the VNA.

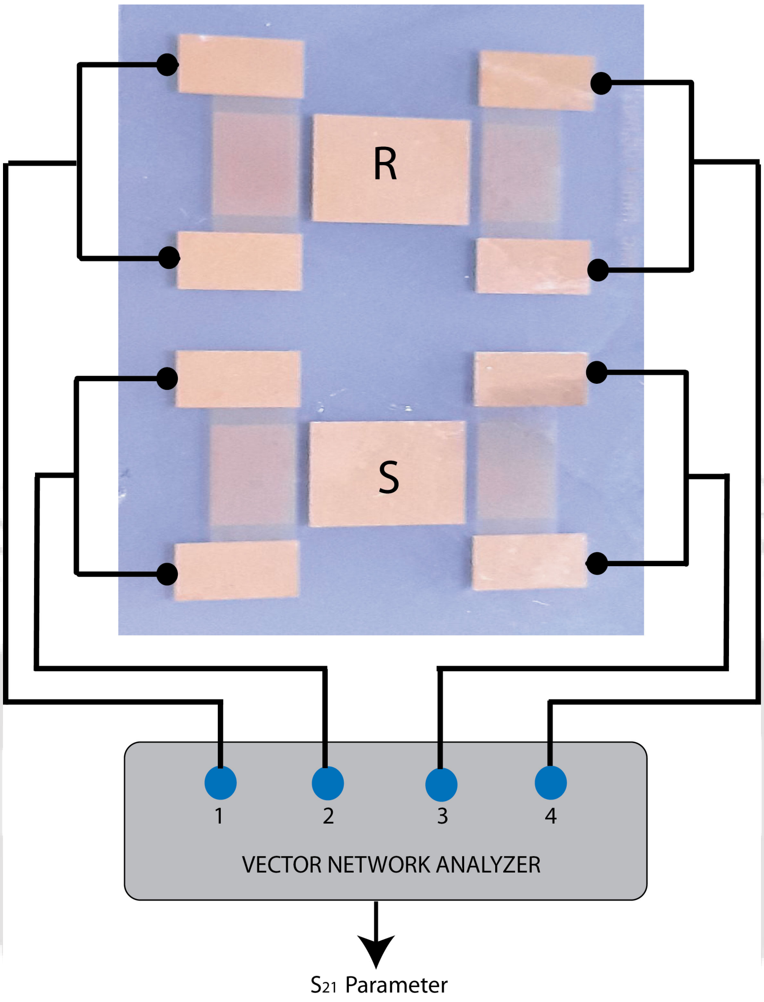

FIGURE 6.3: Measurement of S-parameter with VNA

A regeneration step was included after every reading, which included washing the sensing area with acetate buffer (pH 5.0) to remove the HBsAg bound to the antibody from the earlier sample. After the regeneration, the sensing areas were again washed thrice with PBS to make it ready for subsequent samples. The change in resonant frequency because of regeneration and washing in both channels was taken each time, to compensate for any change in the original resonance frequency of the delay lines. After that, a new sample of HBsAg and PBS were added to the sample and reference channels respectively. Next, the frequency shift of the sample SAW device was subtracted from the frequency shift of the reference SAW device in order to eliminate any changes other than mass change due to the binding of HBsAg.

Figure 6.4 shows the detection scheme followed in the experiments for detection of HBsAg.

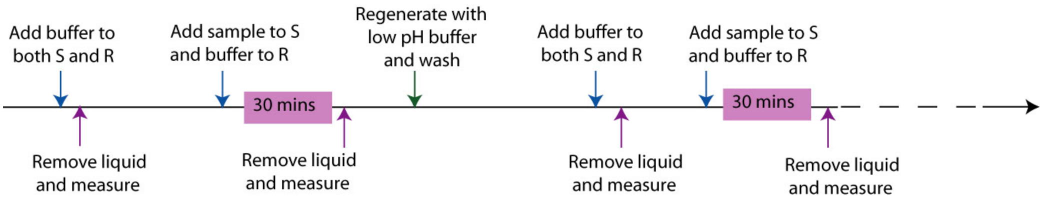

Figure 6.4: HBsAg Detection scheme for multiple samples with intermediate regeneration and washing

Let Δf_S denotes the change in resonant frequency, f_0 in the sample delay line due to the addition of PBS buffer and HBsAg sample, and Δf_R denote the same in the reference delay line due to the addition of PBS once as the buffer, and then as the analyte.

$$\Delta f_S = f_{buffer,S} - f_{sample} \tag{6.1}$$

$$\Delta f_R = f_{buffer,R} - f_{reference} \tag{6.2}$$

The corrected change in frequency Δf_C for each sample is thus obtained by:

$$\Delta f_C = \Delta f_S - \Delta f_R \tag{6.3}$$

If f_0 denotes the resonant frequency of a delay line, the change in resonant frequency due to the addition of reference and sample is graphically shown in Figure 6.5.

Δf_C is plotted against the concentration of the HBsAg sample to obtain the detection profile of the sensor. After the readings for the Mouse Anti-HBsAg antibody are taken, the sensing areas are treated with a solution consisting of 2:1:66 molar ratio of NH_4OH, H_2O_2 and H_2O respectively [136]. This eradicates all linker molecules and antibody attached to the gold surface. The idea behind this step is to regenerate the gold layer, as a result of which the sensor can be reused and thus help in cost-saving. Subsequently,

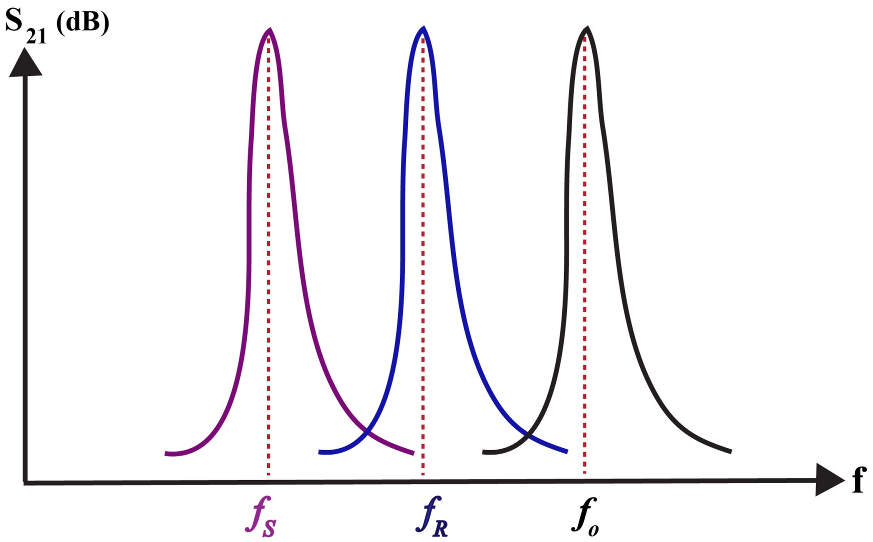

Figure 6.5: Schematic diagram explaining change in resonant frequency

the entire process of functionalisation, as discussed in Chapter 5, is repeated for the anti-HBsAg MBP-scFv. Then, the measurements for Δf_C are taken over the same linear range of concentration of HBsAg. Finally, a comparison is done among the two sets of data.

6.3 Detection Results

Using the method explained in the previous section, experiments were done under varying conditions to derive meaningful insights into the operation of the SAW dual delay line sensor. The different experiments, with the results derived from them, are explained in the following subsections:

6.3.1 Effect of Sample Incubation Time on Measurement

Binding of an antigen to an antibody is a time dependent process. Therefore, we need to check the optimum incubation time required after addition of HBsAg samples, prior to making measurements. The dual delay line sensor on 41°YX $LiNbO_3$, with IDT width 4 μm was first tested for optimizing the incubation time needed for the binding of the

HBsAg onto the Mouse Anti-HBsAg antibody functionalised on the sensing area. 10 ng/ml HBsAg in Phosphate Buffered Saline (PBS) buffer was used as the analyte in the sample line, while PBS was used in the reference line for each measurement. 10 ng/ml Bovine Serum Albumin (BSA) was used as the negative control. Volume of analyte was 30 μl on both the lines. Different incubation times of 2, 5, 10, 15, 20 and 30 minutes were used. The bar diagram in Figure 6.6 below shows the shift in Δf_C (in kHz) for different incubation times.

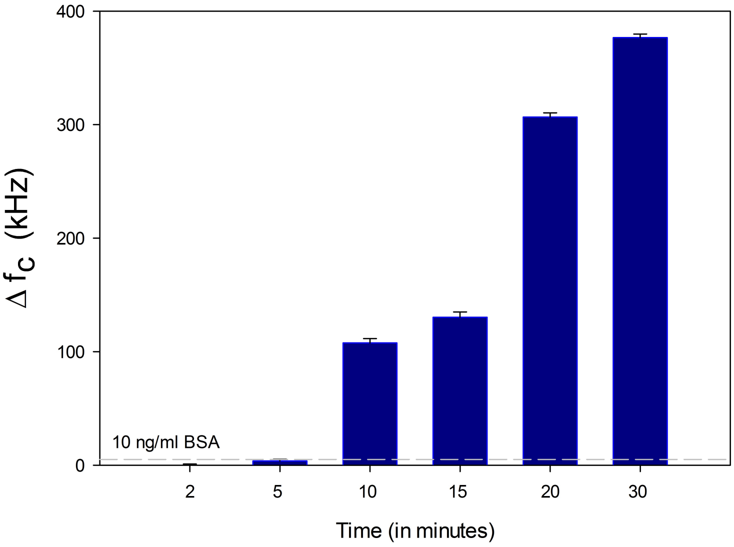

FIGURE 6.6: Identification of suitable incubation time for detection of HBsAg. HBsAg in PBS (10 ng/ml) was used as analyte and incubated for different durations. Subsequently, Δf_C for each sample was measured. The horizontal dotted line represents the reading for 10 ng/ml BSA in PBS incubated for 30 minutes on the sensor. BSA was used as the negative control.

As we can see from the graph, an incubation time of 30 minutes gave the best change in frequency, indicating that proper antigen-antibody binding occurred at the sensing area in this time interval. Hence, from this point onward, all subsequent experiments were performed keeping the incubation time constant at 30 minutes.

6.3.2 Effect of Regeneration on Resonant Frequency

The reusability of the sensor was checked by measuring the resonant frequency of the measuring and reference channel after each round of sample measurement and regeneration. The device used was the dual delay line sensor on 41°YX $LiNbO_3$, with IDT width

4 μm. The graph in Fig. 6.7 shows the variation in resonant frequency of the sample and reference lines for eight sequential samples.

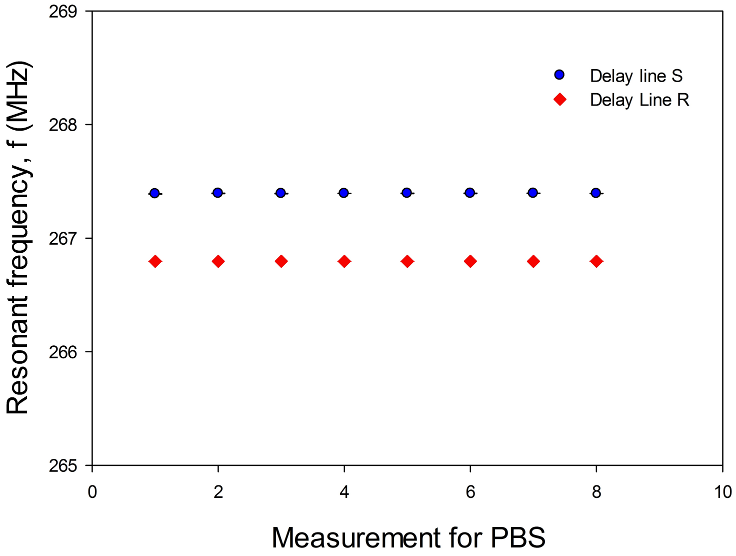

FIGURE 6.7: Effect of regeneration on resonant frequency on both sample and reference delay line

As can be seen from the graph, the change in base response was extremely small. This indicates that proper regeneration has occurred and the sensor can be used to measure as many as eight samples, provided proper regeneration is done as the intermediate step between each sample.

6.3.3 Dose Dependent Detection of the HBsAg

For this experiment, eight samples of HBsAg in a linear range of 0.0818 IU/ml to 818000 IU/ml in PBS was prepared from a stock solution of 8180000 IU/μl. 10 ng/ml Bovine Serum Albumin (BSA) was used as the negative control in each case. Measurements were done for all six devices, and a comparison of the generated data is done, as can be seen in Figure 6.8, 6.9 and 6.10.

Figure 6.8(A) and 6.8(B) show the variation in Δf_C when different concentrations of HBsAg were detected with Mouse Anti-HBsAg antibody functionalised on the sensing surface for three devices on 41°YX $LiNbO_3$ and the 36°YX $LiTaO_3$ substrate, with IDT widths 4 μm, 8 μm, and 12 μm respectively. With Mouse Anti-HBsAg antibody, the highest change in Δf_C for the device with IDT widths 4 μm was found to be 890 kHz on 41°YX $LiNbO_3$ substrate, while it was found to be 576 kHz for the device on 36°YX $LiTaO_3$ substrate.

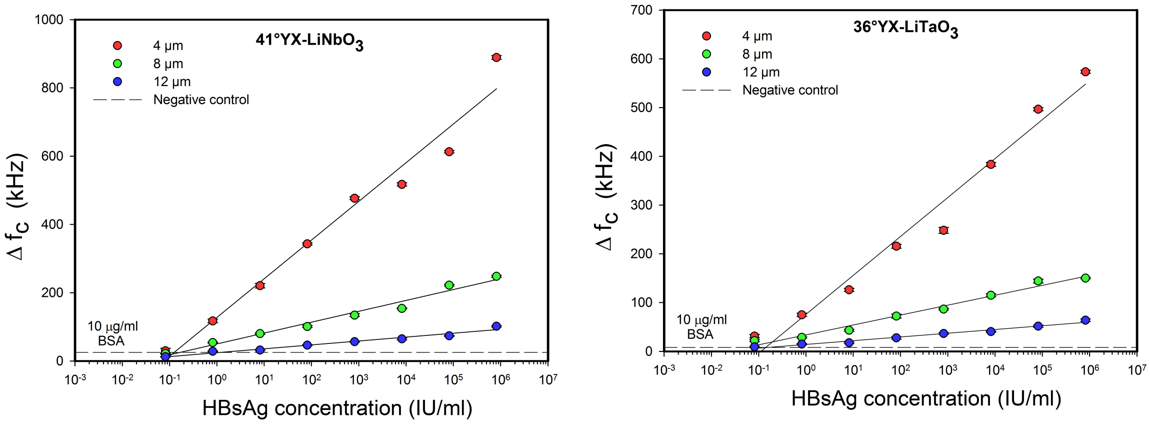

(A) (B)

Figure 6.8: Detection of HBsAg using Mouse Anti-HBsAg antibody for devices with varying IDT widths on (A)41°YX $LiNbO_3$ and (B)36°YX $LiTaO_3$ substrates

Figure 6.9(A) shows the variation in Δf_C when different concentrations of HBsAg are detected with MBP-scFv functionalised on the sensing surface for three devices on 41°YX $LiNbO_3$ substrate, with the same IDT widths mentioned earlier. Figure 6.9(B) shows the same variation for three devices on 36°YX $LiTaO_3$ substrate. With MBP-scFv, the highest change in Δf_C was achieved for the device with IDT width 4 μm, which was found to be 640 kHz on 41°YX $LiNbO_3$ substrate, while it was found to be 410 kHz for the device on 36°YX $LiTaO_3$ substrate. This difference in resonant frequency change can be attributed to the fact that the velocity of SAW is higher in 41°YX $LiNbO_3$, which leads to higher frequency of operation at the same wavelength, and hence higher change in frequency due to mass loading.

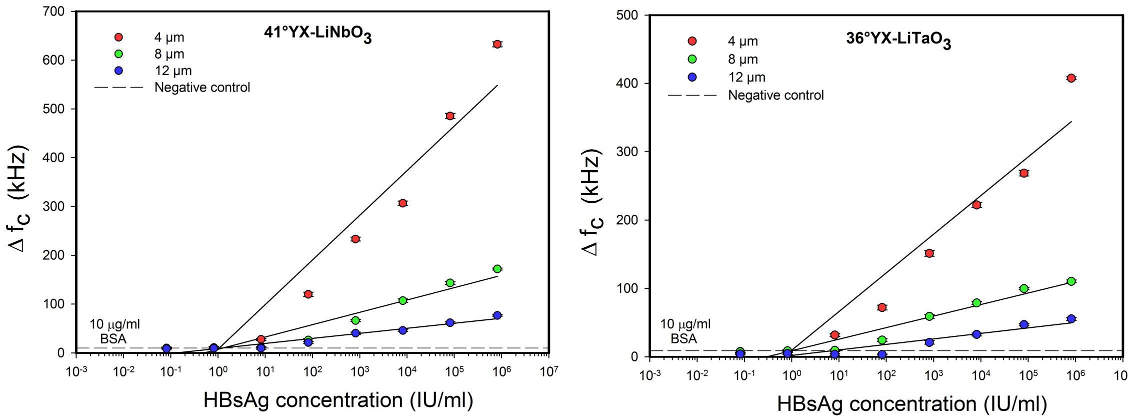

(A) (B)

Figure 6.9: Detection of HBsAg using recombinant MBP-scFv for devices with varying IDT widths on (A) 41°YX $LiNbO_3$ and (B) 36°YX $LiTaO_3$ substrates

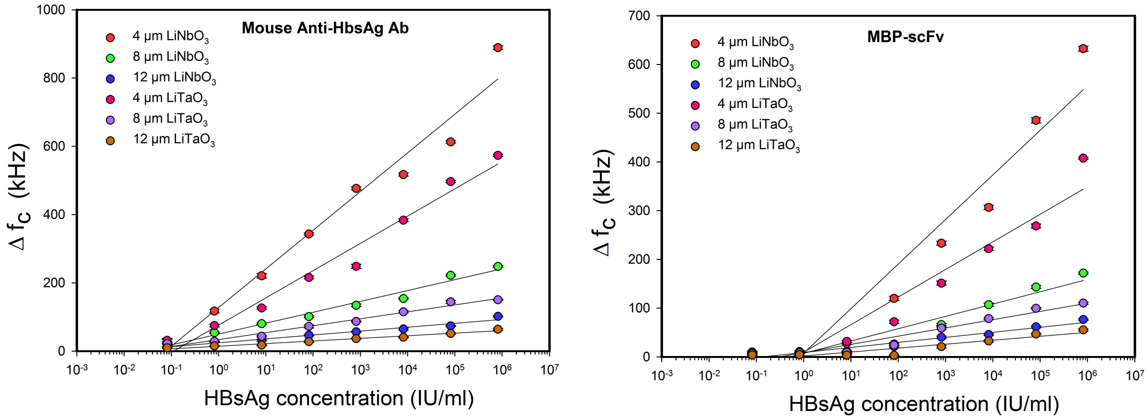

(A) (B)

Figure 6.10: Performance of all six devices with different immobilised antibody

Finally, in Figure 6.10(A) and 6.10(B), a comparison is shown for the Δf_C plotted against the change in concentration of HBsAg for all 6 devices with Mouse Anti-HBsAg and MBP-scFv antibody immobilization respecively. From these graphs, it is evident that the devices fabricated on 41°YX $LiNbO_3$ shows a 1.5 fold increase in Δf_C compared to the devices fabricated on 36°YX $LiTaO_3$. Also, there is a 1.3 fold decrease in Δf_C while detecting MBP-scFv compared to Mouse Anti-HBsAg antibody. This behaviour might be attributed to the repeated stripping and regeneration performed on the sensing layer, which might have led to the deterioration in quality of the gold film.

6.3.4 Detection of HBsAg in Human Serum

In all previous experiments, samples of HBsAg were prepared by dissolving the protein in PBS. To test the ability of the sensors to detect HBsAg in human serum, the measurements were done with the same range of concentration of HBsAg as earlier, but the samples were human serum spiked with HBsAg. As shown in Fig. 6.11, with Mouse Anti-HBsAg antibody functionalised on the sensing surface for the device with IDT width 4 μm on 41°YX $LiNbO_3$ substrate, Δf_C showed a value of 66 kHz for the highest concentration of 818000 IU/ml of HBsAg, and a linear range of operation was seen from 81.8 IU/ml to 818000 IU/ml. The reason for this decrease in quality of performance of the sensor might be due to the decline in the quality of the gold thin film that was used as the sensing area because of repeated regeneration. Thus, the sensor shows prospect to be used as a label-free HBsAg detection sensor.

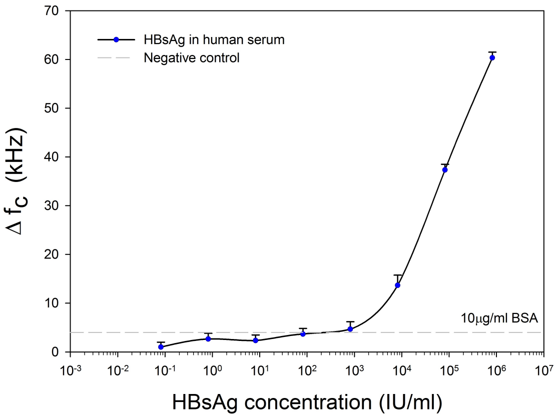

FIGURE 6.11: Detection of HBsAg in human serum

6.3.5 Comparison of Limit of Detection (LoD)

Limit of detection (LoD) can be defined as the lowest quantity of the analyte that can be detected. If σ is the standard deviation in Δf_C, then LoD is calculated by the mathematical expression:

$$\text{LoD} = 3{*}\sigma \tag{6.4}$$

Let us consider the detection of HBsAg in PBS, using the functionalised MBP-scFv and Mouse Anti-HBsAg antibody. As can be seen from the graphs in Figure 6.10, the devices showed a linear relationship between the frequency shift and the antigen concentration in the range of 0.0818 IU/ml to 818000 IU/ml. Sensitivity of the device was evaluated using the slope of the graphs, and the values of LOD are shown in Table 6.1.

TABLE 6.1: Comparison of LoD values

Type of substrate	IDT width (μm)	LOD (Limit of detection) in IU/ml	
		MBP-scFv	Mouse Anti-HBsAg Ab
41°YX $LiNbO_3$	4	1.541	0.183
	8	1.333	0.155
	12	1.364	0.156
36°YX $LiTaO_3$	4	1.592	0.143
	8	1.503	0.139
	12	1.348	0.155

6.4 Summary

In this chapter, we have demonstrated the detection of HBsAg using SAW sensor functionalised with two different antibodies: MBP-scFv and Mouse Anti-HBsAg antibody. The delay line with 4 μm IDT width on 41°YX $LiNbO_3$ substrate was found to outperform the other devices in terms of change in frequency observed. LOD was found to be better in case of the devices functionalised with mouse Anti-HBsAg antibody than in case of the devices functionalised with the recombinant scFv. We have to keep in mind that, first we have functionalised the devices with mouse anti-HBsAg antibody, performed experiments and then stripped off the antibody from the devices. The same devices were functionalised with MBP-scFv. This stripping and regeneration may have affected the performance of the sensors with MBP-scFv.

Chapter 7

Conclusion and Future Prospects

7.1 Conclusion

This chapter outlines the results obtained and gives an insight into the future prospects of the work described in this thesis. The work encompasses the design, simulation and fabrication of a Surface Acoustic Wave based dual delay line device and its use as a sensor for the detection of HBsAg.

The use of COMSOL Multiphysics has been discussed for finite element simulation of six SAW devices with different device dimensions. COMSOL simulation helps to optimise the device characteristics prior to microfabrication. The substrates, 41°YX $LiNbO_3$ and 36°YX $LiTaO_3$ were chosen to generate shear-horizontal SAW to obtain maximum efficiency for liquid sensing applications. The displacement profile, voltage profile and generation of SH-SAW were simulated, and based on these data, the IDT dimensions were finalised to obtain maximum efficiency. These parameters were subsequently used during the microfabrication of the SAW devices. The microfabrication of the SAW delay line was discussed in detail, alongwith the characterisation of the devices. The S-parameters of all devices were measured using a Vector Network Analyzer. Matching networks were designed based on the impedance values obtained from the S-parameters. The values of resonant frequency agreed with the theoretical values, and hence we moved on to the production of an anti-HBsAg scFv antibody. The various attempts to produce the scFv in soluble form have been discussed. Purified MBP-scFv was obtained and then functional assays were done to confirm the binding of the recombinant protein to HBsAg. Immobilisation of the antibody to the sensor surface was achieved using an 11-MUA linker molecule, and the various steps undertaken were analysed by EDX, AFM, FESEM and ATR-FTIR. Also, an ELISA like method was adopted to detect the optimum concentration of antibody for proper immobilization. Next, we have demonstrated the detection of HBsAg using two different antibodies functionalised on the sensor surface: MBP-scFv and Mouse Anti-HBsAg antibody. The delay line with 4 μm IDT width on 41°YX $LiNbO_3$ substrate was found to outperform the other devices in terms of change in frequency observed. Results show that the HBsAg was successfully detected by the devices, with the 4 μm devices showing the highest sensitivity followed by the 8 μm and 12 μm devices. It was also observed that the limit of detection (LoD) was found to be better in case of the devices functionalised with mouse Anti-HBsAg antibody than in case of the devices functionalised with the recombinant scFv. This can be attributed to the fact that first the devices were functionalised with mouse anti-HBsAg antibody, followed by stripping off of the antibody, and again functionalised with MBP-scFv. This stripping and regeneration can be a reason behind the deterioration in the performance of the sensors with MBP-scFv. Out of the six devices, the highest frequency change of 889 kHz, and hence the best sensitivity was shown by the delay line with an IDT width of 4 μm and 41°YX $LiNbO_3$ substrate. The sensor showed a response to HBsAg in a range of 0.0818 IU/ml to 818000 IU/ml. The proposed device was successfully applied to determine the HBsAg in spiked-human serum with a detection limit of 81.8 IU/ml. This is not at par with the clinical methods currently in use in diagnostic centres. However, the reason for this is the reuse of the device, and hence performance can be enhanced if reusability is avoided. The microfabricated SAW dual delay line sensor provided a specific and quantitative detection of HBsAg in PBS and human serum.

The detection experiments performed show that the dual delay line SH-SAW sensor designed and fabricated is sensitive enough to detect the binding of HBsAg to an immobilised layer of anti-HBsAg antibody. Thus, it can be forecasted to have tremendous impact in the field of biosensing applications.

The developed SAW immuno-biosensors showed a limit of detection of approximately 1.5 IU/ml. Table 7.1 gives a comparison of the performance of our sensor against the existing state of the art diagnostic kits. However, we need to note that none of the existing kits use electronic methods of detection. Moreover, our device offers the option of multiple use, which can go a long way in reducing the cost of the diagnostic process.

TABLE 7.1: Comparison of developed SH-SAW sensor with commercially available kits

Name of the kit (Manufacturer)	**Principle of detection**	**Limit of detection**	**Single use/ Multiple use**	**Ref**
Liaison HBsAg (Dia-Sorin)	Direct sandwich chemiluminescence immunoassay	0.050 IU/mL	Multiple	[18]
ICT-CLEIA	Semiautomated immune complex transfer chemiluminescence enzyme immunoassay	0.2 mIU/mL	Multiple	[21]
Architect HBsAg QT assay (Abbott)	Chemiluminescent microparticle immunoassay (CMIA)	0.130 IU/mL	Multiple	[22]
CobasAmpliprep/ CobasTaqMan assay (Cobas)	Molecular techniques	6.25 IU/mL	Single	[24]
Developed SAW device	In vitro SAW device	1.5 IU/ml	Multiple	This work

7.2 Future Prospects

Based on the conclusion of the thesis, the possibility of the SAW dual delay line to be used as a point-of-care device can be predicted. The developed SAW sensor is label-free and detects the sensing signal electrically. The integration of the device with microfluidics can help to enhance its functionality and also decrease the complexity of the detection scheme. The use of an oscillator circuit in lieu of the network analyzer to detect the response can also aid in decreasing the cost of operation of the device.

Appendix A

Materials and Equipments Used

General reagents

Acetic acid, di-sodium hydrogen phosphate, glycerol, hydrochloric acid, isopropyl alcohol, methanol, sulphuric acid, ethanol, sodium chloride (all AR grade) – from HiMedia, India and Merck, India.

Molecular biology grade reagents/ chemicals

Acrylamide, APS, bis-acryl amide, TEMED, APS, EDTA, IPTG, tween 20, triton X 100, Bradford's reagent - from Sigma-Aldrich, USA. Glycine, SDS, tris–base, imidazole, ampicillin- from Himedia, India.

Components for bacterial culture medium

Tryptone, yeast extract, Agar from Himedia, India.

Enzymes

PCR master mix from HiMedia, India. SalI, BamHI and XhoI, from NEB, UK. Quick DNA ligase from NEB, UK.

Blotting Membranes and Filters

PVDF membrane (0.2 μm) - from Millipore, U.S.A. 3mm filter paper - from Whatman, USA.

DNA and protein markers

100 bp and 1 kbp DNA ladder and protein molecular weight marker (11-175KD) - from HiMedia, India.

Plastic and Glasswares

Micro pipette tips, micro centrifuge tubes, petri dishes and other plastic wares- from Tarson Products Pvt. Ltd., India. PCR tubes - from Axygen, USA; Glassware- from Borosil International, India.

Bacterial strains used

1. *E. coli* DH5α : From Novagen.
2. *E. coli* BL21 : From Novagen.

Culture Medium for Bacteria

1. Luria Broth: Tryptone 1.0%, Yeast extract 0.5%, NaCl 1.0%
2. 2xTY: Tryptone 1.6%, Yeast extract 1.0%, NaCl 0.5%

List of Buffers and Solutions

1. TAE : Tris Acetate EDTA buffer, 50x (100ml) 24.2 g Tris base, 5.71 ml CH3COOH, 10 ml of 0.5 M EDTA.
2. Phosphate buffer saline (PBS): 0.137 M NaCl, 2.68 mM KCl, 7.98 mM Na2HPO4, 1.4 mM KH2PO4, pH 7.2.
3. TBS: 50mM tris base, 150mM NaCl.
4. TBST: TBS containing 0.1% Tween-20.

Solutions for competent cell preparation

1. Sterile $CaCl_2$: 50 mM $CaCl_2$ is filter sterilized through a 0.22µ filter (HiMedia)
2. Sterile Glycerol (50%): 20 ml 100% Glycerol is added in 20 ml water and sterilized by autoclaving.

Buffers/solutions for protein purification

1. Stripping Buffer: 20 mM sodium phosphate, 500 mM NaCl, 50 mM EDTA, pH 7.4.
2. Equilibration Buffer: 20 mM sodium phosphate, 500 mM NaCl, 40 mM Imidazole, pH 7.4.

3. Binding Buffer: 20 mM sodium phosphate, 500 mM NaCl, 40 mM Imidazole, pH 7.4.
4. Column Buffer: 20 mM Tris-HCl, 200 mM NaCl, 1 mM EDTA, pH 7.4.
5. Binding Buffer: 20 mM sodium phosphate, 500 mM NaCl, 40 mM Imidazole, pH 7.4.
6. Elution Buffer: 10 mM maltose in column buffer, pH 7.4

Buffers/solutions for SDS-PAGE

1. 30 % acrylamide-bisacrylamide solution (100 ml): 29.2 g Acrylamide, 0.8 g Bisacrylamide.
2. Tris. HCl(pH 6.8) 0.5 M (100 ml): 6.06 g of Tris base, pH adjusted to 6.8 with 2 N HCl.
3. Tris.HCl, pH 8.8, 1.5 M (100 ml): 18.18 g of Tris base, pH adjusted to 8.8 with 2 N HCl.
4. Gel Running Buffer: 25 mM Tris base, 250 mM, 0.1% SDS.
5. Sample Loading Buffer (1X): 50 mM Tris-HCl pH 6.8, 2% SDS, 10% glycerol, 1% β-mercaptoethanol, 0.02 % bromophenol blue.
6. Staining solution: 50% Methanol, 10% Acetic acid, 40% Water, 0.25% CBB R250.
7. Destaining solution: 30% Methanol, 10% Acetic acid, 60% Water.

Buffers/solutions for Western Blot

1. Transfer buffer: 25 mM Tris base, 39 mM Glycine, 20 % Methanol .
2. Ponceau solution (Sigma): 0.1% Ponceau S in 5% acetic acid.
3. Blocking Solution: 3% BSA in TBST.
4. Washing buffer: PBST or TBST

Buffers/Solutions for SPR

1. Amine-coupling reagent(A): 0.4 M 1-ethyl-3-(3-dimethylamino-propyl)carbodiimide hydrochloride in water, pH 7.4
2. Amine-coupling reagent(B): 0.1 M N-hydroxysuccinimide in water,pH 7.4
3. Ethanolamine solution: 1.0 M ethanolamine-HCl, pH 8.5
4. Coupling Buffer: 10 mM sodium acetate, pH 4.0, 4.5, 5.0, 5.5
5. Regeneration Buffer: 10 mM sodium acetate, pH 1.5, 2.0, 2.5, 3.0
6. Running Buffer: 10 mM Na_2HPO_4, NaH_2PO_4, 150 mM NaCl, pH 7.4
7. Equilibration Buffer: 10 mM Na_2HPO_4, NaH_2PO_4, 150mM NaCl, 0.05% Tween 20, pH 7.4

Buffers/Solutions for ELISA

1. Substrate solution: O-phenylenediamine (0.5 mg/ml) diluted in 0.05 M citric acid and 0.1 M Na_2HPO_4 (pH 5.0) and 0.03% H_2O_2.
2. Stop solution 8 N Sulphuric acid.

List of Antibodies

1. Monoclonal Anti-Histidine-tagged protein (Calbiochem, Germany, #0B05).
2. Anti Mouse-HRP (Sigma, U.S.A, #A0412).
3. Monoclonal Anti-MBP antibody (Sigma, U.S.A, #SAB5300427).
4. Monoclonal Anti-HBV antigen HBsAg (Sigma Aldrich, #SAB 4700767)

List of Primers

1. The primers for scFv cloned in pET-22b(+) were:
   T7 Promoter Primer: 5'-TAATACGACTCACTATAGGG-3
   T7 Terminator Primer: 5'-GCTAGTTATTGCTCAGCGG-3

2. The primers for scFv cloned in pMAL-p5x were:
   Forward primer: 5'-GCAAGTCGACGAGGTGCAGCTGCAGCAGC-3
   Reverse primer: 5'-GCAAGGATCCTCACCGTTTGAGTTCCAGCTTG-3

Equipment used in microfabrication

1. Lithography Laser Writer: Heidelberg μPG-501. Micro-pattern generator machine. Manufactured by Heidelberg Instruments Mikrotechnik GmbH, Germany.
2. Tecport Sputter Coater. RF sputtering machine. Manufactured by Tecport Optics, Orlando.
3. Dektak XT surface profiler. Manufactured by Bruker, USA.
4. Wafer dicing machine. EC-400 Semi-automatic model. Manufactured by MTI Corporation, USA.

Bibliography

[1] M. Krajden, G. McNabb, and M. Petric, “The laboratory diagnosis of Hepatitis B Virus,” *Canadian Journal of Infectious Diseases and Medical Microbiology*, vol. 16, no. 2, pp. 65–72, 2005.

[2] N. Gitlin, “Hepatitis B: diagnosis, prevention, and treatment,” *Clinical chemistry*, vol. 43, no. 8, pp. 1500–1506, 1997.

[3] C. W. Shepard, E. P. Simard, L. Finelli, A. E. Fiore, and B. P. Bell, “Hepatitis B virus infection: epidemiology and vaccination,” *Epidemiologic reviews*, vol. 28, no. 1, pp. 112–125, 2006.

[4] T. J. Liang, “Hepatitis B: the virus and disease,” *Hepatology*, vol. 49, no. S5, 2009.

[5] M. Mendy, T. Welzel, O. Lesi, P. Hainaut, A. Hall, M. Kuniholm, S. McConkey, J. Goedert, S. Kaye, S. Rowland Jones *et al.*, “Hepatitis B viral load and risk for liver cirrhosis and hepatocellular carcinoma in the gambia, west africa,” *Journal of viral hepatitis*, vol. 17, no. 2, pp. 115–122, 2010.

[6] M. Krajden, G. McNabb, and M. Petric, “The laboratory diagnosis of Hepatitis B virus,” *Canadian Journal of Infectious Diseases and Medical Microbiology*, vol. 16, no. 2, pp. 65–72, 2005.

[7] S. H. Kim, “Elisa for quantitative determination of Hepatitis B virus surface antigen,” *Immune network*, vol. 17, no. 6, pp. 451–459, 2017.

[8] A. Valanne, S. Huopalahti, R. Vainionpää, T. Lövgren, and H. Härmä, “Rapid and sensitive hbsag immunoassay based on fluorescent nanoparticle labels and time-resolved detection,” *Journal of virological methods*, vol. 129, no. 1, pp. 83–90, 2005.

[9] H. J. Lee, K. Namkoong, E. C. Cho, C. Ko, J. C. Park, and S. S. Lee, “Surface acoustic wave immunosensor for real-time detection of Hepatitis B surface antibodies in whole blood samples,” *Biosensors and Bioelectronics*, vol. 24, no. 10, pp. 3120–3125, 2009.

[10] T. Xu, J. Miao, Z. Wang, L. Yu, and C. M. Li, “Micro-piezoelectric immunoassay chip for simultaneous detection of Hepatitis B virus and α-fetoprotein,” *Sensors and Actuators B: Chemical*, vol. 151, no. 2, pp. 370–376, 2011.

[11] S. Lee, J. Cho, Y. Lee, S. Jeon, H. J. Cha, and W. Moon, “Measurement of Hepatitis B surface antigen concentrations using a piezoelectric microcantilever as a mass sensor,” *Journal of Sensors*, vol. 2012, 2012.

[12] Y. J. Huang, C. W. Huang, T. H. Lin, C. T. Lin, L. G. Chen, P. Y. Hsiao, B. R. Wu, H. T. Hsueh, B. J. Kuo, H. H. Tsai *et al.*, “A CMOS cantilever-based label-free dna SoC with improved sensitivity for Hepatitis B virus detection,” *IEEE Transactions on Biomedical Circuits and systems*, vol. 7, no. 6, pp. 820–831, 2013.

[13] Z. Tan, M. Li, X. Kuang, Y. Tang, Y. Fan, G. Deng, Y. Wang, and D. He, “Clinical implications of Hepatitis B surface antigen quantitation in the natural history of chronic Hepatitis B virus infection,” *Journal of Clinical Virology*, vol. 59, no. 4, pp. 228–234, 2014.

[14] K. Oh, Y. S. Choi, H. Y. Yoon, N. Park, J. Kim, and Y. K. Kim, “Immunochromatographic assay of Hepatitis B surface antigen using magnetic nanoparticles as signal materials,” *IEEE Transactions on Magnetics*, vol. 50, no. 11, pp. 1–4, 2014.

[15] S. Chevaliez, D. Challine, H. Naija, T. C. Luu, S. Laperche, L. Nadala, J. P. Allain, H. H. Lee, and J. M. Pawlotsky, “Performance of a new rapid test for the detection of Hepatitis B surface antigen in various patient populations,” *Journal of Clinical Virology*, vol. 59, no. 2, pp. 89–93, 2014.

[16] “HBsAg (HBs) assay for the detection of Hepatitis B surface antigen,” *ADVIA Centaur Assay Manual*, vol. 07064134, 2005.

[17] “HBsAg ULTRA,” *Monolisa kit Manual (Bio-Rad)*, vol. 883614, 2011.

[18] “Liaison® XL murex HBsAg quant,” *DiaSorin*, vol. 12297, 2013.

[19] “Vikia HBsAg rapid diagnostic test,” *Biomerieux*, vol. 3.

[20] “HBsAg (v2),” *Abbott AXSYM System*, vol. 2, 2005.

[21] K. Takeda, M. Maruki, T. Yamagaito, M. Muramatsu, Y. Sakai, H. Tobimatsu, H. Kobayashi, Y. Mizuno, and Y. Hamaguchi, “Highly sensitive detection of Hepatitis B virus surface antigen using a semi-automated immune complex transfer chemiluminescent enzyme immunoassay,” *Journal of clinical microbiology*, pp. JCM–00 324, 2013.

[22] “HBsAg qualitative,” *Architect system*, vol. B1P970, 2009.

[23] “One step HBsAg test,” *InTec PRODUCTS, INC.*, vol. ITP01001, 2013.

[24] M. Ghosh, S. Nandi, S. Dutta, and M. K. Saha, “Detection of Hepatitis B virus infection: a systematic review,” *World journal of hepatology*, vol. 7, no. 23, p. 2482, 2015.

[25] “Determine Hapatitis B,” *Inverness Medical*, vol. 2.0, 2007.

[26] A. Moulin, S. O’shea, and M. E. Welland, “Microcantilever-based biosensors,” *Ultramicroscopy*, vol. 82, no. 1-4, pp. 23–31, 2000.

[27] M. Joshi, N. Kale, S. Mukherji, R. Lal, and V. R. Rao, “Affinity cantilever sensors for cardiac diagnostics,” 2007.

[28] B. N. Johnson and R. Mutharasan, “Biosensing using dynamic-mode cantilever sensors: A review,” *Biosensors and bioelectronics*, vol. 32, no. 1, pp. 1–18, 2012.

[29] L. Beardslee, F. Josse, S. M. Heinrich, I. Dufour, and O. Brand, “Geometrical considerations for the design of liquid-phase biochemical sensors using a cantilever’s fundamental in-plane mode,” *Sensors and Actuators B: Chemical*, vol. 164, no. 1, pp. 7–14, 2012.

[30] J. Zhang, H. P. Lang, F. Battiston, N. Backmann, F. Huber, and C. Gerber, “Development of robust and standardized cantilever sensors based on biotin/neutravidin coupling for antibody detection,” *Sensors*, vol. 13, no. 4, pp. 5273–5285, 2013.

[31] Y. J. Huang, C. W. Huang, T. H. Lin, C. T. Lin, L. G. Chen, P. Y. Hsiao, B. R. Wu, H. T. Hsueh, B. J. Kuo, H. H. Tsai *et al.*, “A CMOS cantilever-based label-free DNA SoC with improved sensitivity for Hepatitis B virus detection,” *IEEE Transactions on Biomedical Circuits and systems*, vol. 7, no. 6, pp. 820–831, 2013.

[32] H. Wohltjen and R. Dessy, “Surface acoustic wave probe for chemical analysis. I. Introduction and instrument description,” *Analytical Chemistry*, vol. 51, no. 9, pp. 1458–1464, 1979.

[33] Y. W. Kim, S. E. Sardari, M. T. Meyer, A. A. Iliadis, H. C. Wu, W. E. Bentley, and R. Ghodssi, “An ALD aluminum oxide passivated surface acoustic wave sensor for early biofilm detection,” *Sensors and Actuators B: Chemical*, vol. 163, no. 1, pp. 136–145, 2012.

[34] P. Zheng, D. W. Greve, and I. J. Oppenheim, “Langasite surface acoustic wave gas sensors: Modeling and verification,” *IEEE transactions on ultrasonics, ferroelectrics, and frequency control*, vol. 60, no. 3, pp. 579–586, 2013.

[35] A. Binder, G. Bruckner, N. Schobernig, and D. Schmitt, “Wireless surface acoustic wave pressure and temperature sensor with unique identification based on $LiNbO_3$,” *IEEE Sensors Journal*, vol. 13, no. 5, pp. 1801–1805, 2013.

[36] P. Dineva, D. Gross, R. Müller, and T. Rangelov, “Piezoelectric materials,” in *Dynamic Fracture of Piezoelectric Materials*. Springer, 2014, pp. 7–32.

[37] B. A. Auld, *Acoustic fields and waves in solids*. Wiley Interscience Publication, 1973.

[38] D. Morgan, *Surface acoustic wave filters: With applications to electronic communications and signal processing*. Academic Press, 2010.

[39] M. Thompson and D. C. Stone, *Surface-launched acoustic wave sensors: chemical sensing and thin-film characterization*. Wiley-Interscience, 1997, vol. 195.

[40] H. Wohltjen, “Mechanism of operation and design considerations for surface acoustic wave device vapour sensors,” *Sensors and Actuators*, vol. 5, no. 4, pp. 307–325, 1984.

[41] S. Martin and G. Frye, “Surface acoustic wave response to changes in viscoelastic film properties,” *Applied physics letters*, vol. 57, no. 18, pp. 1867–1869, 1990.

[42] W. Buff, S. Klett, M. Rusko, J. Ehrenpfordt, and M. Goroli, “Passive remote sensing for temperature and pressure using saw resonator devices,” *IEEE transactions on ultrasonics, ferroelectrics, and frequency control*, vol. 45, no. 5, pp. 1388–1392, 1998.

[43] B. Drafts, "Acoustic wave technology sensors," *IEEE Transactions on microwave theory and techniques*, vol. 49, no. 4, pp. 795–802, 2001.

[44] A. D'amico and E. Verona, "Saw sensors," *Sensors and Actuators*, vol. 17, no. 1-2, pp. 55–66, 1989.

[45] A. Mauder, "Saw gas sensors: comparison between delay line and two port resonator," *Sensors and Actuators B: Chemical*, vol. 26, no. 1-3, pp. 187–190, 1995.

[46] I. Avramov, A. Voigt, and M. Rapp, "Rayleigh saw resonators using gold electrode structure for gas sensor applications in chemically reactive environments," *Electronics Letters*, vol. 41, no. 7, pp. 450–452, 2005.

[47] M. Penza, P. Aversa, G. Cassano, W. Wlodarski, and K. Kalantar-Zadeh, "Layered saw gas sensor with single-walled carbon nanotube-based nanocomposite coating," *Sensors and actuators B: Chemical*, vol. 127, no. 1, pp. 168–178, 2007.

[48] J. E. Roederer and G. J. Bastiaans, "Microgravimetric immunoassay with piezoelectric crystals," *Analytical Chemistry*, vol. 55, no. 14, pp. 2333–2336, 1983.

[49] R. C. Ebersole and M. D. Ward, "Amplified mass immunosorbent assay with a quartz crystal microbalance," *Journal of the American Chemical Society*, vol. 110, no. 26, pp. 8623–8628, 1988.

[50] J. Kondoh, Y. Matsui, and S. Shiokawa, "New biosensor using shear horizontal surface acoustic wave device," *Japanese journal of applied physics*, vol. 32, no. 5S, p. 2376, 1993.

[51] C. Déjous, M. Savart, D. Rebière, and J. Pistré, "A shear-horizontal acoustic plate mode (SH-APM) sensor for biological media," *Sensors and Actuators B: Chemical*, vol. 27, no. 1-3, pp. 452–456, 1995.

[52] G. Harding, J. Du, P. Dencher, D. Barnett, and E. Howe, "Love wave acoustic immunosensor operating in liquid," *Sensors and Actuators A: Physical*, vol. 61, no. 1-3, pp. 279–286, 1997.

[53] F. Josse, F. Bender, and R. W. Cernosek, "Guided shear horizontal surface acoustic wave sensors for chemical and biochemical detection in liquids," *Analytical chemistry*, vol. 73, no. 24, pp. 5937–5944, 2001.

[54] K. Kalantar-Zadeh, W. Wlodarski, Y. Y. Chen, B. N. Fry, and K. Galatsis, "Novel love mode surface acoustic wave based immunosensors," *Sensors and Actuators B: Chemical*, vol. 91, no. 1-3, pp. 143–147, 2003.

[55] D. W. Branch and S. M. Brozik, "Low-level detection of a bacillus anthracis simulant using love-wave biosensors on 36°YX-LiTaO$_3$," *Biosensors and Bioelectronics*, vol. 19, no. 8, pp. 849–859, 2004.

[56] M. D. Schlensog, T. M. Gronewold, M. Tewes, M. Famulok, and E. Quandt, "A love-wave biosensor using nucleic acids as ligands," *Sensors and Actuators B: Chemical*, vol. 101, no. 3, pp. 308–315, 2004.

[57] E. Berkenpas, S. Bitla, P. Millard, and M. P. Da Cunha, "Pure shear horizontal SAW biosensor on langasite," *IEEE transactions on ultrasonics, ferroelectrics, and frequency control*, vol. 51, no. 11, pp. 1404–1411, 2004.

[58] Y. Hur, J. Han, J. Seon, Y. E. Pak, and Y. Roh, "Development of an SH-SAW sensor for the detection of DNA hybridization," *Sensors and Actuators A: Physical*, vol. 120, no. 2, pp. 462–467, 2005.

[59] N. Moll, E. Pascal, D. H. Dinh, J. P. Pillot, B. Bennetau, D. Rebiere, D. Moynet, Y. Mas, D. Mossalayi, J. Pistré *et al.*, "A love wave immunosensor for whole e. coli bacteria detection using an innovative two-step immobilisation approach," *Biosensors and Bioelectronics*, vol. 22, no. 9-10, pp. 2145–2150, 2007.

[60] J. Sakong, H. Roh, and Y. Roh, "Surface acoustic wave DNA sensor with microfluidic channels," *Japanese Journal of Applied Physics*, vol. 46, no. 7S, p. 4729, 2007.

[61] M. Bisoffi, B. Hjelle, D. Brown, D. Branch, T. Edwards, S. Brozik, V. Bondu-Hawkins, and R. Larson, "Detection of viral bioagents using a shear horizontal surface acoustic wave biosensor," *Biosensors and Bioelectronics*, vol. 23, no. 9, pp. 1397–1403, 2008.

[62] N. Moll, E. Pascal, D. H. Dinh, J. L. Lachaud, L. Vellutini, J. P. Pillot, D. Rebière, D. Moynet, J. Pistré, D. Mossalayi *et al.*, "Multipurpose love acoustic wave immunosensor for bacteria, virus or proteins detection," *Irbm*, vol. 29, no. 2-3, pp. 155–161, 2008.

[63] K. Länge, B. E. Rapp, and M. Rapp, "Surface acoustic wave biosensors: a review," *Analytical and bioanalytical chemistry*, vol. 391, no. 5, pp. 1509–1519, 2008.

[64] M. I. Rocha Gaso, C. March Iborra, Á. Montoya Baides, and A. Arnau Vives, "Surface generated acoustic wave biosensors for the detection of pathogens: A review," *Sensors*, vol. 9, no. 7, pp. 5740–5769, 2009.

[65] N. Fourati, M. Lazerges, C. Vedrine, J. M. Fougnion, C. Zerrouki, L. Rousseau, P. Lepeut, J. J. Bonnet, and C. Pernelle, "Surface acoustic waves sensor for dna-biosensor development," *Sensor letters*, vol. 7, no. 5, pp. 847–850, 2009.

[66] D. S. Lee, J. H. Lee, J. Luo, Y. Fu, W. I. Milne, S. Maeng, M. Y. Jung, S. H. Park, and H. C. Yoon, "A surface acoustic wave-based immunosensing device using a nanocrystalline Zno film on Si," *Journal of nanoscience and nanotechnology*, vol. 9, no. 12, pp. 7181–7185, 2009.

[67] Y. Bergaoui, C. Zerrouki, J. Fougnion, N. Fourati, and A. Abdelghani, "Sensitivity estimation and biosensing potential of lithium tantalate shear horizontal surface acoustic wave sensor," *Sensor letters*, vol. 7, no. 5, pp. 1001–1005, 2009.

[68] C. Zerrouki, N. Fourati, R. Lucas, J. Vergnaud, J. M. Fougnion, R. Zerrouki, and C. Pernelle, "Biological investigation using a shear horizontal surface acoustic wave sensor: Small "click generated" dna hybridization detection," *Biosensors and Bioelectronics*, vol. 26, no. 4, pp. 1759–1762, 2010.

[69] G. De Simoni, G. Signore, M. Agostini, F. Beltram, and V. Piazza, "A surface-acoustic-wave-based cantilever bio-sensor," *Biosensors and Bioelectronics*, vol. 68, pp. 570–576, 2015.

[70] T. M. Gronewold, "Surface acoustic wave sensors in the bioanalytical field: Recent trends and challenges," *analytica chimica acta*, vol. 603, no. 2, pp. 119–128, 2007.

[71] K. Länge, B. E. Rapp, and M. Rapp, "Surface acoustic wave biosensors: a review," *Analytical and bioanalytical chemistry*, vol. 391, no. 5, pp. 1509–1519, 2008.

[72] E. Timurdogan, B. E. Alaca, I. H. Kavakli, and H. Urey, "MEMS biosensor for detection of Hepatitis A and C viruses in serum," *Biosensors and Bioelectronics*, vol. 28, no. 1, pp. 189–194, 2011.

[73] E. Nuxoll, "BioMEMS in drug delivery," *Advanced drug delivery reviews*, vol. 65, no. 11-12, pp. 1611–1625, 2013.

[74] S. C. Gopinath, T. H. Tang, M. Citartan, Y. Chen, and T. Lakshmipriya, "Current aspects in immunosensors," *Biosensors and Bioelectronics*, vol. 57, pp. 292–302, 2014.

[75] M. O. Noor and U. J. Krull, "Silicon nanowires as field-effect transducers for biosensor development: A review," *Analytica chimica acta*, vol. 825, pp. 1–25, 2014.

[76] G. Harding, J. Du, P. Dencher, D. Barnett, and E. Howe, "Love wave acoustic immunosensor operating in liquid," *Sensors and Actuators A: Physical*, vol. 61, no. 1-3, pp. 279–286, 1997.

[77] J. Kondoh, Y. Matsui, and S. Shiokawa, "New biosensor using shear horizontal surface acoustic wave device," *Japanese journal of applied physics*, vol. 32, no. 5S, p. 2376, 1993.

[78] K. Kalantar Zadeh, W. Wlodarski, Y. Y. Chen, B. N. Fry, and K. Galatsis, "Novel Love mode surface acoustic wave based immunosensors," *Sensors and Actuators B: Chemical*, vol. 91, no. 1-3, pp. 143–147, 2003.

[79] Y. Hur, J. Han, J. Seon, Y. E. Pak, and Y. Roh, "Development of an SH-SAW sensor for the detection of DNA hybridization," *Sensors and Actuators A: Physical*, vol. 120, no. 2, pp. 462–467, 2005.

[80] N. Moll, E. Pascal, D. H. Dinh, J. P. Pillot, B. Bennetau, D. Rebiere, D. Moynet, Y. Mas, D. Mossalayi, J. Pistré *et al.*, "A Love wave immunosensor for whole E. coli bacteria detection using an innovative two-step immobilisation approach," *Biosensors and Bioelectronics*, vol. 22, no. 9-10, pp. 2145–2150, 2007.

[81] M. Bisoffi, B. Hjelle, D. Brown, D. Branch, T. Edwards, S. Brozik, V. Bondu-Hawkins, and R. Larson, "Detection of viral bioagents using a shear horizontal surface acoustic wave biosensor," *Biosensors and Bioelectronics*, vol. 23, no. 9, pp. 1397–1403, 2008.

[82] S. Krishnamoorthy, A. A. Iliadis, T. Bei, and G. P. Chrousos, "An interleukin-6 ZnO/SiO_2/Si surface acoustic wave biosensor," *Biosensors and Bioelectronics*, vol. 24, no. 2, pp. 313–318, 2008.

[83] L. Schmid, A. Wixforth, D. A. Weitz, and T. Franke, "Novel surface acoustic wave (saw)-driven closed PDMS flow chamber," *Microfluidics and nanofluidics*, vol. 12, no. 1-4, pp. 229–235, 2012.

[84] F. Di Pietrantonio, D. Cannatà, M. Benetti, E. Verona, A. Varriale, M. Staiano, and S. D'Auria, "Detection of odorant molecules via surface acoustic wave biosensor array based on odorant-binding proteins," *Biosensors and Bioelectronics*, vol. 41, pp. 328–334, 2013.

[85] M. Cole, I. Spulber, and J. W. Gardner, "Surface acoustic wave electronic tongue for robust analysis of sensory components," *Sensors and Actuators B: Chemical*, vol. 207, pp. 1147–1153, 2015.

[86] Y. W. Kim, M. T. Meyer, A. Berkovich, S. Subramanian, A. A. Iliadis, W. E. Bentley, and R. Ghodssi, "A surface acoustic wave biofilm sensor integrated with a treatment method based on the bioelectric effect," *Sensors and Actuators A: Physical*, vol. 238, pp. 140–149, 2016.

[87] S. Cular, S. K. Sankaranarayanan, and V. R. Bhethanabotla, "Enhancing effects of microcavities on shear-horizontal surface acoustic wave sensors: A finite element simulation study," *Applied Physics Letters*, vol. 92, no. 24, p. 244104, 2008.

[88] M. Richardson, S. Sankaranarayanan, and V. Bhethanabotla, "Shear-horizontal surface acoustic wave phononic device with high density filling material for ultra-low power sensing applications," *Applied Physics Letters*, vol. 104, no. 25, p. 253501, 2014.

[89] S. U. Senveli and O. Tigli, "A novel approach for differentiation of liquid samples with surface acoustic wave transducers and embedded microcavities," *Sensors and Actuators B: Chemical*, vol. 196, pp. 272–281, 2014.

[90] M. Richardson, S. Cheemalapati, R. Everly, S. K. Sankaranarayanan, A. Pyayt, and V. R. Bhethanabotla, "Design and fabrication of a SAW device with Ta filled microcavities inserted into its delay path for improved power transfer," *Journal of Vacuum Science & Technology B, Nanotechnology and Microelectronics: Materials, Processing, Measurement, and Phenomena*, vol. 33, no. 2, p. 022001, 2015.

[91] S. U. Senveli and O. Tigli, "A novel surface acoustic wave sensor for microparticle sensing and quantification," *IEEE Sensors Journal*, vol. 15, no. 10, pp. 5748–5754, 2015.

[92] S. U. Senveli, Z. Ao, S. Rawal, R. H. Datar, R. J. Cote, and O. Tigli, "A surface acoustic wave biosensor for interrogation of single tumour cells in microcavities," *Lab on a Chip*, vol. 16, no. 1, pp. 163–171, 2016.

[93] S. Li, S. K. Sankaranarayanan, C. Fan, Y. Su, and V. R. Bhethanabotla, "Achieving lower insertion loss and higher sensitivity in a SAW biosensor via optimization of waveguide and microcavity structures," *IEEE Sensors Journal*, vol. 17, no. 6, pp. 1608–1616, 2017.

[94] J. C. Eijkel and A. Van Den Berg, "Nanofluidics: what is it and what can we expect from it?" *Microfluidics and Nanofluidics*, vol. 1, no. 3, pp. 249–267, 2005.

[95] K. Länge, G. Blaess, A. Voigt, R. Götzen, and M. Rapp, "Integration of a surface acoustic wave biosensor in a microfluidic polymer chip," *Biosensors and Bioelectronics*, vol. 22, no. 2, pp. 227–232, 2006.

[96] A. Jung, T. M. Gronewold, M. Tewes, E. Quandt, and P. Berlin, "Biofunctional structural design of SAW sensor chip surfaces in a microfluidic sensor system," *Sensors and Actuators B: Chemical*, vol. 124, no. 1, pp. 46–52, 2007.

[97] J. Sakong, H. Roh, and Y. Roh, "Surface acoustic wave DNA sensor with microfluidic channels," *Japanese Journal of Applied Physics*, vol. 46, no. 7S, p. 4729, 2007.

[98] T. Dung Luong and N. Trung Nguyen, "Surface acoustic wave driven microfluidics-A Review," *Micro and Nanosystems*, vol. 2, no. 3, pp. 217–225, 2010.

[99] D. Matatagui, J. L. Fontecha, M. J. Fernández, I. Gràcia, C. Cané, J. P. Santos, and M. C. Horrillo, "Love-wave sensors combined with microfluidics for fast detection of biological warfare agents," *Sensors*, vol. 14, no. 7, pp. 12 658–12 669, 2014.

[100] Y. Kwon and Y. Roh, "Development of SH-SAW sensors for underwater measurement," *Ultrasonics*, vol. 42, no. 1-9, pp. 409–411, 2004.

[101] I. Leonte, G. Sehra, M. Cole, P. Hesketh, and J. Gardner, "Taste sensors utilizing high-frequency SH-SAW devices," *Sensors and Actuators B: Chemical*, vol. 118, no. 1-2, pp. 349–355, 2006.

[102] F. Di Pietrantonio, M. Benetti, D. Cannatà, E. Verona, M. Girasole, M. Fosca, S. Dinarelli, M. Staiano, V. Marzullo, A. Capo *et al.*, "A shear horizontal surface acoustic wave biosensor for a rapid and specific detection of D-serine," *Sensors and Actuators B: Chemical*, vol. 226, pp. 1–6, 2016.

[103] J. Hechner and W. Soluch, "Pseudo surface acoustic wave dual delay line on 41°YX-$LiNbO_3$ for liquid sensors," *Sensors and Actuators B: Chemical*, vol. 111, pp. 436–440, 2005.

[104] F. M. Zhou, Z. Li, L. Fan, S. Y. Zhang, and X. J. Shui, "Experimental study of love-wave immunosensors based on $ZnO/LiTaO_3$ structures," *Ultrasonics*, vol. 50, no. 3, pp. 411–415, 2010.

[105] J. P. Folkers, P. E. Laibinis, and G. M. Whitesides, "Self-assembled monolayers of alkanethiols on gold: comparisons of monolayers containing mixtures of short-and long-chain constituents with methyl and hydroxymethyl terminal groups," *Langmuir*, vol. 8, no. 5, pp. 1330–1341, 1992.

[106] N. K. Chaki and K. Vijayamohanan, "Self-assembled monolayers as a tunable platform for biosensor applications," *Biosensors and Bioelectronics*, vol. 17, no. 1-2, pp. 1–12, 2002.

[107] P. Jiang, Z. F. Liu, and S. M. Cai, "Growing monodispersed PbS nanoparticles on self-assembled monolayers of 11-Mercaptoundecanoic Acid on Au (111) substrate," *Langmuir*, vol. 18, no. 11, pp. 4495–4499, 2002.

[108] A. Tlili, A. Abdelghani, S. Hleli, and M. A. Maaref, "Electrical characterization of a thiol SAM on gold as a first step for the fabrication of immunosensors based on a quartz crystal microbalance," *Sensors*, vol. 4, no. 6, pp. 105–114, 2004.

[109] J. C. Love, L. A. Estroff, J. K. Kriebel, R. G. Nuzzo, and G. M. Whitesides, "Self-assembled monolayers of thiolates on metals as a form of nanotechnology," *Chemical reviews*, vol. 105, no. 4, pp. 1103–1170, 2005.

[110] F. Cecchet, M. Marcaccio, M. Margotti, F. Paolucci, S. Rapino, and P. Rudolf, "Redox mediation at 11-Mercaptoundecanoic Acid self-assembled monolayers on gold," *The Journal of Physical Chemistry B*, vol. 110, no. 5, pp. 2241–2248, 2006.

[111] E. Briand, C. Gu, S. Boujday, M. Salmain, J. M. Herry, and C. Pradier, "Functionalisation of gold surfaces with thiolate SAMs: Topography/bioactivity relationship–A combined FT-RAIRS, AFM and QCM investigation," *Surface Science*, vol. 601, no. 18, pp. 3850–3855, 2007.

[112] D. J. Kim, R. Pitchimani, D. E. Snow, and L. J. Hope Weeks, “A simple method for the removal of thiols on gold surfaces using an NH_4OH–H_2O_2–H_2O solution,” *Scanning: The Journal of Scanning Microscopies*, vol. 30, no. 2, pp. 118–122, 2008.

[113] Z. Lv, J. Wang, L. Deng, and G. Chen, “Preparation and characterization of covalently binding of rat anti-human IgG monolayer on thiol-modified gold surface,” *Nanoscale research letters*, vol. 4, no. 12, p. 1403, 2009.

[114] Z. Lv, J. Wang, G. Chen, and L. Deng, “Probing specific interaction forces between human IgG and rat anti-human IgG by self-assembled monolayer and atomic force microscopy,” *Nanoscale research letters*, vol. 5, no. 6, p. 1032, 2010.

[115] M. Yoon, H. J. Hwang, and J. H. Kim, “Immobilization of antibodies on the self-assembled monolayer by antigen-binding site protection and immobilization kinetic control,” *Journal of Biomedical Science and Engineering*, vol. 4, no. 04, p. 242, 2011.

[116] P. Bhadra, M. Shajahan, E. Bhattacharya, and A. Chadha, “Studies on varying n-alkanethiol chain lengths on a gold coated surface and their effect on antibody–antigen binding efficiency,” *RSC Advances*, vol. 5, no. 98, pp. 80 480–80 487, 2015.

[117] D. A. Frickey, “Conversions between s, z, y, h, abcd, and t parameters which are valid for complex source and load impedances,” *IEEE Transactions on microwave theory and techniques*, vol. 42, no. 2, pp. 205–211, 1994.

[118] H. J. Lee, K. Namkoong, E. C. Cho, C. Ko, J. C. Park, and S. S. Lee, “Surface acoustic wave immunosensor for real-time detection of Hepatitis B surface antibodies in whole blood samples,” *Biosensors and Bioelectronics*, vol. 24, no. 10, pp. 3120–3125, 2009.

[119] A. A. Mohanan, M. S. Islam, S. H. M. Ali, R. Parthiban, and N. Ramakrishnan, “Investigation into mass loading sensitivity of Sezawa wave mode-based surface acoustic wave sensors,” *Sensors*, vol. 13, no. 2, pp. 2164–2175, 2013.

[120] M. H. Hafezi and T. Kundu, “Peri-ultrasound modeling for surface wave propagation,” *Ultrasonics*, vol. 84, pp. 162–171, 2018.

[121] S. Trivedi and H. B. Nemade, “Finite element simulation of a highly sensitive SH-SAW delay line sensor with SiO_2 micro-ridges,” *Microsystem Technologies*, pp. 1–11, 2018.

[122] B. Bose, D. A. Chugh, M. Kala, S. K. Acharya, N. Khanna, and S. Sinha, “Characterization and molecular modeling of a highly stable anti-Hepatitis B surface antigen scFv,” *Molecular immunology*, vol. 40, no. 9, pp. 617–631, 2003.

[123] E. Pensa, E. Cortes, G. Corthey, P. Carro, C. Vericat, M. H. Fonticelli, G. Benitez, A. A. Rubert, and R. C. Salvarezza, “The chemistry of the sulfur–gold interface: in search of a unified model,” *Accounts of chemical research*, vol. 45, no. 8, pp. 1183–1192, 2012.

[124] J. Coates, “Interpretation of infrared spectra, a practical approach,” *Encyclopedia of analytical chemistry*, vol. 12, pp. 10 815–10 837, 2000.

LIST OF PUBLICATIONS

Patent

- Goswami N., Paily R. P., & Bose B. (2019),"**Surface Acoustic Wave Based Biosensor for Detection of Hepatitis B Surface Antigen**," Indian Patent, 2973/IITG

Journals

- Goswami N., Paily R. P., & Bose B., "**Surface Acoustic Wave Based Biosensor for Detection of Hepatitis B Surface Antigen**," Manuscript under preparation.
- Barman, U., Mukhopadhyay, G., Goswami, N., Ghosh, S. S., & Paily, R. P. (2017), "**Detection of Glutathione by Glutathione-S-Transferase-Nanoconjugate Ensemble Electrochemical Device**," IEEE transactions on nanobioscience, 16(4), 271-279.
- Kalita, A., Hussain, S., Malik, A. H., Barman, U., Goswami, N., & Iyer, P. K. (2016). "**Anion-exchange induced strong π-π interactions in single crystalline naphthalene diimide for nitroexplosive sensing: an electronic prototype for visual on-site detection**," ACS applied materials & interfaces, 8(38), 25326-25336.

Conferences

- Goswami N., Barman U., Paily R. P., Bose B., & Ghosh S. S. (2014), "**A Highly Sensitive Lithium-Niobate Based Micro cantilever for Biosensing Applications, Elsevier proceedings**," ICETREE, 2014.
- Barman, U., Goswami, N., Ghosh, S. S., & Paily, R. P. (2017), "**Chemiresistive device for detection of glutathione**," ICANN-2017, IIT Guwahati.

- Barman, U., Goswami, N., Ghosh, S. S., & Paily, R. P. (2017), "**Size Dependence of Intrinsic Band gap of ZnO Nanoparticles**," ICANN-2017, IIT Guwahati.
- Goswami N., Barman U., & Paily R. P. (2018), "**Fabrication of SAW dual delay line for biosensing applications**", International Workshop on NANO/MICRO 2D-3D Fabrication, Manufacturing of Electronic-Biomedical Devices and Applications, IIT Mandi.
- Barman, U., Goswami, N., Ghosh, S. S., & Paily, R. P. (2018), "**Simulation studies of ZnO nanoparticle based FET device for possible biosensing applications**," IEEE NANO-2018, Cork, Ireland.